

The background of the entire image is a deep space photograph featuring a nebula with intricate, swirling patterns of blue, green, and yellow. Numerous small stars of varying brightness are scattered across the dark blue background.

KRITTIKA SUMMER PROJECTS

Binary Stars

Bhavesh Rajpoot, B. Malavika, Mohammad Saad,
Namitha LS, Neev Shah, Rohan Sanghai, Sahil Jhawar,
Soumyadeep Bhattacharjee, Ananya Burli, Soham
Purohit, and Vedant Shenoy

KRITTIKA SUMMER PROJECTS

Binary Stars

Bhavesh Rajpoot¹, B. Malavika², Mohammad Saad³, Namitha LS⁴, Neev Shah⁵,
Rohan Sanghai⁶, Sahil Jhawar⁷, Soumyadeep Bhattacharjee⁸, Ananya Burli⁹,
Soham Purohit⁹, and Vedant Shenoy⁹

¹Fergusson College, Pune 411004, India

²Indian Institute of Technology Bombay, Powai, Mumbai 400076, India

³Indian Institute of Technology Kanpur, Kanpur 208016, India

⁴University of Hyderabad, Hyderabad 500046, India

⁵Indian Institute of Science Education and Research, Homi Bhabha Rd, Pashan, Pune 411008, India

⁶MIT-World Peace University, Pune 411038, India

⁷Christ(Deemed to be University), Bengaluru 560029, India

⁸Indian Institute of Science, Bangalore 560012, India

⁹Krittika-The Astronomy Club of IIT Bombay, Powai, Mumbai 400076, India

Copyright © 2020 Krittika IITB

PUBLISHED BY KRITTIKA: THE ASTRONOMY CLUB OF IIT BOMBAY

[GITHUB.COM / KRITTIKAIITB](https://github.com/KRITTIKAIITB)

First Release, August 2020

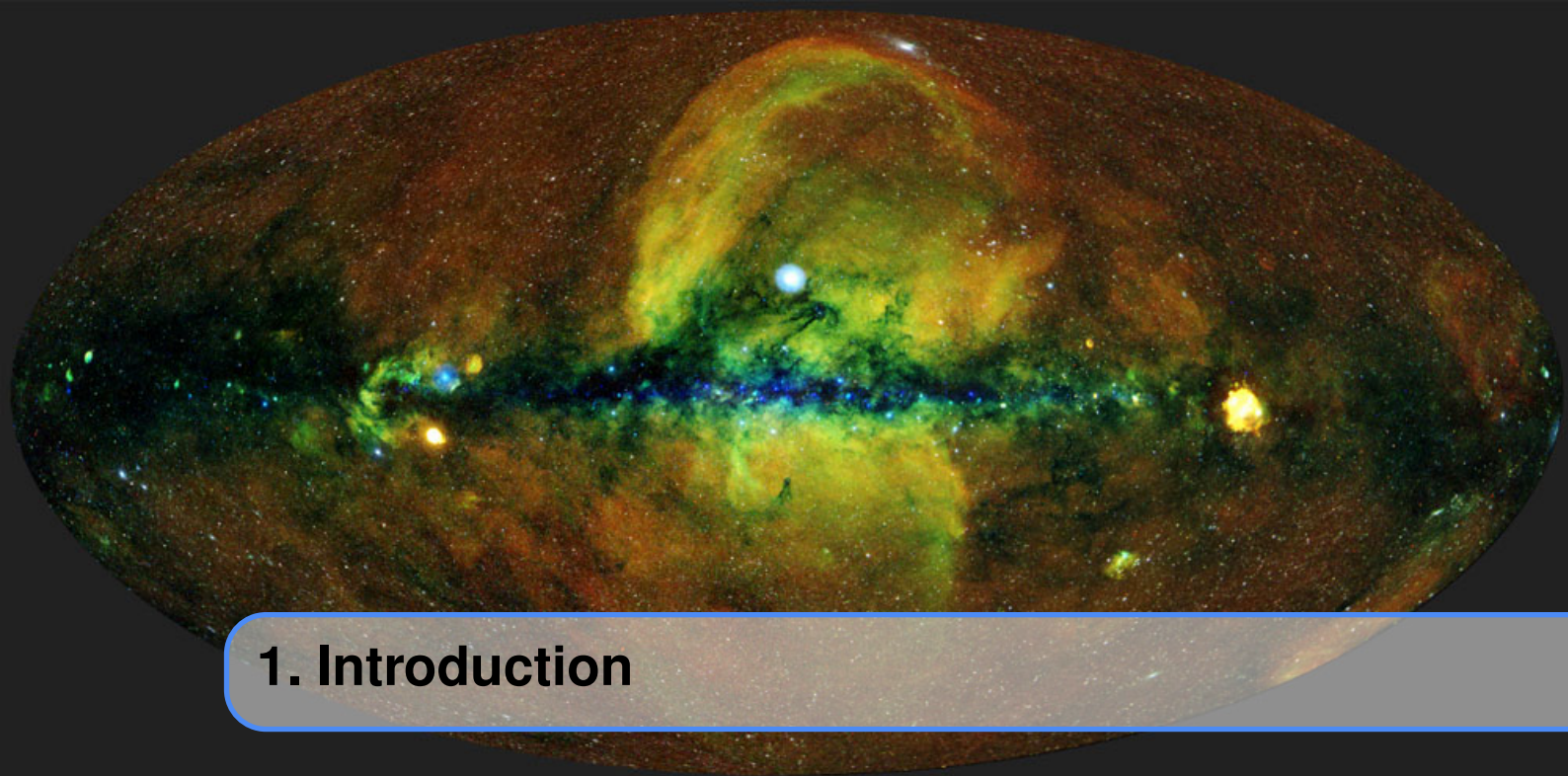


Contents

1	Introduction	7
1.1	Paragraphs of Text	7
1.2	Citation	7
1.3	Lists	7
1.3.1	Numbered List	7
1.3.2	Bullet Points	7
1.3.3	Descriptions and Definitions	8
2	Preliminaries	9
2.1	Orbital Parameters	9
2.1.1	Defining the Ellipse	9
2.1.2	Orbital Parameters	10
2.1.3	Anomalies	11
2.2	Transformations	13
3	Binary Star Systems	15
3.1	Eclipsing Binaries	15
3.2	Spectroscopic Binaries	16
3.3	Astrometric Binaries	17
3.4	Types of Binaries	18
4	Modelling of Binary Systems	21
4.1	Radial velocities	21
4.1.1	Edge-on circular orbits	21
4.1.2	Non-edge-on circular orbits	22

4.1.3	Elliptical orbits in COM frame	23
4.1.4	Adding The Orbital Parameters	25
4.1.5	Interactive Plot	27
4.2	Light Curves	27
4.2.1	Limb Darkening	28
4.2.2	Some Results	30
4.3	Rossiter-McLaughlin Effect	31
4.3.1	Theory	31
4.3.2	Implementation	32
4.3.3	Results	35
4.4	Ellipsoidal Variation	36
4.4.1	Deviation from Spherical Shape	36
4.4.2	The Lobed Shape	36
4.4.3	The Light Curve Variation	37
4.4.4	Method Used to Model	38
4.4.5	Results	39
5	Analyzing Observations	41
5.1	Spectroscopic Binaries	41
5.1.1	The Data	41
5.1.2	The Equations	41
5.1.3	Algorithm	42
5.1.4	Best Fit Results	43
5.2	Eclipsing Binaries	44
5.2.1	The Data	44
5.2.2	The Equations	45
5.2.3	Effects of Photometric Variation	46
5.3	Estimation of Parameters	47
5.3.1	The Approach of Model Fitting	47
5.3.2	Period	47
5.3.3	The Fitting	47
5.3.4	Combined Parameters	47
5.3.5	Circular Orbits	49
5.3.6	Elliptical Orbits	49
6	Alcor-Mizar: A Case Study	51
6.1	Mizar and Alcor : the Famous Double Star	51
6.1.1	Observation and Analysis of System in Radio at 1420 MHz	53
6.1.2	Optical Analysis of the Binary System using Aperture Photometry Tool	57
7	More Complex Systems	61
7.1	Types of Binaries	61
7.2	Stability of Complex Systems	61
7.3	Contact Binary Systems from an Observer's Perspective	63

8	Visualizations	69
8.1	Introduction	69
8.2	About the Software and the Tools Used	69
8.2.1	Blender - a Brief Introduction	69
8.2.2	Blender Python	70
8.2.3	Tools Used	70
8.2.4	Python Modules Used	70
8.3	Topic of the Animation	70
8.3.1	Revisiting few Terms	71
8.4	The Animation and its Making	72
8.5	The Main Formation Pathway	72
8.5.1	Texture and Modelling	72
8.5.2	Images of the Major Events	73
8.6	The BNS Merger	75
8.6.1	Modelling and Texture	75
8.6.2	Images	75
8.7	Detection from Earth	76
8.8	Putting the parts together	76
A	Appendix	77
A.1	Two Body Problem	77
A.1.1	Angular Momentum	77
A.1.2	Deriving the Orbit	78
A.1.3	Laplace-Runge-Lenz Vector (Alternate Way)	79
B	Replicating this work	81
B.1	RV Curves	81
B.2	Analysis	81
	References	83



1. Introduction

1.1 Paragraphs of Text

Hello this is an intro.

1.2 Citation

Inline citations are done via `\citet`, as proposed in Doe (2013). Another way to cite is using `\citep` (Smith, 2012). You can also combine citations (Doe, 2013; Smith, 2012). If you want to use inline citation as is done in Doe (2013); Smith (2012), you are free to do so. You can export citations from ADS for your bib file.

Rossiter (1924, Figure 5) shows how to cite a figure in text. In parenthesis, it is different (Rossiter, 1924, Figure 2). Suppose that this is a figure caption. Credits: da Vinci, 1490.

1.3 Lists

Lists are useful to present information in a concise and/or ordered way¹.

1.3.1 Numbered List

1. The first item
2. The second item
3. The third item

1.3.2 Bullet Points

- The first item
- The second item
- The third item

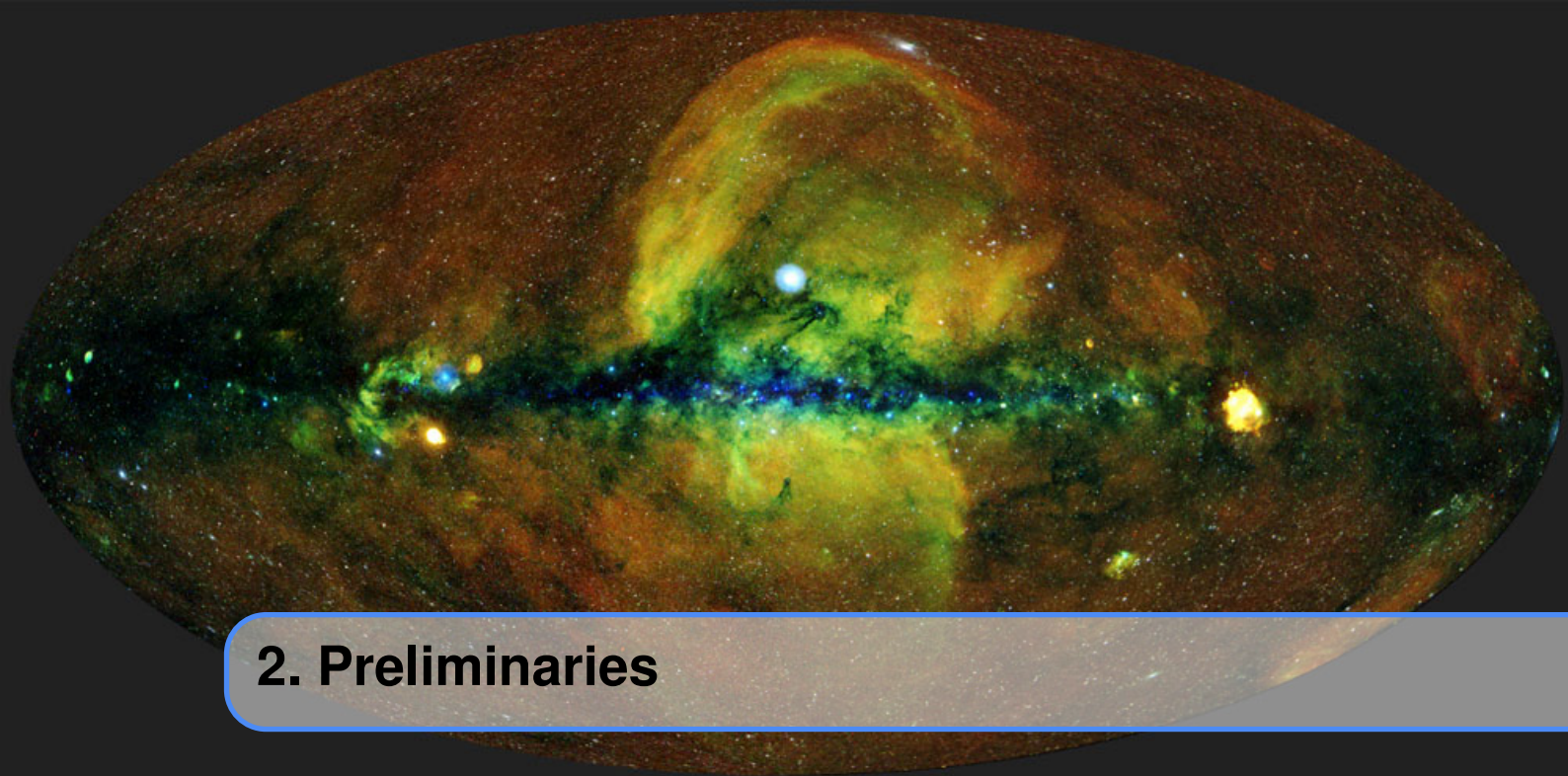
¹Footnote example...

1.3.3 Descriptions and Definitions

Name Description

Word Definition

Comment Elaboration



2. Preliminaries

2.1 Orbital Parameters

In the two body problem, the path followed by each of the bodies is a conic section (see Appendix A for a derivation). In bound binary systems like binary stars or planetary systems, the path followed by both the objects is either an ellipse or a circle (parabolic and hyperbolic orbits are both unbound). Newton's Laws of Motion gives a second order differential equation, generally in 3 dimensions (x, y, z). Thus to uniquely specify the path, we need 6 initial conditions; for example, the initial position and the velocity vectors. Inherent symmetries in the 2-body problem allow us to work with different parameters. These are

1. eccentricity (e)
2. semi-major axis (a)
3. inclination (i)
4. argument of periapsis (ω)
5. longitude of ascending node (Ω)
6. true anomaly at some epoch

2.1.1 Defining the Ellipse

One of the many definitions of an ellipse is the following: Given two points A and B, and a constant C whose value is greater than the distance between A and B. Then, the locus of all the points such that the sum of distances from A and B is C defines an ellipse. The two points A and B are called the focii of the ellipse; if they are degenerate, then the ellipse reduces to a circle. The trajectory of a bound body under gravitational force takes the form of an ellipse or a circle, with the 'source' of the force at one of the focii of the ellipse. For a binary system, the the centre of mass (or the barycentre) of the system serves as the focus for the trajectory of both the components.

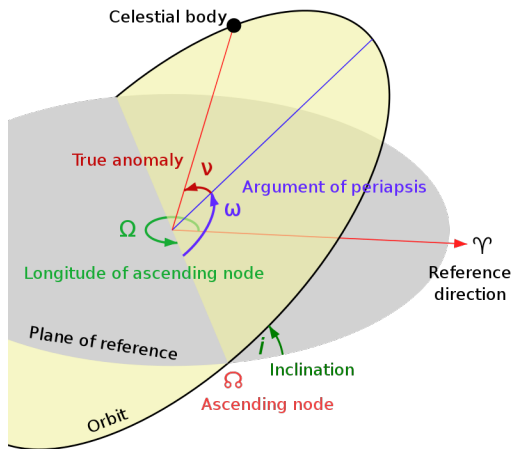


Figure 2.1: Orbital Parameters: Center is primary, these uniquely determine the orientation of an orbit with respect to an observer

2.1.2 Orbital Parameters

The first two parameters (eccentricity and semi-major axis) describe the shape of the ellipse. The eccentricity is a measure of the ‘skewness’ of the ellipse, with an eccentricity of 0 giving a circle. The eccentricity can be defined as the ratio of the distance between the two focii, and that between the two farthest points on the ellipse. The semi-major axis is the length of the line joining the centre of the ellipse and the farthest point on the ellipse from the centre.

The next 3 parameters determine the orientation of the ellipse in space. To describe this orientation, we first define a reference coordinate system. Figure 2.1 marks a plane of reference in grey. Observations from Earth for distant objects usually define this as the plane perpendicular to the line of sight to the binary system. For such observation, it is possible only to observe the relative motion of the two bodies (choosing one body as the ‘stationary’ primary and the other as the revolving ‘secondary’). The relative path of the secondary is also an ellipse (Refer Appendix A) and from now, we shall assume that the ellipse in Figure 2.1 is this ellipse, and the primary is at a focus. We also need to define a reference direction to completely specify the coordinate system (assuming right-handedness). This can be the direction from the binary system (or more accurately, the primary) to the North Celestial Pole or to the Vernal Equinox. Now, we are in a position to define the orientation of the ellipse.

The inclination is the angle between the plane of the ellipse and the plane of reference (this is the same as the angle between the angular momentum of the binary system and the line of sight). $i = 90^\circ$ gives an edge-on ellipse and $i = 0^\circ$ gives a face-on ellipse.

When the inclination is not 0° , then there will be two points where the plane of reference intersects the ellipse. The point where the secondary moves above the reference plane is called the ascending node (the other one is the descending node). The angle between the reference direction and the ascending node as seen from the primary is called the longitude of ascending node (Ω). By convention, the angle is measured in an anticlockwise sense.

The third parameter that defines the orientation is the argument of periapsis (ω). This is defined as the angle on the plane of ellipse from the ascending node to the periapsis of the elliptical orbit as seen from the primary. Note that although ω and Ω are both measured with respect to the primary, they are on different planes. The last orbital

parameter simply defines the position of the secondary on the, now uniquely described, elliptical orbit. The true anomaly is the angle between the secondary and the periapsis as seen from the primary. Defining this at some epoch (time of measurement) now defines completely the trajectory of the secondary with respect to the primary.

2.1.3 Anomalies

Just as we defined the true anomaly in Section 2.1.2, we can define two more angles which will be convenient later. These are the eccentric anomaly E and the mean anomaly M (see Figure 2.2 and Figure 2.3 respectively).

Eccentric anomaly (E): Consider a circle with the same centre as the ellipse and radius equal to the semi-major axis, in the plane of the ellipse. This circle is called the auxiliary circle of the ellipse. We drop a perpendicular from the secondary to the semi major axis. Extending this line in the direction of the secondary, we intersect the auxilliary circle at a point (P'). The angle made by the line joining the centre of the ellipse and P' with the semi-major axis is called the eccentric anomaly of the secondary.

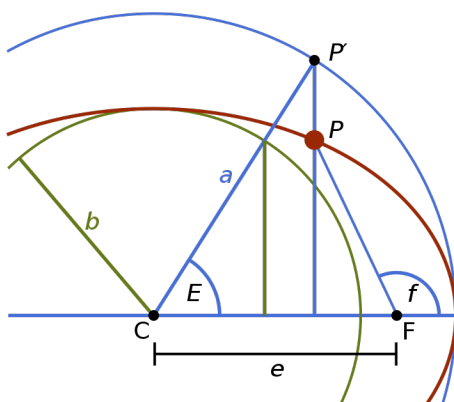


Figure 2.2: Eccentric anomaly: As the secondary moves along the ellipse, the eccentric anomaly also changes accordingly. The auxiliary circle is the blue outer circle, C denotes the centre of the ellipse, F the focus (or the position of the secondary), P the position of the primary. f here is the true anomaly.

Mean anomaly (M): Mean anomaly is equivalent to time. It is the angle made by an imaginary body moving in a circular orbit around the primary with the same period as the secondary, both of which start from the periapsis.

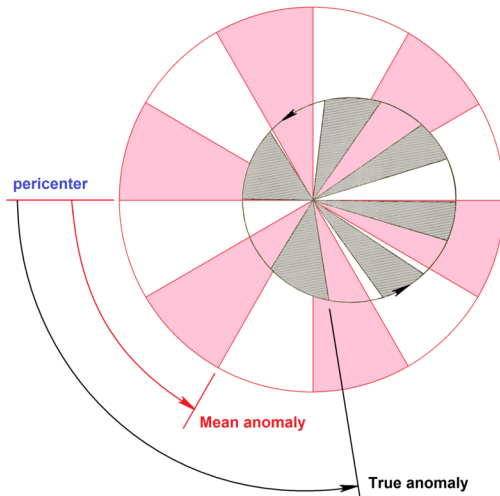


Figure 2.3: Mean Anomaly: The pink arc is the trajectory of the imaginary object, the grey is the actual orbit of the secondary. The grey and pink triangles are the areas swept at a specific time interval. Both sweep out equal areas in equal times, but the angular rate of sweep varies for the elliptical orbit and is constant for the circular orbit.

Find actual credits and put them in the captions. Image credits : Wikipedia and then remove this

2.2 Transformations

Consider the coordinate system defined in Section 2.1.2. We define this system in cartesian coordinates (X, Y, Z), by assigning the Z axis to the line of sight vector (perpendicular to the reference plane) and X axis to the reference direction (compare Figures 2.1 and 2.4).

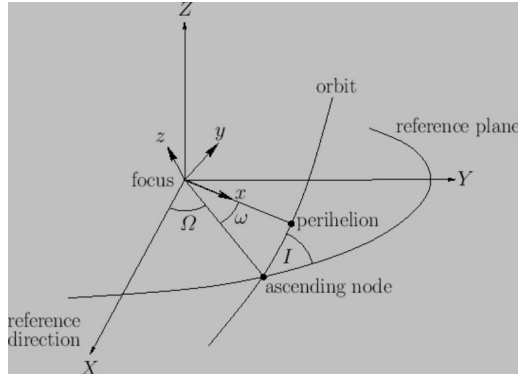


Figure 2.4: A figure depicting a general orbit. Here, you can see all the orbital parameters as seen from the reference direction, with the focus as the origin. Credits: Fitzpatrick, Richard (2016, Figure 4.6)

Let us define a second Cartesian coordinate system (x, y, z) , also centered on the primary. The xy plane coincides with the plane of the orbit, the x axis points towards the orbit's periapsis. We can transform from the (x, y, z) system to the (X, Y, Z) system via a series of three rotations of the coordinate system: first, a rotation through an angle ω about the z -axis; second, a rotation through an angle i about the new x -axis; and finally, a rotation through an angle Ω about the new z -axis. This can be represented in matrix form¹ as

$$\begin{pmatrix} X \\ Y \\ Z \end{pmatrix} = \begin{pmatrix} \cos \Omega & -\sin \Omega & 0 \\ \sin \Omega & \cos \Omega & 0 \\ 0 & 0 & 1 \end{pmatrix} \begin{pmatrix} 1 & 0 & 0 \\ 0 & \cos i & -\sin i \\ 0 & \sin i & \cos i \end{pmatrix} \begin{pmatrix} \cos \omega & -\sin \omega & 0 \\ \sin \omega & \cos \omega & 0 \\ 0 & 0 & 1 \end{pmatrix} \begin{pmatrix} x \\ y \\ z \end{pmatrix} \quad (2.1)$$

We can represent any curve in the x - y plane by its polar coordinates (r, θ) such that $x = r \cos \theta$ and $y = r \sin \theta$ and $z = 0$. In the (X, Y, Z) coordinate system this is

$$X = r [\cos \Omega \cos (\omega + \theta) - \sin \Omega \sin (\omega + \theta) \cos I] \quad (2.2)$$

$$Y = r [\sin \Omega \cos (\omega + \theta) - \cos \Omega \sin (\omega + \theta) \cos I] \quad (2.3)$$

$$Z = r \sin (\omega + \theta) \sin I \quad (2.4)$$

In, polar coordinates, the equation of the elliptical orbit is given by

$$r = \frac{h^2/k}{(1 + e \cos(\theta - \theta_0))} \quad (2.5)$$

This is derived in Appendix A (Equation A.16). Then Equations (2.2 - 2.4) can be used to find the cartesian coordinates of the secondary for various values of θ ($\theta = 0$ corresponds to the periapsis). Figures 2.5 and 2.6 reconstruct these orbits using parameters of two binary systems. Figure 2.5 shows the plot of the apparent orbit of a system with $i = 90^\circ$ which corresponds to an edge-on orbit. We therefore see a straight line which can be

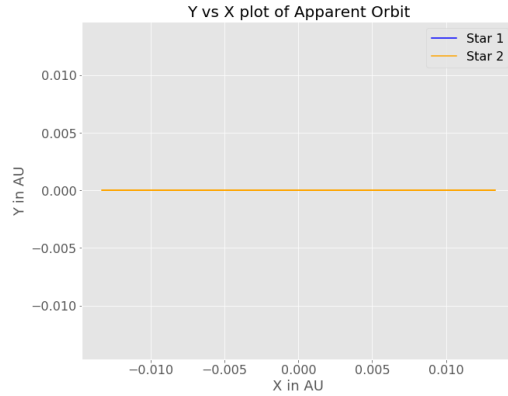


Figure 2.5: X-Y plot: Apparent orbit of binary system RS Ind as seen on the plane of sky, which has an inclination of 90°

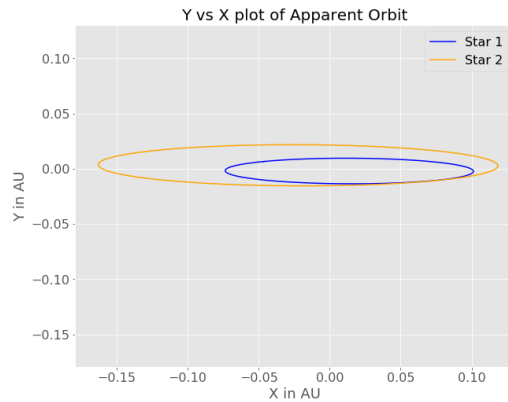


Figure 2.6: X-Y plot: Apparent orbit of binary system V380 Cyg as seen on the plane of sky, which has an inclination of 82.4°

verified by putting $i = 90^\circ$ in Equations (2.2 - 2.3) Figure 2.6 shows the X – Y plot of the apparent orbit. The system has an inclination of 82.4° which is why it has been flattened along the Y axis.

We shall now consider the special case where the two bodies are stars, and discuss the different observables for the various types of binary star systems.

¹this transformation is the same as Euler Rotations



3. Binary Star Systems

3.1 Eclipsing Binaries

If the plane of a binary system lies almost or precisely edge-on with respect to the observer ($i \approx 90^\circ$), the components are observed to eclipse each other periodically. Photometry of such sources give light curves that show periodic dips in brightness. The size of the dip depends on their radii, effective temperatures, the proportion of the occulted star **what does this mean?** and the relative brightness of the stars. The deeper eclipse (when the dimmer star occults the brighter one) is said to be '**primary**' eclipse and the shallower eclipse (when the dimmer star is occulted by the brighter one) is the '**secondary**' eclipse. If these binaries are also spectroscopic (Section 3.2), then their orbital elements and their masses can also be inferred. **More details! Give info about how they are useful for distance measurements.** maybe rephrase. just giving examples sounds a bit weird here **HIP 59683, SV Cam, Algol** are some examples of eclipsing binaries.

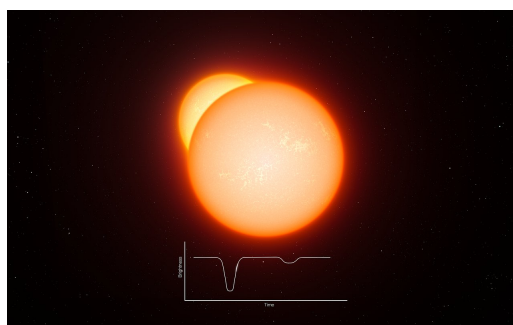


Figure 3.1: Artistic Impression of Eclipsing Binaries, Credits: Calçada, 6 March 2013

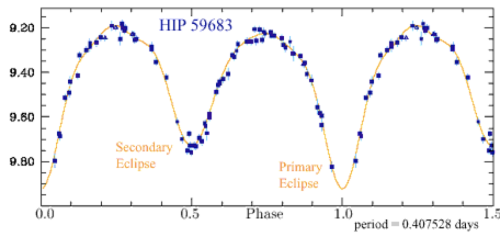


Figure 3.2: Light Curve of HIP 59683, an eclipsing binary. Credits: atnf.csiro.au

3.2 Spectroscopic Binaries

Most binary stars are too distant to be resolved even with a large telescope. These binary systems have been detected by Doppler shifts in their spectral lines and are known as Spectroscopic Binaries. As the two stars orbit around each other (about their common centre of mass) the radial components of their velocities with respect to the observer periodically changes. This results in a periodic change in the measured wavelengths of the spectra of the two components. The shift in wavelength is also dependent on the inclination of the binary system; face-on binaries will not show such a shift in the spectra.

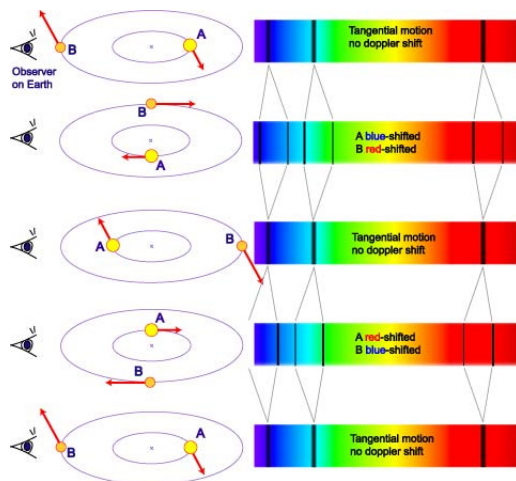


Figure 3.3: A Spectroscopic Binary system in which a high-mass star A and low-mass B orbit around a common centre of mass. The observed combined spectrum shows periodic splitting and shifting of spectral lines. The amount of shift is a function of the alignment of the system to us and the orbital speed of the stars. Credits: Australia Telescope National Facility

The radial velocity curve (radial velocity vs time) can be used to determine orbital parameters including period, eccentricity and argument of periastron. [ref section here](#).

In some spectroscopic binaries, spectral lines from both stars can be observed and they are known as double-lined spectroscopic binary (Denoted as "SB2"). If only one set of lines is present they are called single-lined spectroscopic binary (Denoted as "SB1"). The mass ratios can be found for the SB2 binaries but only the mass function can be derived if one spectrum alone is observed. [ref the section here](#)

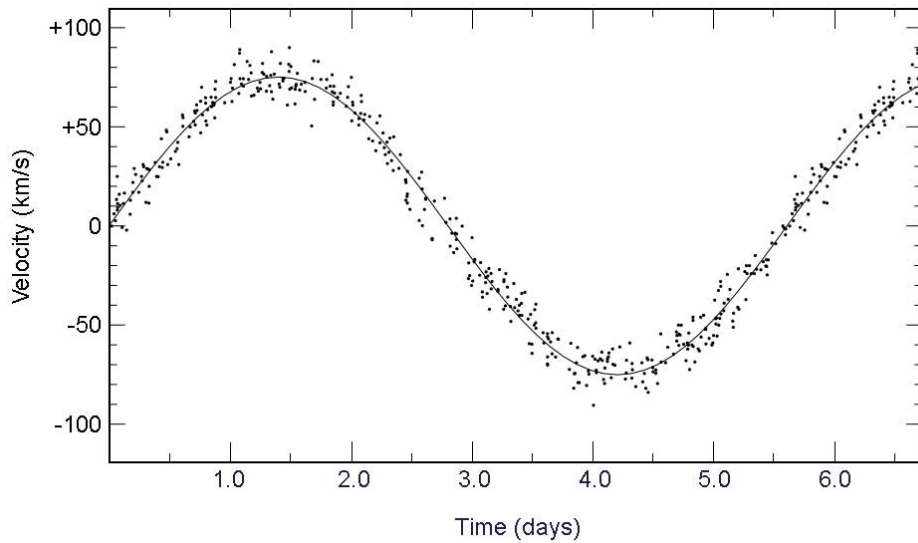


Figure 3.4: A radial velocity curve of accumulated data, obtained through redshift measurements after corrections, represented as points on the graph, compared with theoretical curve, denoted by the solid line, Credits: ([Brocksopp et al., 1999](#))

3.3 Astrometric Binaries

Astrometric binaries are relatively nearby stars which can be seen to wobble around a point in space, with no visible companion. The most famous example of an astrometric binary system is Sirius.

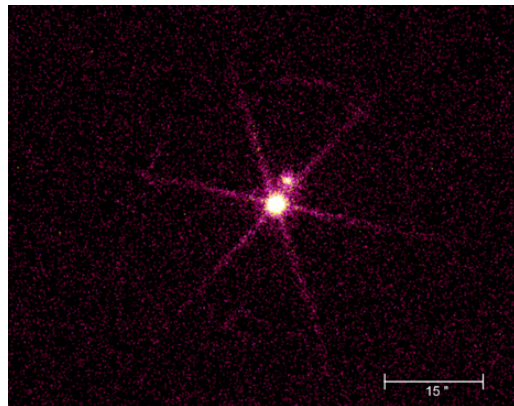


Figure 3.5: Chandra X-ray Image of the Sirius system. Credit: [NASA/CXC/SAO, 2000](#)

Sirius A (also known as the ‘Dog star’) is the brightest star in the night sky and it was in 1844 that Friedrich Bessel pointed out that it had a wobble in its proper motion [[citation needed](#)]. Its dim companion Sirius B (affectionately known as the ‘Pup’) was only seen telescopically by Alvan Clark in 1862 and is now known to be a dim white dwarf. [[citation needed](#)].

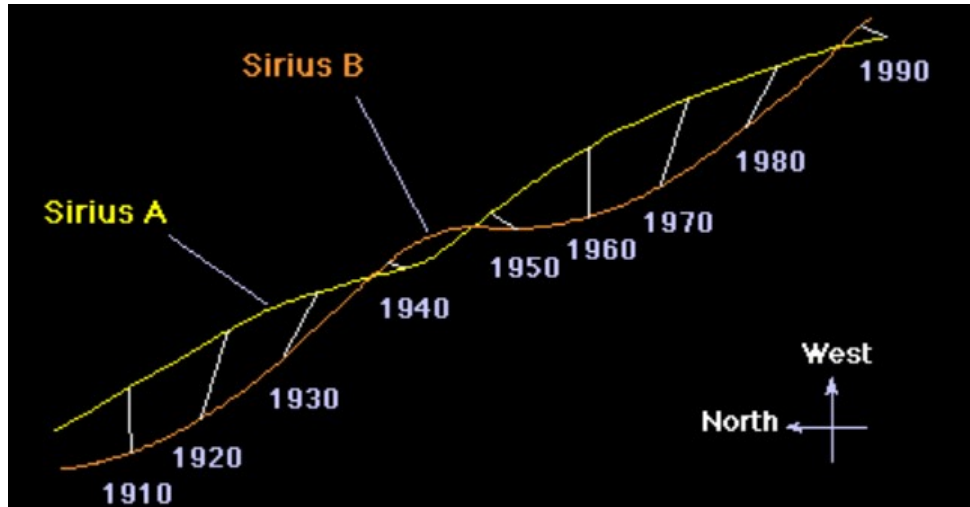


Figure 3.6: This diagram shows the proper motion, the motion with respect to the background of stationary stars as seen from Earth, of the Sirius system over 80 years. Credit: Courtesy of Mike Guidry, University of Tennessee.

Presently, interferometric analysis can be used to apprehend compact binary systems that require the use of high-resolution techniques to study them. For more details on interferometric analysis of binaries, refer to Boffin (2016) [Hmm, thinking of maybe cutting this out. seems out of nowhere in a new para.](#)

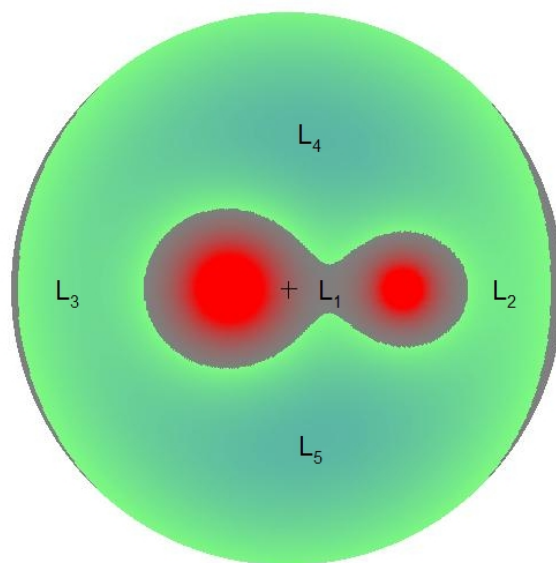
3.4 Types of Binaries

[Hmm, Binary classification based on ...? instead. Not edited yet. go through.](#)

- **Detached Binaries:** The most commonly observed binary systems^[citation needed], in which the stars maintain a distance large enough to prevent any material from entering into the Roche Lobe (check Semi-detached binaries) of the other star. All sections in this report regarding observations have been of the detached systems type.
- **Semi-detached Binaries:** Here, first we'll get introduced to the concept of a Roche Lobe. In a two body system, there is a region of space around each body within which orbiting material is gravitationally bound to that particular body. Which essentially means that the surface of the Roche Lobe is the smallest equipotential that can exist around the bodies.

Here is where the difference between a star and a planet comes into importance. Stars essentially consist of fluids, i.e., gas and plasma, which, on entering the Roche Lobe of the other star, would lead to a mass transfer taking place, which is called Roche Lobe Overflow. In the case of semi-detached binaries, only one out of the two stars has its material extending into the Roche Lobe of the other, thus leading to a mass transfer of the former to the latter. This leads to formation of an accretion disc and may subsequently evolve into a contact binary system ([give ref](#) theory of stability and evolution is discussed in the chapter titled 'Complex Systems').

- **Contact Binaries:** The situation when both the stars have material extending into the other's Roche Lobes, thus forming a common envelope of material, is called a Contact Binary system. Contact binaries may form due to evolution of a detached/semi-detached system through means such as stellar wind and magnetic braking, or may form when the protostar undergoes fission in the early stages (more details of this in



Above: A plot of the Roche potential for a mass ratio (M_2/M_1 with $M_2 = 2 \times M_1$). The cross indicates the centre-of-mass of the system and L_1 to L_5 are the Lagrange points.

Figure 3.7: Potential contours depicting Roche Lobe and Lagrangian points

the Complex Systems chapter).

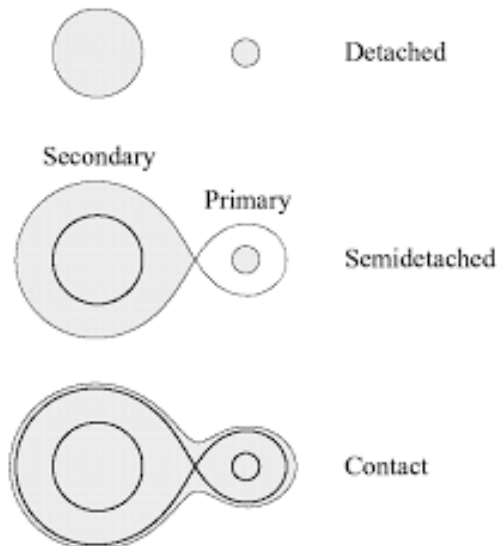
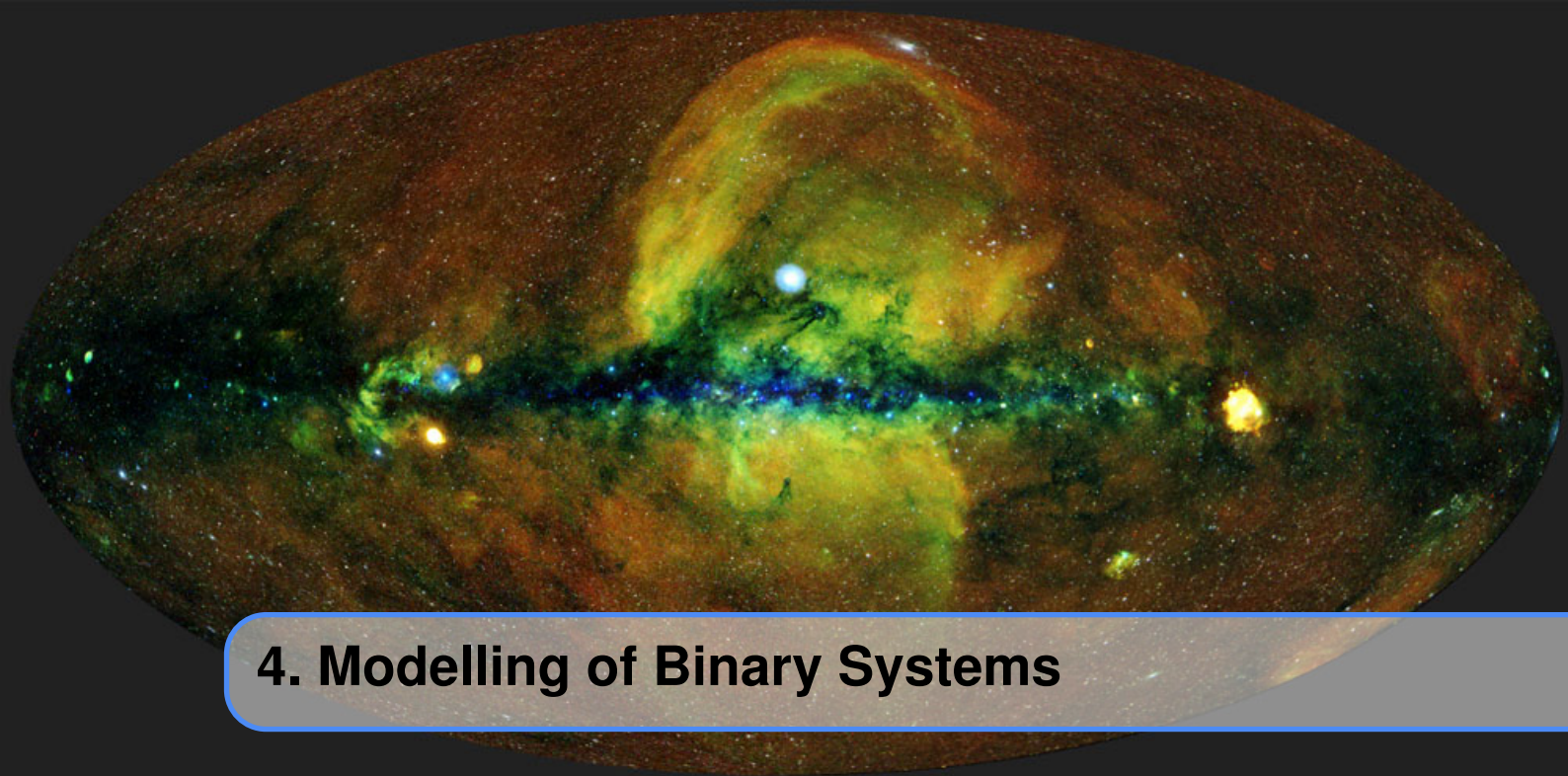


Figure 3.8: Types of binaries highlighted with the use of Roche Lobes, the shaded portion represents presence of matter



4. Modelling of Binary Systems

put in stuff here. In this chapter we will do this this this.

4.1 Radial velocities

put in stuff here. In this section we will do this this this.

4.1.1 Edge-on circular orbits

The simplest case of motion of binary stars comprises circular orbital motion. The two stars orbit their barycentre (centre of mass, CoM) in concentric circular paths, at the opposite ends of their CoM. In edge-on orbits, the plane of motion is parallel to the line of sight ($i = 90^\circ$).

Method

Different name? Derivation maybe? Let there be light. Let there be less 'Let's' Let the masses of the stars be m_1 and m_2 . Let their total mass be $M = m_1 + m_2$. Let the distance between them be d . Let their time period of revolution be P and angular velocity be ω . Now, let r_1 and r_2 be orbital radii of star 1 and star 2 respectively. We know that, ok F. you dont define align like this. Also make the equations more compact, probably 2 in a line

$$m_1 r_1 = m_2 r_2 \quad (4.1)$$

$$r_1 = \frac{m_2}{M} d \quad (4.2)$$

$$r_2 = \frac{m_1}{M} d \quad (4.3)$$

$$\omega = \frac{2\pi}{P} \quad (4.4)$$

From Kepler's third law,

$$d^3 = \frac{GM P^2}{4\pi^2} \quad (4.5)$$

Let θ be the angle formed by the line-of-sight (LOS) and the line joining the barycentre to the star. Let the time of epoch be $t = T$. Hence,

$$\theta = \omega(t - T) \quad (4.6)$$

The LOS velocities observed will be the projection of the star's velocity (entirely tangential). The second star has angular position shifted by 180° , in comparison to that of star 1. Further, let the CoM velocity be V_γ .

Hence, using Equations 4.2, 4.3, 4.4, 4.5 and 4.6, you used split here but not above. confused noises.

$$\begin{aligned} v_{1,\text{LOS}} &= V_\gamma + \omega r_1 \sin(\theta) \\ &= V_\gamma + \left(\frac{2\pi G}{PM^2} \right)^{\frac{1}{3}} m_2 \sin \left(\frac{2\pi}{P}(t - T) \right) \end{aligned} \quad (4.7)$$

$$\begin{aligned} v_{2,\text{LOS}} &= V_\gamma + \omega r_2 \sin(\theta + \pi) \\ &= V_\gamma - \left(\frac{2\pi G}{PM^2} \right)^{\frac{1}{3}} m_1 \sin \left(\frac{2\pi}{P}(t - T) \right) \end{aligned} \quad (4.8)$$

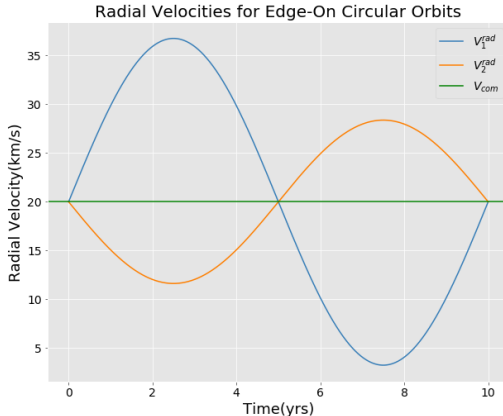


Figure 4.1: Radial velocity curve with the following parameters: Masses- $M_1 = 2M_\odot$, $M_2 = 4M_\odot$, Time period- $T = 10$ yrs, Velocity- $V_\gamma = 20$ km/s, Inclination- $i = 90^\circ$.

4.1.2 Non-edge-on circular orbits

General circular orbits? Consider circular orbits of stars in planes that are inclined at an angle that is not 90° . In this case, the LOS velocity is simply the projection of the velocities of the edge on orbits onto the plane parallel to the LOS.

$$v_{1,\text{LOS}} = V_\gamma + \sin(i) \left(\frac{2\pi G}{PM^2} \right)^{\frac{1}{3}} m_2 \sin \left(\frac{2\pi}{P}(t - T) \right) \quad (4.9)$$

$$v_{2,\text{LOS}} = V_\gamma - \sin(i) \left(\frac{2\pi G}{PM^2} \right)^{\frac{1}{3}} m_1 \sin \left(\frac{2\pi}{P}(t - T) \right) \quad (4.10)$$

Note that, on substituting $i = 90^\circ$ in the above equations, we obtain the expressions in Section 4.1.1. **RV1 AND RV3 IMAGES ARE THE SAME! GET THE CORRECT ONE FROM WHOEVER MADE THIS SECTION! IMP**

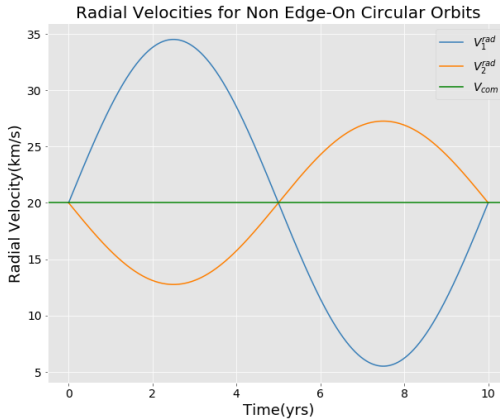


Figure 4.2: Radial Velocity curve with the following parameters: Masses- $M_1 = 2M_\odot$, $M_2 = 4M_\odot$, Time period- $T = 10$ yrs, Velocity- $V_\gamma = 20$ km/s, Inclination- $i = 60^\circ$

4.1.3 Elliptical orbits in COM frame

Consider the stars to have a non-zero eccentricity of their orbital paths. Their orbits would be elliptical ($0 < e < 1$). Let them be edge-on. They will have the same eccentricity, angular velocity and will share a focus, which is their barycentre.

Method

The input parameters to the simulation were the masses of the stars m_1 and m_2 in solar masses, the sum of their semi-major axes / semi-major axis of their relative orbit a in AU and the eccentricity e of the orbits. Let the total mass be M ; let a_1 and a_2 be the semi-major axes of orbits of star 1 and 2 respectively. Let P be the time period of the stars. Let T be the time of periastron epoch. **look at the 'let's again**

Using Kepler's Second Law,

$$r^2\dot{\theta} = \text{constant} = \frac{2\pi a^2 \sqrt{1 - e^2}}{P} \quad (4.11)$$

For an ellipse, in COM frame (COM at rest), where origin lies at the common focus i.e the barycentre, taking positive x axis going from barycentre to the second focus of m_1 (Note, θ is the true anomaly of star 1), **the spacing of the equations seems a bit too much, plus its different from previous equations, non uniformity does'nt look good**

$$\hat{r} = \cos \theta \hat{i} + \sin \theta \hat{j} \quad (4.12)$$

$$\mathbf{r}_1 = \frac{a_1(1 - e^2)}{(1 + e \cos \theta)} \hat{r} \quad (4.13)$$

$$\mathbf{r}_2 = -\frac{a_2(1 - e^2)}{(1 + e \cos \theta)} \hat{r} \quad (4.14)$$

Differentiating the two wrt time,

$$\frac{d\mathbf{r}_1}{dt} = -\frac{a_1 e \sin \theta (1 - e^2)}{(1 + e \cos \theta)^2} \dot{\theta} \hat{\mathbf{r}} \quad (4.15)$$

$$\frac{d\mathbf{r}_2}{dt} = \frac{a_2 e \sin \theta (1 - e^2)}{(1 + e \cos \theta)^2} \dot{\theta} \hat{\mathbf{r}} \quad (4.16)$$

$$\mathbf{v}_1 = \dot{r}_1 \hat{\mathbf{r}} + r_1 \dot{\theta} \hat{\theta} \quad (4.17)$$

$$\begin{aligned} v_1^2 &= \dot{r}_1^2 + r_1^2 \dot{\theta}^2 \\ &= (1 + e^2 + 2e \cos \theta) \frac{4\pi^2 a_1^2}{P^2 (1 - e^2)} \end{aligned} \quad (4.18)$$

Since this is the COM frame,

$$\mathbf{v}_2 = \frac{-m_1}{m_2} \mathbf{v}_1 \quad (4.19)$$

Also,

$$\frac{m_1}{m_2} = \frac{a_2}{a_1} \quad (4.20)$$

Hence, from Equations 4.18, 4.19 and 4.20,

$$v_2^2 = (1 + e^2 + 2e \cos \theta) \frac{4\pi^2 a_2^2}{P^2 (1 - e^2)} \quad (4.21)$$

Using $a = a_1 + a_2$ and from Kepler's third law,

$$P^2 = \frac{4\pi^2 a^3}{GM} \quad (4.22)$$

Hence,

$$v_1 = m_2 \sqrt{\frac{G(1 + e^2 + 2e \cos \theta)}{(1 - e^2)Ma}} \quad (4.23)$$

And,

$$v_2 = m_1 \sqrt{\frac{G(1 + e^2 + 2e \cos \theta)}{(1 - e^2)Ma}} \quad (4.24)$$

From Equations 4.11 and 4.13,

$$\int_0^\theta \frac{d\theta}{(1 + e \cos \theta)^2} = \int_T^t \frac{2\pi dt}{T(1 - e^2)^{\frac{3}{2}}} \quad (4.25)$$

This equation, after feeding to an online integral calculator, yielded,

$$\frac{e \sin \theta}{(1 - e^2)(e \cos \theta + 1)} - \frac{2 \arctan\left(\frac{(1-e)\tan(\frac{\theta}{2})}{\sqrt{1-e^2}}\right)}{(1 - e^2)^{\frac{3}{2}}} = \frac{2\pi(t - T)}{P(1 - e^2)^{\frac{3}{2}}} \quad (4.26)$$

Let E be the **eccentric anomaly**.

We get,

$$\cos E = \frac{\cos \theta + e}{1 + e \cos \theta} \quad (4.27)$$

$$\sin E = \frac{\sqrt{1 - e^2} \sin \theta}{1 + e \cos \theta} \quad (4.28)$$

$$\tan\left(\frac{E}{2}\right) = \sqrt{\frac{1-e}{1+e}} \tan\left(\frac{\theta}{2}\right) \quad (4.29)$$

Simplifying Equation 4.26 using the equations above, we get,

$$\mathcal{M} = E - e \sin E = \frac{2\pi(t - T)}{P} \quad (4.30)$$

where, \mathcal{M} is defined as the **mean anomaly**.

Thus, the velocities of the stars in the barycentre frame can be implicitly expressed using Equations 4.23, 4.24 and 4.26.

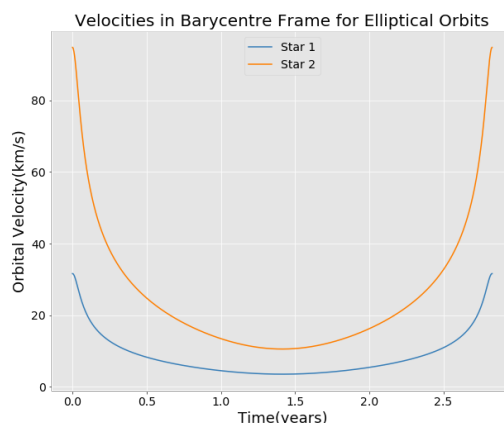


Figure 4.3: Velocities in the Barycenter (center of mass) reference frame, with the following parameters: Masses- $M_1 = 6M_{\odot}$, $M_2 = 2M_{\odot}$, Eccentricity- $e = 0.8$, Semi-major axis- $a = 4AU$, Time period- $T = 10yrs$

4.1.4 Adding The Orbital Parameters

The orbital parameters have already been discussed earlier. There are six of them - i) inclination(ii) ii) The argument of periapsis (ω) iii) The eccentricity of orbit (e) iv) the semimajor axis (a) v) Longitude of ascending node (Ω) and the vi) True anomaly at the epoch.

Circular orbits

For the circular orbits, $e = 0$. As this makes the orbit symmetrical with respect to the barycentre (the centre of revolution), the parameters Ω, ω are of no use (all values of them mean the same). The semi-major axis becomes the radius. The only two parameters that remain are i and the epoch position. The use of these parameters has been discussed in Section 4.1.2.

Elliptical orbits

Firstly, it is easy to see that the parameter Ω has no effect in the LOS velocity. This is because Ω is defined as the angle between periapsis (periastron) and the reference direction in a reference plane. The reference plane is perpendicular to the LOS and the angle is measured in this plane. Thus, this does not have any effect on the LOS direction which is perpendicular to the plane.

For ease of discussion we will take the epoch position as corresponding to a true anomaly of 0° . Also, we will work from the perspective of one of the stars in the binary. From this star, the other star is seen as an ellipse. The eccentricity remains the same as the eccentricity of the individual orbits, the semi-major axis becomes the sum of the semi-major axes of the orbits of both the stars. We will refer to the relative elliptical orbit (secondary with respect to primary).

Now first let $i = 90^\circ$. In such case, the angle between the periapsis and the LOS is $(\omega - \frac{\pi}{2})$. Thus, at time when the true anomaly of the star in orbit is θ , the angle with respect to the LOS is $(\theta + \omega - \frac{\pi}{2})$.

A simple diagram will show that if at that time, the velocity of the star is decomposed to v_r and v_θ (the radial and angular velocity respectively) with respect to the focus of the ellipse,

$$\begin{aligned} v_{\text{rel,LOS}} &= v_r \cos \left(\theta + \omega - \frac{\pi}{2} \right) - v_\theta \sin \left(\theta + \omega - \frac{\pi}{2} \right) \\ &= v_r \sin(\theta + \omega) + v_\theta \cos(\theta + \omega) \end{aligned} \quad (4.31)$$

where r is given by,

$$r = \frac{a(1-e^2)}{(1+e \cos \theta)} \quad (4.32)$$

We separate the components of velocity along r and θ by writing them as

$$\begin{aligned} v_r &= \dot{r} \\ &= \frac{a(1-e^2)}{(1+e \cos \theta)^2} e \sin \theta \dot{\theta} \end{aligned} \quad (4.33)$$

$$\begin{aligned} v_\theta &= r \dot{\theta} \\ &= \frac{a(1-e^2)}{(1+e \cos \theta)} \dot{\theta} \end{aligned} \quad (4.34)$$

Using simple trigonometric manipulation, the radial velocity comes out in another form given by,

$$v_{\text{rel,LOS}} = K' [\cos(\theta + \omega) + e \cos \omega] \quad (4.35)$$

where $K' = \frac{2\pi a}{P\sqrt{1-e^2}}$.

Now coming to the general case, where $i \neq 90^\circ$, there is an additional factor of $\sin(i)$. Thus, the final form becomes,

$$v_{\text{rel,LOS}} = K [\cos(\theta + \omega) + e \cos \omega] \quad (4.36)$$

where $K = \frac{2\pi a \sin(i)}{P\sqrt{1-e^2}}$. Why is there a sudden change in size? Check and change

Alternately, using Equation 2.4 in Section 2.2, we can differentiate the Z-coordinate of the star in the relative orbit wrt time t. This Z-component of v_{rel} is the LOS velocity.

$$\begin{aligned} v_{\text{rel,LOS}} &= \dot{z} \\ &= \dot{r} \sin(\omega + \theta) \sin(i) + r \dot{\theta} \cos(\omega + \theta) \sin(i) \\ &= v_r \sin(\theta + \omega) + v_\theta \cos(\theta + \omega) \end{aligned} \quad (4.37)$$

which yields the same equations. Thus, the final LOS velocity in the Earth's frame is,

$$v_{\text{LOS}} = V_Y + K [\cos(\theta + \omega) + e \cos \omega] \quad (4.38)$$

4.1.5 Interactive Plot

Based on Equation 4.38, interactive plot has been made which is used to visualise the Radial Velocity curve of the SB2 system. Variable parameters includes e & ω . Although, eccentricity of the orbit is still given as a parameter of the function to plot the curve.

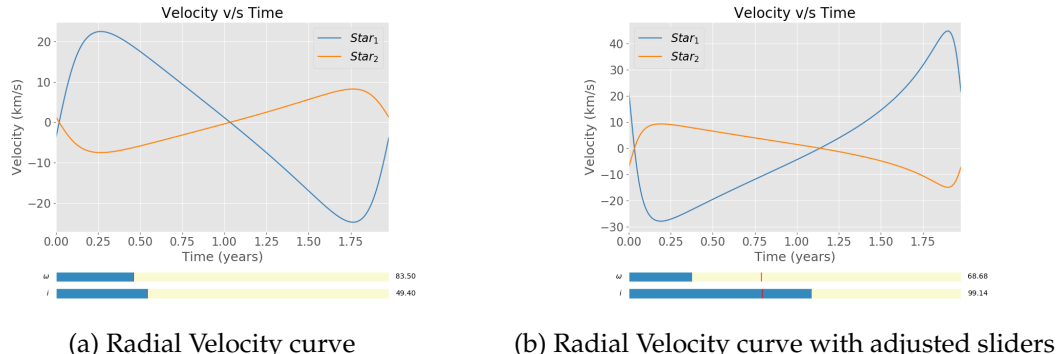


Figure 4.4: Parameters for the above figures: Masses- $M_1 = 1M_\odot$, $M_2 = 3M_\odot$, Semi-major axis- $a = 2.5\text{AU}$, Eccentricity- $e = 0.64$

In Figure 4.4a, the slider value of e & ω has been kept constant as given in the parameter of the function. Where as, in Figure 4.4b the values of e & ω has been adjusted and corresponding to that, the shape of the curve changes. what exactly does slider mean?

4.2 Light Curves

Binary Star Systems which orbit in a plane close to our line of sight will periodically eclipse each other from our point of view. We can detect these eclipses by measuring the total flux received from the system. In a single orbital period, there are two dips seen in the light curves which correspond to the primary and secondary eclipses. Whenever one star passes in front of the other, it blocks a certain fraction of the light coming from the star that is being eclipsed. The dips in the light curves depend on the inclination of the system as well as their fractional radii.

To a first approximation, the stars can be modelled as surfaces at some temperature T emitting black-body radiation. Departures from an ideal black-body will be studied in the next section. For this simple model, we take two stars with radii R_1 and R_2 having a surface temperature of T_1 and T_2 having a constant surface intensity of

$$I_1 = \sigma T_1^4 \quad (4.39)$$

$$I_2 = \sigma T_2^4 \quad (4.40)$$

where σ is the Stefan-Boltzmann Constant. Consequently, the luminosity of the stars is simply the total radiation emitted and is given by

$$\mathcal{L}_1 = I_1 4\pi R_1^2 \quad (4.41)$$

$$\mathcal{L}_2 = I_2 4\pi R_2^2 \quad (4.42)$$

The flux received by the observer can be written in the general form as

$$\mathcal{F} = C \left(\mathcal{L}_1 (1 - f_1) + \mathcal{L}_2 (1 - f_2) \right) \quad (4.43)$$

where C is a constant factor which accounts for the distance to the system and other parameters. f_1, f_2 refer to the fraction of the stellar disks that are eclipsed at any given moment. These can be computed by considering simple geometric arguments to the intersection of the two stellar disks of given radii and the distance between their centres. Maximum flux is received when the stars do not eclipse each other and can be written as

$$\mathcal{F}_{\max} = C (\mathcal{L}_1 + \mathcal{L}_2) \quad (4.44)$$

Now we can compute the relative Flux F/F_{\max} which is given by

$$\mathcal{F}_{\text{rel}} = \frac{\mathcal{L}_1 (1 - f_1) + \mathcal{L}_2 (1 - f_2)}{\mathcal{L}_1 + \mathcal{L}_2} \quad (4.45)$$

4.2.1 Limb Darkening

Limb darkening is a an optical effect seen in stars, where the centre of the star appears to be brighter than the edge, or limb.

The loss of light $\Delta\mathcal{L}$ suffered at any phase of the eclipse can be expressed as

$$\Delta\mathcal{L} = \int_s J \cos \gamma \, d\sigma \quad (4.46)$$

where J represents the distribution of brightness over the apparent disc of the star undergoing eclipse, of surface element $d\sigma$; and γ , the angle of foreshortening (where $\gamma \leq 90^\circ$); while the range s of integration is to be extended over the entire eclipsed area.

The distribution of brightness J , for spherical stars is approximated to (Kopal, 1979)

$$J = H (1 - u_1 - u_2 - \dots - u_\Lambda + u_1 \cos \gamma + u_2 \cos^2 \gamma + \dots + u_\Lambda \cos^\Lambda \gamma) \quad (4.47)$$

where H stands for the intensity of radiation emerging normally to the surface, and the u_j 's are the 'coefficients of limb-darkening' of j -th degree ($j = 1, 2, 3, \dots, \Lambda$).

The fractional loss of light during the eclipse of a star whose surface brightness falls off from centre to limb in accordance with a law of Λ -th degree of the form (4.47) is given by

$$f = \frac{\int J \cos \gamma d\sigma}{\int J \cos \gamma d\sigma} \quad (4.48)$$

where s is the eclipsed area and S denotes the total area of the hemisphere of star that is directed towards us. Evaluating the integral we find that

$$f = \sum_{l=0}^{\Lambda} C^{(l)} \alpha_l^0 \quad (4.49)$$

where,

$$C^{(0)} = \frac{1 - u_1 - u_2 - \dots - u_{\Lambda}}{1 - \sum_{l=1}^{\Lambda} \frac{l u_l}{l+2}} \quad (4.50)$$

while for $l > 0$,

$$C^{(l)} = \frac{u_l}{1 - \sum_{l=1}^{\Lambda} \frac{l u_l}{l+2}} \quad (4.51)$$

and α_l^0 are the integrated alpha functions computed by Kopal (1979)

The total luminosities L_1 and L_2 , of each star, limb-darkened in accordance with Equation (4.47) can then be given by

$$L_1 = \mathcal{L}_1(1 - f_1) \quad (4.52)$$

$$L_2 = \mathcal{L}_2(1 - f_2) \quad (4.53)$$

where f_1 and f_2 are fractional losses of light for the primary and secondary respectively, given by Equation (4.48) - (4.49)

Therefore flux can be calculated as per Equations (4.43) - (4.45)

Limb Darkening can be incorporated by using various laws which have surfaced in the last few decades by Kopal (1979), Schwarzschild (1906). Some of these laws are,

$I(\mu) = I_0$	(uniform)
$I(\mu) = I_0[1 - c_1(1 - \mu)]$	(linear)
$I(\mu) = I_0[1 - c_1(1 - \mu) - c_2(1 - \mu)^2]$	(quadratic)
$I(\mu) = I_0[1 - c_1(1 - \mu) - c_2(1 - \sqrt{\mu})]$	(square-root)
$I(\mu) = I_0[1 - c_1(1 - \mu) - c_2 \mu \ln \mu]$	(logarithmic)
$I(\mu) = I_0[1 - c_1(1 - \mu_2^{\xi})]$	(power2)
$I(\mu) = I_0[1 - c_1(1 - \mu^{1/2}) - c_2(1 - \mu) - c_3(1 - \mu^{3/2}) - c_4(1 - \mu^2)]$	(nonlinear)

where, $\mu = \sqrt{1 - x^2}$, $0 \leq x \leq 1$ - Normalized Radial Coordinate, I - Integrated Stellar Intensity, & I_0 - Normalization constant such that I is unity.

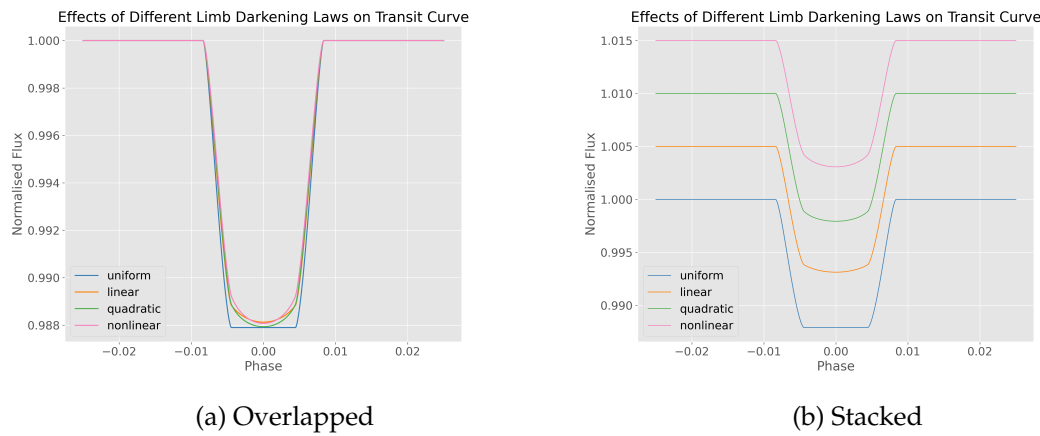


Figure 4.5: Effects of Different Limb Darkening Laws on Transit Curve

4.2.2 Some Results

No Limb Darkening Effect

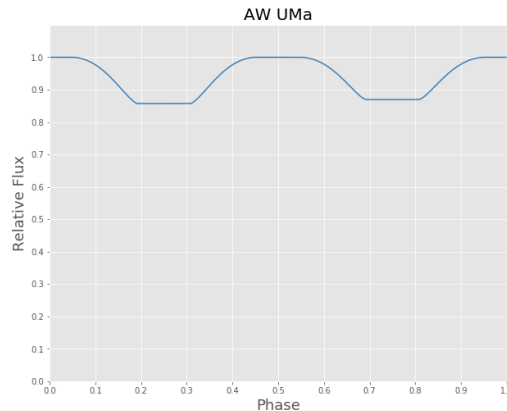


Figure 4.6: Light Curve for AW UMa Binary System

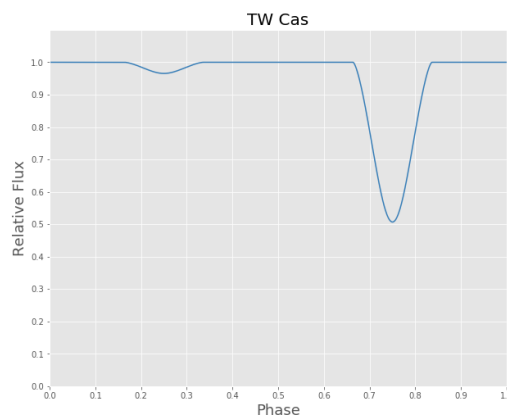


Figure 4.7: Light Curve for TW Cas Binary System

To see the real and simulated data as well as the stellar and orbital parameters for the light curves of the systems shown in Figures (4.6) and (4.7), refer to this [Eclipsing Binary](#)

Simulator

Limb Darkening Effect

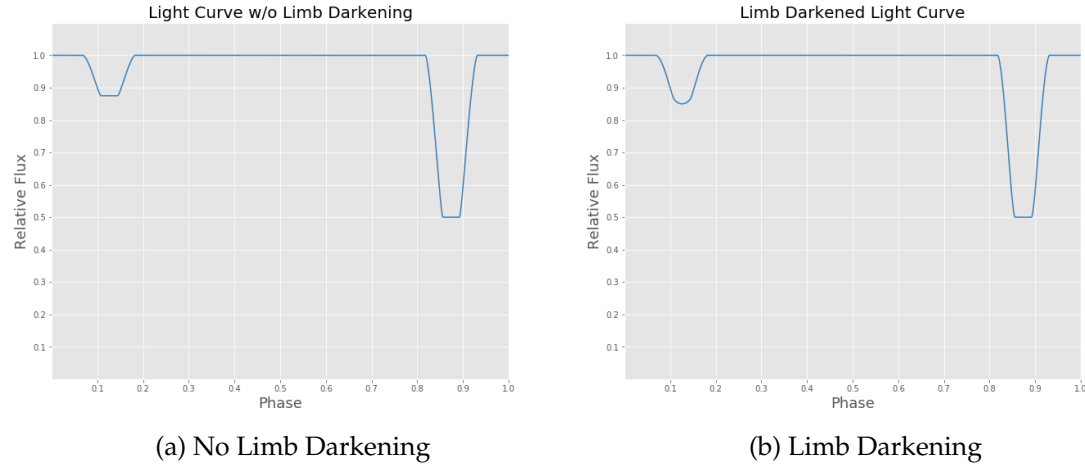


Figure 4.8: Effect of Limb Darkening on Light Curves

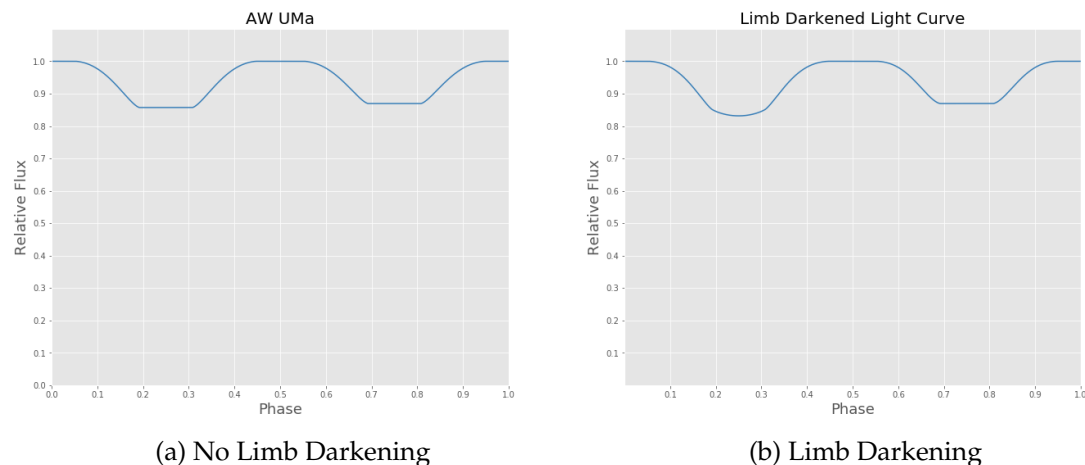


Figure 4.9: Effect of Limb Darkening on AW UMa

Note : For the Light Curves with Limb Darkening, The Linear Limb Darkening Model has been implemented with Limb Darkening Coefficient, $u = 0.6$ under the Eddington Approximation to the Grey Atmosphere Problem in Stellar Atmospheres.

4.3 Rossiter-McLaughlin Effect

4.3.1 Theory

It is a spectrometric phenomenon which was first observed by Rossiter (1924). This is also independently detected (McLaughlin, 1924) in the case of eclipsing systems β Lyrae and the Algol system, respectively. The phenomenon occurs when an object moves across the face of a rotating star.

The spectral data of a star is the result of the star moving either away from us or towards us which shows up as shifts in the wavelength of the radiation observed. Due

to rotation, one limb of the star apparently moves away from us thus causing a redshift and the other limb moves towards us thus causing a blueshift. When the whole face of the star is visible, this symmetrical broadening of the spectral lines due to equal and opposite velocities averages out to give the actual velocity of the star. But when some part of the face is covered, either due to a transiting planet or the second star of the binary system, the broadening is asymmetrical thus giving a different measure of the star's velocity.

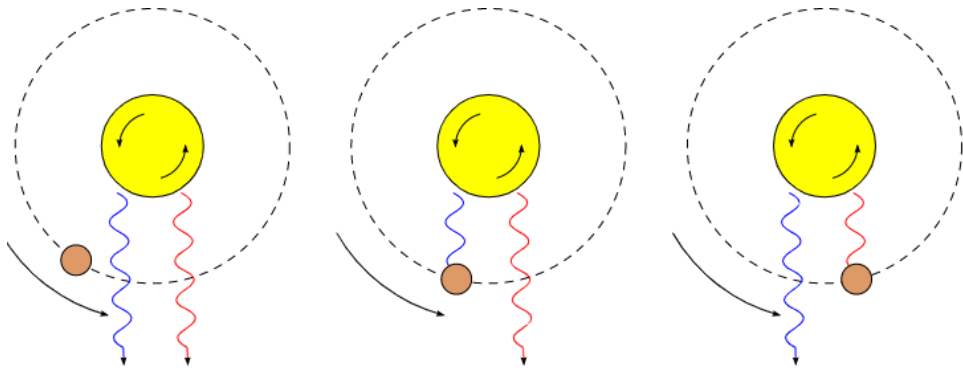


Figure 4.10: The viewer is situated at the bottom. Light from the anticlockwise-rotating star is blue-shifted on the approaching side, and red-shifted on the receding side. As the planet passes in front of the star it sequentially blocks blue- and red-shifted light, causing the star's apparent radial velocity to change when it in fact does not. Credits: [Nicholas Shanks, 2005](#)

As given in Takeda et al. (2015), the apparent change in velocity δV is given by:

$$\delta V = \frac{\int_A v_{\text{rad}} I dA}{\int_A I dA} \quad (4.54)$$

where v_{rad} is the radial velocity of the small element dA on the star's face, A is the area visible during the eclipse at a certain instant and I is the star's intensity.

4.3.2 Implementation

Consider an eclipsing circular binary of radius a with the orbital plane MM' inclined at an angle i with the line of sight and the stellar radii being R_1 and R_2 where $R_1 > R_2$. The phase angle is defined as $\theta = 0$ when O and M coincide. The larger star spins with an angular velocity Ω_s about an axis making an angle ϕ with the line of sight, refer to 4.11b.

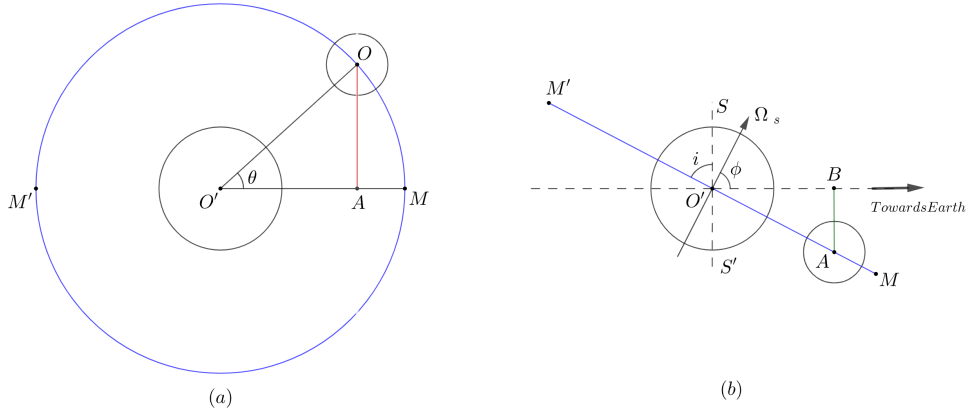


Figure 4.11: (a) The system when viewed perpendicular to the orbital plane. (b) The system when viewed along AO such that the orbital plane appears to be a line.

For a given θ , we set up two Cartesian coordinate systems, one at the center of the larger star's stellar disc (O') and the other at the center of the smaller star's stellar disc (O) as shown in 4.12. We now proceed to obtain the expressions for X and Y as they will be required further when we transit from one system to the other.

In 4.11a, we have $OO' = a$, thus $OA = a \sin \theta$. By visualizing a circular orbit one can infer that inclination does not affect the horizontal distance. As can be seen in 4.11b, if the inclination i was 90° , the center of the smaller star would also pass through the line of sight and thus O and O' would coincide along that line. But due to inclination, the vertical distance observed from earth is AB . We have, $O'A = a \cos \theta$ and since $\angle BAO' = i$, the length $AB = a \cos \theta \cos i$.

Considering the relative position of the two stars (refer to 4.12) and the definition of θ stated above, we have:

$$(X, Y) \equiv (-a \sin \theta, a \cos \theta \cos i) \quad (4.55)$$

If the spin axis is along the line of sight then the stellar rotation will contribute nothing to the radial velocity of any point on the star's disc. Thus, we consider only that component of rotation which is perpendicular to the line of sight, that is, $\Omega_s \sin \phi$, along the axis SS' . Consider any point $P(x', y')$ on the larger star's stellar disc in the coordinate system O' . As can be seen in 4.12, the radial velocity of P will be:

$$v_{\text{rad}} = x' \Omega_s \sin \phi \quad (4.56)$$

We have the coordinate transformation:

$$(x', y') = (x - X, y - Y) \quad (4.57)$$

Applying 4.57 to 4.56, we finally get:

$$v_{\text{rad}} = (x - X) \Omega_s \sin \phi \quad (4.58)$$

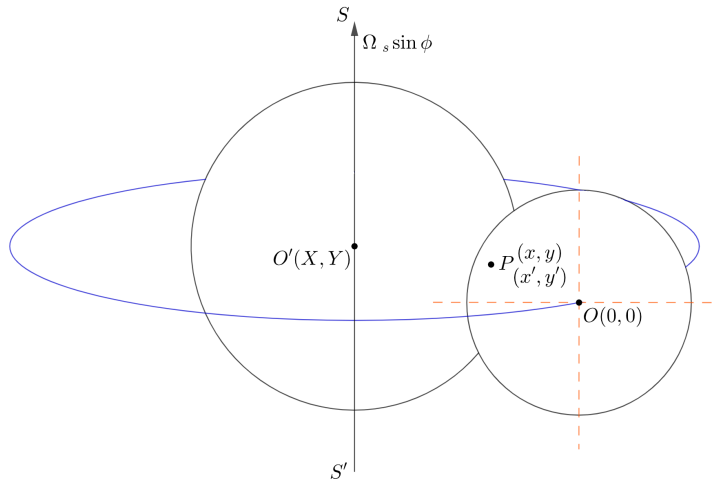


Figure 4.12: The system when viewed along the line of sight. The smaller star moves from left to right.

Since, we have an intensity term in 4.54 thus the radial velocity measured depends on the intensity at that point. We assume the stellar disk to follow linear limb darkening, thus, intensity at $P(x', y')$ is given as:

$$I(x', y') = I_o \left(1 - \mu \frac{\sqrt{x'^2 + y'^2}}{R_1} \right) \quad (4.59)$$

where, μ is the limb darkening coefficient. Again applying the coordinate transformation 4.57, we get:

$$I(x, y) = I_o \left(1 - \mu \frac{\sqrt{(x-X)^2 + (y-Y)^2}}{R_1} \right) \quad (4.60)$$

We have obtained, v_{rad} and I , the quantities required in 4.54. To compute the integral we need to divide one of the two stellar discs into a grid of small regions dA , determine the region of integration A , calculate the integrand at all of the desired dAs and finally sum over all such dAs to get the numerical value of the integral. The reason for expressing all quantities in terms of coordinate system O must be clear now. We divide the smaller disc into a grid so as to make the implementation less computationally expensive and achieve better accuracy¹.

Let's divide the smaller disc into a grid of squares of size $\Delta x \times \Delta y$ and let $P(x, y)$ represent the small region enclosed between x and $x + \Delta x$, and, y and $y + \Delta y$. As stated before, the region of integration(A) in 4.54 is the visible part of the larger stellar disc. Since P denotes the small grid square on the smaller stellar disc, we can integrate only over the eclipsed region, which is actually complementary to A and thus denoted by A' . To tackle this problem, we use the fact that the two integrals in 4.54, when evaluated over complete larger disc, result to a constant value. When evaluated over complete disc, the integral in the numerator results into zero as expected because in such a case there would be no RM effect in action and the integral in denominator results into total flux given by (@Vedant

¹We could divide the larger disc into a grid but to achieve the same accuracy as in the other case, the grid would need to be finer and hence more number of iterations will make it computationally expensive.

should i give the solution of integral for F in Appendix? It would be just half a page so i dont feel like mentioning it, more like "left as an exercise for the reader":P):

$$\begin{aligned} F &= \int_{A \cup A'} I dA \\ &= \pi R_1^2 \left(1 - \frac{2u}{3} \right) \end{aligned} \quad (4.61)$$

For the integral in the numerator we have:

$$\begin{aligned} \int_A v_{rad} IdA + \int_{A'} v_{rad} IdA &= 0 \\ \Rightarrow \int_A v_{rad} IdA &= - \int_{A'} v_{rad} IdA \\ \Rightarrow \int_A v_{rad} IdA &= - \sum_{(x,y) \in A'} v_{rad} I \Delta x \Delta y \end{aligned} \quad (4.62)$$

And for the integral in denominator:

$$\begin{aligned} \int_A IdA + \int_{A'} IdA &= F \\ \Rightarrow \int_A IdA &= F - \int_{A'} IdA = 0 \\ \Rightarrow \int_A IdA &= F - \sum_{(x,y) \in A'} I \Delta x \Delta y \end{aligned} \quad (4.63)$$

Therefore, finally we get:

$$\delta V = \frac{\int_A v_{rad} IdA}{\int_A IdA} = \frac{- \sum_{(x,y) \in A'} v_{rad} I \Delta x \Delta y}{F - \sum_{(x,y) \in A'} I \Delta x \Delta y} \quad (4.64)$$

where v_{rad} , I and F are as given in equations 4.58, 4.60 and 4.61.

4.3.3 Results

The above implementation was executed for a circular binary system with stellar radii $1.2R_\odot$ and $0.8R_\odot$ with the separation between the two stars being $40R_\odot$ and considering linear limb darkening coefficient as $\mu = 0.5$. Other parameters were varied so that the corresponding variation in the curve can be seen.

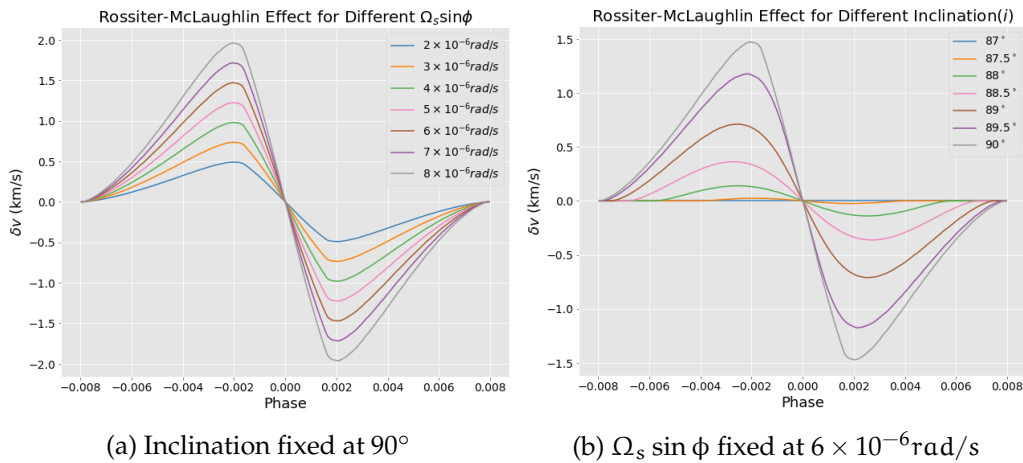


Figure 4.13: **(a)** As can be inferred from the equations, the change in angular velocity simply changes the peak of the curve. **(b)** As the inclination changes the phases at which eclipse starts and ends also change and after a certain inclination no RM effect is observed because then there is no eclipse. The curve will remain exactly the same on changing the inclination on either side of 90° by an equal amount.

4.4 Ellipsoidal Variation

4.4.1 Deviation from Spherical Shape

A binary system is a system of two stars. The two stars interact with each other through gravitational pull. This often leads to distortion of the star shape and deviation from the spherical geometry. This can be simply realised this way - a spherical geometry requires a spherical symmetry in a force field. For an isolated star, formed from collapsing gas cloud, matter collapses towards a dense 'centre' which eventually forms the fuel burning core of the star. The collapse is spherically symmetric as the gravitational field due to the dense core is spherically symmetric (Some deformation may occur due to rotation of the star - the equator bulges out due to centrifugal force, which breaks the symmetry). But when a second star is brought near it, the symmetry is broken, and matter feels an extra pull towards the second star. This leads to deformation of the stars.

4.4.2 The Lobed Shape

Circularization of Orbits

Orbits of most interacting binary systems are circularized. This is because of drain in energy due to tidal interactions. There are several theories that explain this circularization. One of them (Darwin) shows that the interaction causes a bulge in one or both the stars. These bulges actually do shift from the line joining the centres of the stars. This in turn leads to gravitational torques, exchanges of angular momentum, circularization and synchronization. Another theory (Zahn) adds viscosity in consideration and shows how the various layers inside the stars with their deformed shape suffers viscous drag and thus dissipates energy. Another theory (Cowling, Zahn) describes circularization when the stars are not in hydrodynamics equilibrium which leads to time varying gravitational potential and excitation oscillations. All these leads to drain of energy from the system and circularization of the orbit - which can be thought of as orbit of least energy given an angular momentum as the latter is fairly conserved. This also leads to tidal locking of the two stars.

The Roche Potential

Thus for binaries with ellipsoidal variations, we can safely assume that the orbits have been circularized. Most close binaries with short periods get circularized in the main sequence phase. For those which do not circularize in this phase, they circularize in the post main sequence phase. This is because, as one of the stars evolves to a giant, its size and thus the interaction increases significantly, which leads to effective energy dissipation and circularization. For such a circularized orbit, we can define a potential around the stars that a third body would feel when co-rotating with the system. This is called the Roche potential and has contribution from the gravitational potential from the two stars and the potential arising due to the centrifugal force. Suppose the two stars are on the y axis with the origin on star with mass m_1 and m_2 (with respect to some reference frame). The net potential is -

$$\Phi = -\frac{Gm_1}{r_1} - \frac{Gm_2}{r_2} - \frac{\omega^2}{2}(x^2 + (y - \frac{m_2}{M})^2) \quad (4.65)$$

This forms lobe shaped equipotential surfaces around the stars. As the stars interact, the deformed star starts approaching these lobe shapes thus deviating from the spherical shape. One of the equipotential surface surrounds the two stars with lobed shape and also converge at a point between the two stars called the 1st Lagrange Point (L1). This is a potential extremum. These lobe shapes are called the Roche Lobe. This is the maximum deformation that can occur. After that events like mass transfer or envelope formation takes place.

4.4.3 The Light Curve Variation

A sphere has a uniform projection when seen from any distance. Thus the light flux received by us is constant. But for non spherical shape, the cross section is not always the same, and depends on the direction of view. A skewed shape like Roche lobe is not easy to work with. To start with, let's take the shape of the stars to be ellipses. This is a crude approximation for interacting binaries - tear drop shaped lobes approximate to be ellipses. For the rest of the section, ellipses will be considered. Depending on the line of sight, the flux received will vary as the projected area will vary. To mention here, several other factors apart from projected area govern the flux received. The most important is limb darkening. But in this section, we will stick to just the ellipsoidal shape. Consider an ellipsoid with centre as the origin. The following equation represents the ellipsoid.

$$\frac{x^2}{a^2} + \frac{y^2}{b^2} + \frac{z^2}{c^2} = 1 \quad (4.66)$$

with a, b, c not all same. Now, consider two different line of sight, one along the x axis and the other along the y axis. Let's assume we see from very far. Now the projected outline is given by the points on the ellipsoid whose normal is perpendicular to line of site at that point. Considering viewing from far away, the LOS is the x axis and points satisfying the above condition can be found by taking the partial derivative of the above function and putting it to zero. Here it is easily seen that imposing this condition gives $x = 0$. Putting this back in Eq. 4.66, we find that the projected figure is given by

$$\frac{y^2}{b^2} + \frac{z^2}{c^2} = 1 \quad (4.67)$$

This is an ellipse with area πbc . Similarly viewing from y axis similarly gives the projected figure to be:

$$\frac{x^2}{a^2} + \frac{z^2}{c^2} = 1 \quad (4.68)$$

This is an ellipse with area πac . When a and b are not equal, the areas are not equal, thus it is seen that line of sight can vary the projected area and if we consider this a star with uniform surface luminosity, this changes the flux received and gives a variation in light curve (this is because as the star revolves, we see the ellipsoidal star from different directions). This is what is meant by Ellipsoidal Variation or Ellipsoidal Modulation of light curves.

4.4.4 Method Used to Model

Here, we have simulated a very simplified model of ellipsoidal variation. Suppose we start with an ellipsoid given by: maybe keep z1,etc as subscripts

$$\frac{(x_1 - a)^2}{a^2} + \frac{y_1^2}{b^2} + \frac{z_1^2}{c^2} = 1 \quad (4.69)$$

x_1, y_1, z_1 is a fixed reference coordinate frame. Here we consider a binary system with the stars located along the x_1 axis and the star with centre at $x_1 = a$ is ellipsoidal due to tidal stretching by the companion. As the stretching is along x_1 axis we may assume that $a > b = c$. Though the model does not demand this last assumption but for ease of visualization we can assume that. Now suppose the system starts revolving around the z_1 axis. Let's assume it has moved an angle θ in the clockwise direction with respect to the positive z_1 axis. Now we assume two things - first is orbit is circular, secondly, stars are tidally locked i.e. the rotation (about axis) time period is equal to the orbital time period. With the the equation of the ellipse with its new position is given by:

$$\frac{(x_1 \cos(\theta) - z_1 \sin(\theta) - a)^2}{a^2} + \frac{y_1^2}{b^2} + \frac{(x_1 \sin(\theta) + z_1 \cos(\theta))^2}{c^2} = 1 \quad (4.70)$$

Now, let x, y, z be the coordinate axes for the viewer and let the viewer's axis be rotated about the x_1 axis by an angle $\frac{\pi}{2} - i$ where i ranges from 0 to $\frac{\pi}{2}$. Now it is easily seen that the i is nothing but the inclination of the orbit. Now, due to this rotation, the coordinates transform as follows:

$$x_1 = x \text{ again, subscripts} \quad (4.71)$$

$$y_1 = y \cos(\pi/2 - i) + z \sin(\pi/2 - i) \quad (4.72)$$

$$z_1 = -y \sin(\pi/2 - i) + z \cos(\pi/2 - i) \quad (4.73)$$

Substituting the above three equations to Eq 4.70 gives us the equation of ellipse as seen by the observer. Now, employing the same method as before - by taking the derivative with respect to z and substituting back to get the projected area will be tiresome. Instead, the following method was used -

The LOS is the z axis. Thus several points on the $x - y$ plane were chosen. For each point it was checked whether any z value (within some reasonable limit depending on the a, b, c values) satisfies Eqs 4.70, 4.71, 4.72, 4.73. If yes, that point on the $x - y$ plane is "shadowed" by the ellipsoid. But it can be understood that the outline of the shadow is nothing but the projected outline of the ellipsoid on the plane perpendicular to line of site. Thus the area of the shadow is nothing but the measure of the projected area of the ellipsoid, and thus the flux received. And as the area is proportional to the number of x, y for which there exists a z such that the above mentioned equations are satisfied, the count of the number of such (x, y) pair gives a measure of the flux. This has been used to plot the light curves. Two extreme cases have been plotted in the next section, $i = \pi/2$ and $i = 0$.

4.4.5 Results

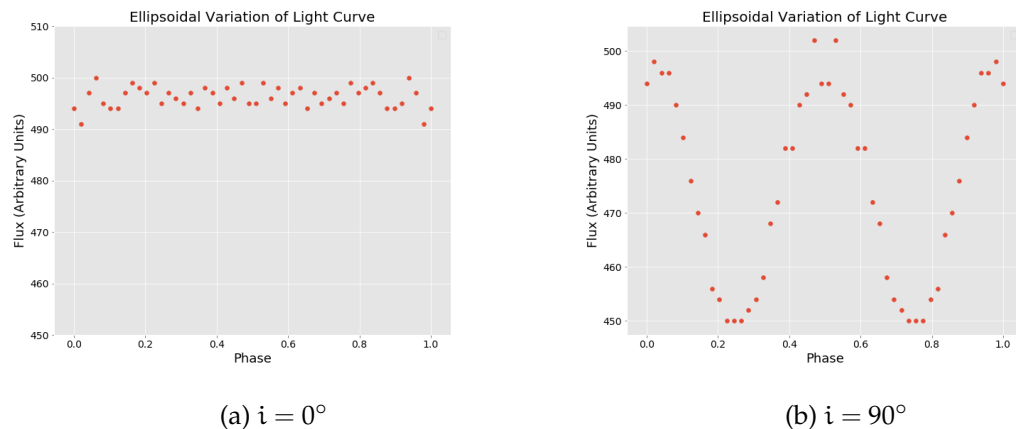
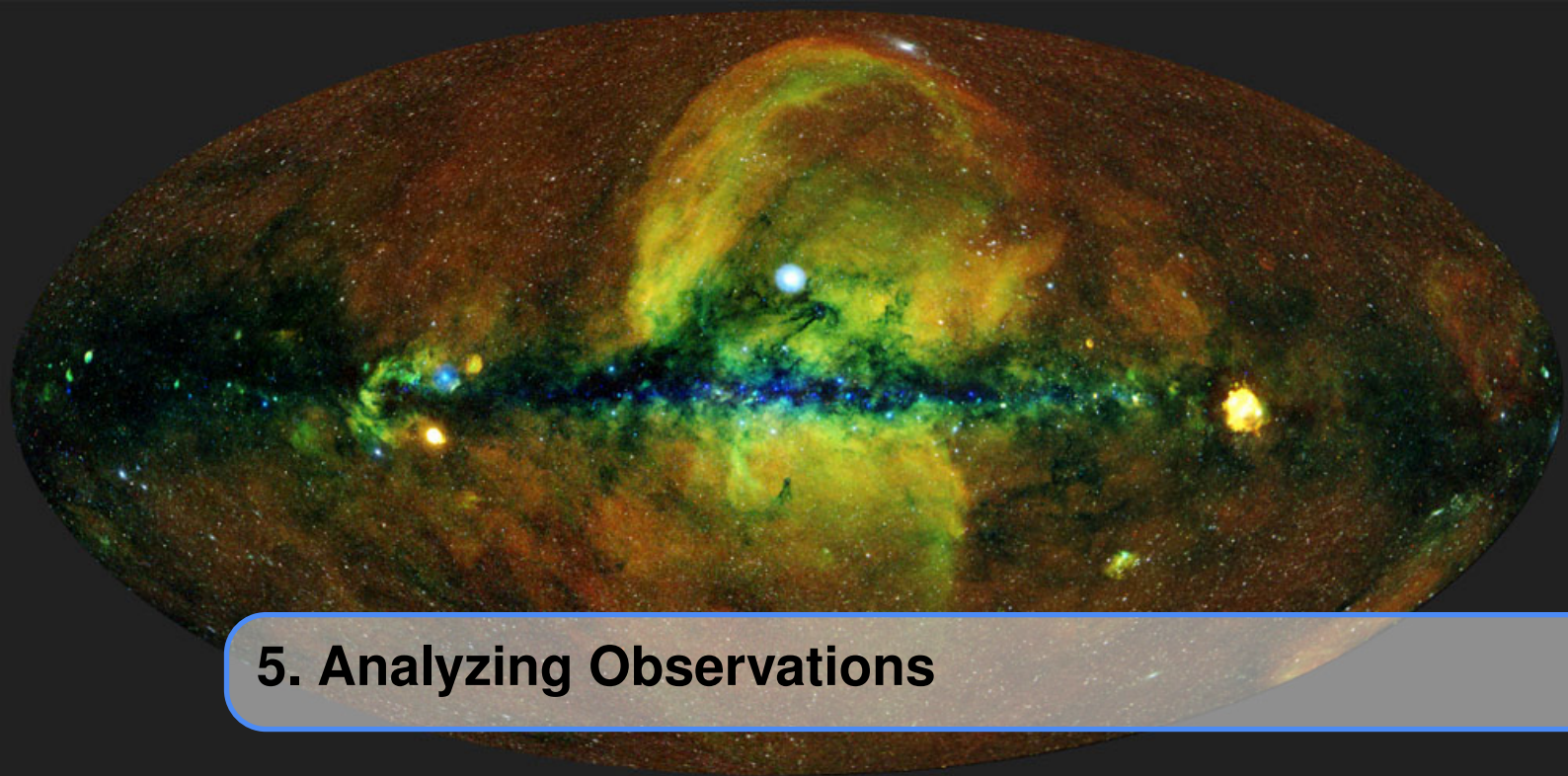


Figure 4.14: Figures showing the ellipsoidal variation in light curves at two extreme inclinations for an ellipsoidal shaped with the principal axes being 10, 9, 9 (solar radius). The larger axis length is along the line joining the centres of this star and its companion.

When $i = 0$, the plane of the circle is perpendicular to the plane of the ellipse. Thus we see only one cross section - the elliptical cross section with axes lengths as 10 and 9 solar radius. Thus, we should expect a fairly constant light curve. Fig 4.14 a shows the light curve as it is fairly constant within the error limits.

When $i = 90$, here we see significant variation of light curve. Here the projected area varies from being a circle of radius 9 solar radius and an ellipse with axes length of 10 and 9 solar radii. Thus we get a variable light curve as shown in Fig 4.14 b. From the graph it is seen, the maximum flux is around 495 units and the minimum around 450 units. The ratio of the maximum and minimum values should be the ratio of the maximum and minimum projected area i.e. $\frac{90}{81} = 1.11$. The model gives the value around $\frac{495}{450} = 1.1$ which is fairly close to the expected. Intermediate inclination will give the light curve, with the amplitude depending on the inclination value (for a given dimensions of the ellipsoid).



5. Analyzing Observations

5.1 Spectroscopic Binaries

The spectral data available from the spectroscopic binaries can be used to obtain the radial velocities of the components using Doppler red-shift. Analysis of the radial velocity data reveals many parameters describing the system. One major drawback is that unless the spectral data is complemented with photometric data, the inclination and hence a few properties of the system remain undetermined.

5.1.1 The Data

We use the system HIP61732 (RA:189.80°, Dec:+16.51°) for analysis. the observations were performed at the T193 telescope of the Haute-Provence Observatory, with the [SOPHIE](#) spectrograph. The data was used for analysis in [Halbwachs et al. \(2020\)](#) and we use their results to compare our results.

5.1.2 The Equations

In section [4.1.4](#) we derived the radial velocities of the binary components as a function of their true anomalies. The observational data obtained is the velocity at certain time instants. Hence, for the analysis we use the following equations connecting the radial velocity with time:

$$\frac{2\pi}{P}(t - T) = E - e \sin E$$

$$\tan\left(\frac{\theta}{2}\right) = \sqrt{\frac{1+e}{1-e}} \tan\left(\frac{E}{2}\right)$$

$$v_{\text{LOS}} = K[\cos(\theta + \omega) + e \cos \omega] + V_\gamma$$

use equation environment where the respective variables have the same meaning as mentioned in section 4.1.4. The above equations were the modelling equations using which we try to fit the data. The parameters that can be obtained by the analysis of the radial velocity data of a SB2 system are given in table 5.1.

Once these parameters are obtained, we can go on to determine the minimum masses and projected semi major axes. As given by equation 4.38:

$$K = \frac{2\pi a \sin i}{P\sqrt{1-e^2}} \quad (5.1)$$

Thus, we get projected semi major axis of each component as:

$$a_{1,2} \sin i = \frac{K_{1,2} P \sqrt{1-e^2}}{2\pi} \quad (5.2)$$

According to the Kepler's third law we have:

$$\begin{aligned} P^2 &= \frac{4\pi^2(a_1 + a_2)^3}{G(m_1 + m_2)} \\ \Rightarrow m_1 + m_2 &= \frac{4\pi^2(a_1 + a_2)^3}{GP^2} \end{aligned} \quad (5.3)$$

We know that the masses are inversely proportional to the semi-major axes (refer equation 4.20), thus using 5.2, we get: **ghichmidkala (looks messy)**

$$\begin{aligned} m_1 + \frac{m_1 K_1}{K_2} &= \frac{4\pi^2 \times \frac{P^3(1-e^2)^{\frac{3}{2}}}{8\pi^3 \sin^3 i} (K_1 + K_2)^3}{GP^2} \\ \Rightarrow \frac{m_1(K_1 + K_2)}{K_2} &= \frac{P(1-e^2)^{\frac{3}{2}}(K_1 + K_2)^3}{2\pi G \sin^3 i} \end{aligned}$$

And thus we have the minimum masses:

$$m_{1,2} \sin^3 i = \frac{P(1-e^2)^{\frac{3}{2}} K_{2,1} (K_1 + K_2)^3}{2\pi G} \quad (5.4)$$

Since, radial velocity curves provide no information regarding the inclination, we obtain just the lower limit of the masses, that is, $m \sin i^3$.

5.1.3 Algorithm

We employ Nonlinear Least Squares methodology **unnecessary capitalisation in a lot of places** to fit the radial velocity data and obtain the best fit parameters. Let the modelling equation be defined as $v_{cal}(t)$ defined by the parameters $(P, T, e, K, V_\gamma, \omega)$ and v_i be the data point obtained via observations at time t_i . The task is to minimise the sum of square of differences to obtain the best fit parameters. The sum S is defined as:

$$S = \sum_{i=1} [v_i - v_{cal}(t_i)]^2 \quad (5.5)$$

The minima occurs when,

$$\frac{\partial S}{\partial P} = \frac{\partial S}{\partial T} = \frac{\partial S}{\partial e} = \frac{\partial S}{\partial K} = \frac{\partial S}{\partial V_\gamma} = \frac{\partial S}{\partial \omega} = 0 \quad (5.6)$$

Light Curves		Radial Velocity Curves	
Name	Symbol	Name	Symbol
Period	P	Period	P
Fractional Radii	$r_{1,2}$	Semi-Amplitude	$K_{1,2}$
Inclination	i	Systematic Velocity	V_Y
Eccentricity	e	Eccentricity	e
Argument of Periastron	ω	Argument of Periastron	ω
Ratio of Stellar Radii	$k = R_2/R_1$	Projected Semi-Major Axis	$a \sin i$
Surface Temperature of Primary Star	$T_{\text{eff},1}$	Minimum Masses	$m_{1,2} \sin^3 i$
Surface Temperature of Secondary Star	$T_{\text{eff},2}$	Mass Function	$f(m)$
Distance	d	Time of Periastron Passage	T

Combined	
Name	Symbol
Mass of Primary Star	M_1
Mass of Secondary Star	M_2
Radius of Primary Star	R_1
Radius of Secondary Star	R_2
Surface Gravity of Primary Star	$\log g_1$
Surface Gravity of Secondary Star	$\log g_2$
Luminosity of Primary Star	\mathcal{L}_1
Luminosity of Secondary Star	\mathcal{L}_2
Density of Primary Star	ρ_1
Density of Secondary Star	ρ_2

Table 5.1: Table of Parameters obtained from RVs and LCs.

Since these partial derivatives are functions of both independent variable and parameters, a closed form solution does not exist. Instead, initial values must be chosen for the parameters. Then, the parameters are refined by iterating, that is, the values are obtained by successive approximation.

The above algorithm is implemented by `scipy.optimize.curve_fit` function of Python3 which we used in analysing the radial velocity data and obtain the best fit parameters. We used the Lomb-Scargle Periodogram (VanderPlas, 2018), a classic method for finding periodicity in irregularly-sampled data, to obtain the initial guess for P, which gave a fairly good value, usually within 5% error range on providing a rough range in which P would be lying. The periodogram can be implemented through `astropy.timeseries.LombScargle` class in Python3. Our curve fit code was sensitive to the initial guess value of eccentricity hence we iterated from 0 to 1 at the step of 0.1, providing at each iteration the respective value as the guess for eccentricity and finally obtain the best fit parameters.

5.1.4 Best Fit Results

On giving the range for period P as 300 to 900 days, the LombScargle Periodogram gave the approximate value of period as 583.828 days. Using that, the following best-fit parameters were obtained:

Parameter	Our Result	Halbwachs et al. (2020)
Period(days)	595.214	595.18 ± 0.20
Systemic Velocity(km/s)	-15.774	-15.956 ± 0.032
Eccentricity	0.3394	0.3393 ± 0.0019
Argument of Periastron(degs)	64.584	64.85 ± 0.67
Time of Periastron Passage(days)	117.581	118.62
Semi-Amplitudes(km/s)	K_1 K_2	9.207 13.057
Projected axes(Gm)	$a_1 \sin i$ $a_2 \sin i$	70.895 100.540
Minimum Masses(M_{\odot})	$m_1 \sin^3 i$ $m_2 \sin^3 i$	0.3323 0.2343
		0.3326 ± 0.0022 0.2341 ± 0.0014

Table 5.2: Comparison of our results with the values given in [Halbwachs et al. \(2020\)](#)

Note: Due to periodic motion, several values of time of periastron passage(T) will give the same RV values. This happens for values of $T - P$, T , $T + P$, $T + 2P$ and so on. Therefore, we mention here the $T \bmod P$ value which tallies and provides confirmation that our result is correct.

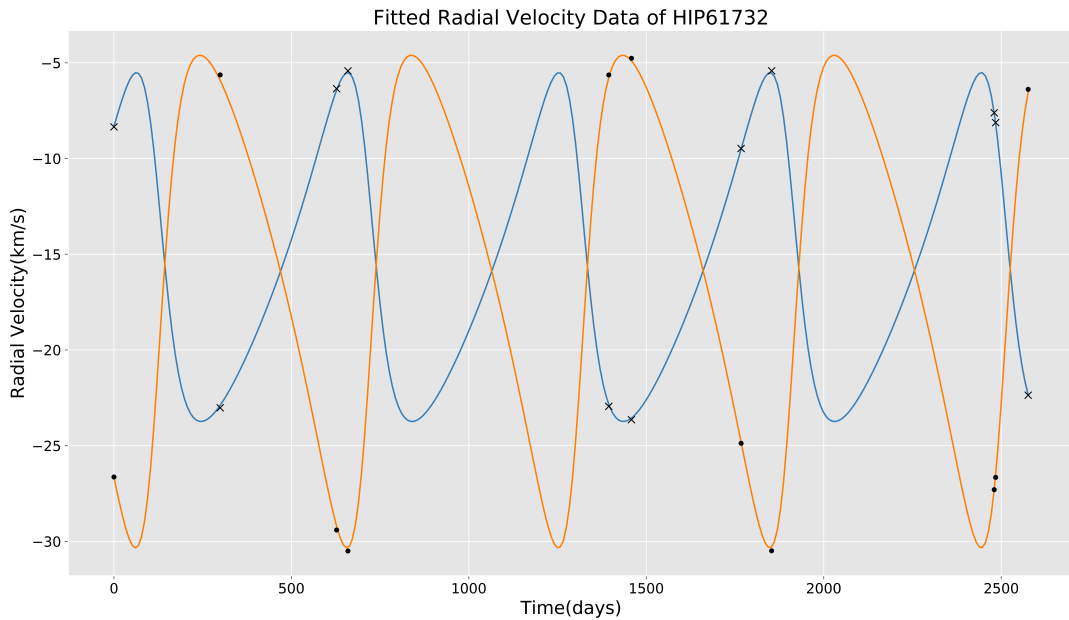


Figure 5.1: The radial velocity curve plotted using obtained parameters. The crosses and dots represent the observed data of individual component of the system.

5.2 Eclipsing Binaries

The orbital and physical parameters of the eclipsing binary systems can be measured to high accuracy and precision by analysing the radial velocity curves and light curves of the systems, which are obtained from the spectroscopic and photometric Observations of them respectively. The basic parameters which can be obtained are mentioned in [5.1](#).

5.2.1 The Data

The light curve data used in the analysis was taken from MAST archive (Mikulski Archive for Space Telescopes). This archive contains the data from different instruments like

Kepler, TESS, Pan-STARRS, Hubble Space Telescope and the upcoming James Webb Space Telescope. The data was accessed from the MAST portal¹ are we using footnotes anywhere else? If not let's keep it uniform to href things¹, which gives the data according to the target object. Even though *Kepler* and TESS mainly searches for exoplanets, they contain light curves for eclipsing binaries as well.

5.2.2 The Equations

In order to analyse the data, we need to understand which values of the curve will give which parameter. The mathematical foundations to achieve this was laid by Russell (1912); Kopal (1979).

The shape and symmetry of the light curves depends on the fractional radii ($r_{1,2} = R_{1,2}/a$), eccentricity(e), argument of periastron (ω), orbital inclination(i) and the ratio of stellar radii (k).

Fig.[] shows a typical light curve and depicts parameters such as Period, Eclipse Duration and Depths which will prove useful to constrain the system's parameters.

The Fractional Radii of Stars unnecessary capitalisation in a lot of places, check can be written in terms of Flux Ratio and Eclipse Duration as,

$$r_1 = \frac{R_1}{a} = \frac{1}{2\sqrt{k}} \sqrt{\sin^2 M_1 - \sin^2 M_2} \quad (5.7)$$

$$r_2 = \frac{R_2}{a} = \frac{\sqrt{k}}{2} \sqrt{\sin^2 M_1 - \sin^2 M_2} \quad (5.8)$$

here, k is the ratio of Stellar Radii unnecessary capitalisation in a lot of places and is given by,

$$k^2 = \left(\frac{r_2}{r_1} \right)^2 = \left(\frac{R_2}{R_1} \right)^2 = \frac{\ell_{\text{tot}} - \ell_{\text{tra}}}{\ell_{\text{occ}}} \quad (5.9)$$

where, $\ell_{\text{tot}} = \ell_1 + \ell_2$ - total brightness of stars, ℓ_{tra} - brightness during transit, and ℓ_{occ} - brightness during occultation.

Once Fractional Radii unnecessary capitalisation in a lot of places are determined, one can estimate the Orbital Inclination of the Eclipsing Binary System by,

$$\cos^2 i = (r_1 + r_2)^2 - \sin^2 M_1 = (r_1 - r_2)^2 - \sin^2 M_2 \quad (5.10)$$

As the eqs. 5.7, 5.8 & 5.10 depends on the Mean Anomaly unnecessary capitalisation in a lot of places (M), it is attributed as,

$$M_1 = \frac{\pi}{P}(t_4 - t_1) \quad M_2 = \frac{\pi}{P}(t_3 - t_2) \quad (5.11)$$

where, $t_4 - t_1$ - Duration of Eclipse, and $t_3 - t_2$ - Duration of Total Eclipse.

The above equations holds good for Eclipsing Binaries with circular orbits or with nearly circular orbits ($e < 0.1$). But for elliptical orbits, things change. Kopal (1979) shows that how orbital eccentricity can effects the timing and duration of eclipses. The relative time of eclipses and duration gives the estimate of Poincare Elements, $e \cos \omega$ & $e \sin \omega$, as

$$e \cos \omega = \frac{\pi}{1 + \csc^2 i} (\phi_{\text{sec}} - \phi_{\text{pri}} - 0.5) \quad (5.12)$$

$$e \sin \omega = \left[\frac{d_{\text{sec}} - d_{\text{pri}}}{d_{\text{sec}} + d_{\text{pri}}} \right] \left[\frac{\alpha^2 - \cos^2 i}{\alpha^2 - 2 \cos^2 i} \right] \quad (5.13)$$

¹<https://mast.stsci.edu/portal/Mashup/Clients/Mast/Portal.html>

where, α is abbreviated as,

$$\alpha = \frac{R_1 + R_2}{a(1 - e^2)} \approx r_1 + r_2 \quad (5.14)$$

Owing to the fact that Eclipsing Binaries have $i \approx 90^\circ$ and less eccentricity, one can simplify the equations in approximate relations as,

$$e \cos \omega \approx \frac{\pi}{2} (\phi_{sec} - \phi_{pri} - 0.5) \quad (5.15)$$

$$e \sin \omega \approx \frac{d_{sec} - d_{pri}}{d_{sec} + d_{pri}} \quad (5.16)$$

where, $\phi_{pri, sec}$, $d_{pri, sec}$ - Phase and Duration of Primary and Secondary Eclipse.

If the photometric data of EBs is present in more than one filter band, such as in U, B, V bands (Johnson & Morgan (1953)), then we can estimate the effective Surface Temperature of stars with Color Index (Ballesteros (2012)) by the formula,

$$T_{eff} = 4600 \left(\frac{1}{0.92(B-V) + 1.7} + \frac{1}{0.92(B-V) + 0.62} \right) K \quad (5.17)$$

where, $B - V$ is the color index in B and V bands and is represented as the difference of magnitudes in different photometric bands.

$$B - V = m_B - m_V = M_B - M_V \quad (5.18)$$

$$= -2.5 \log \left(\frac{\mathcal{F}(B)}{\mathcal{F}(V)} \right) \quad (5.19)$$

Eclipsing Binaries are widely used as Distance estimators as they offer direct method to determine it to an improved 5% level of accuracy ((Rucinski, 1997); (Southworth et al., 2004); (Kang et al., 2007)). The Surface Brightness (S) and Effective Temperature(T_{eff}) of the EBs can be used to constrain the photometric distance of these systems (J. Southworth, 2004). The expression provides an empirical relation between the Distance (d), Wavelength-dependent Surface Brightness of a star (S_{m_λ}), Apparent Magnitude of Star in filter λ (m_λ), Zeroth-Magnitude Angular Diameter ($\phi^{(m_\lambda=0)}$) and Stellar Radii($R_{A,B}$).

$$d = 10^{0.2m_\lambda} \sqrt{\left[\frac{2R_A}{\phi_A^{(m_\lambda=0)}} \right]^2 + \left[\frac{2R_B}{\phi_B^{(m_\lambda=0)}} \right]^2} \quad (5.20)$$

where, $\phi^{(m_\lambda=0)}$ is abbreviated as,

$$\phi^{(m_\lambda=0)} = \phi \cdot 10^{m_\lambda/5} = \frac{S_{m_\lambda}}{5} \quad (5.21)$$

5.2.3 Effects of Photometric Variation

The shape of light curves are often effected due to the photometric variations. These variations can occur due to the change of brightness of stars across their surface (Limb Darkening and Gravity Darkening), due to the presence of a nearby star (Reflection Effect, Ellipsoidal Modulation) and due to relativistic effects (Lensing, Doppler Beaming).

In practise, one need to first incorporate the effects in the fitting model in order to avoid errors in the estimation of parameters. Limb Darkening can be incorporated by using various laws mentioned in 4.2.1.

5.3 Estimation of Parameters

There are two approaches by which we can estimate the parameters of an eclipsing binary system. First approach is to use the equations mentioned in 5.2.2. This approach yields good results for edge-on orbits with less eccentricity but cannot account for the photometric variations. The another approach, which is more efficient and robust, is to fit a model to the light curve and estimate the parameters. Section 5.3.5 talks about this in much detail.

5.3.1 The Approach of Model Fitting

This method approaches the problem in a different but more efficient way. A light curve depends upon the configuration of the positions of stars and their shapes. This approach provides a more generalised way to solve the light curve.

According to the configuration, such detached or semi-detached, circular or elliptic, head-on or inclined, etc., a model is created which takes some input parameters and gives the associated light curve as a result.

This light curve is then fitted to these models, such as Nelson-Davis model ([Nelson & Davis, 1972](#)), Wilson-Devinney model ([Wilson & Devinney, 1971](#)), etc., which are now implemented under the codes JKTEBOP ([Popper & Etzel \(1981\)](#), [Southworth et al. \(2004\)](#), [Southworth \(2013\)](#)) and PHOEBE 2.2 ([Prša et al. \(2016\)](#)) respectively, and their parameters are optimised various diverse techniques such as χ^2 -Minimization or Markov Chain Monte Carlo (MCMC) algorithms.

Apart from this, one can use Allesfitter ([Günther & Daylan, 2020, 2019](#)) to achieve light curve fitting. The python package has both GUI and command-line feature and can fit the curves with Nested and MCMC sampling.

5.3.2 Period

After selecting the eclipsing binary stars, their period can be calculated from the light curves. Even though Lomb-Scarlge method is commonly used for finding period of pulsating objects, this method fails to give accurate results for eclipsing binary stars.

Therefore, the Box-fitting Least Square (BLS) algorithm was used to determine the period of the light curve collected from the database. Unlike the other period-finding methods, Box-fitting Least Square algorithm does not search for signals that are continuously variable over the full phase curve, but instead searches for periodic box-shaped dips in a light curve ([Hartman & Bakos \(2016\)](#)). Hence, this algorithm provides an efficient means of identifying eclipsing binary light curves and transiting planet signals. For a periodic signal with a set of data points, the algorithm will estimate parameters including Period and epoch of transit ([Kovács et al. \(2002\)](#)).

In the analysis of light curves it is preferable to have period before hand as BLS fails on some light curves which has similar eclipse depths.

5.3.3 The Fitting

The `aggregate_downsample()` function was used to bin values from a time series into bins of equal time, using a custom function (median). This operation returns a `BinnedTimeSeries`. Then plotted the results together with data points.

5.3.4 Combined Parameters

The properties of Eclipsing binary stars can be derived by observing and analysing them Spectroscopically (Radial Velocity curves) and Photometrically (Light Curves).

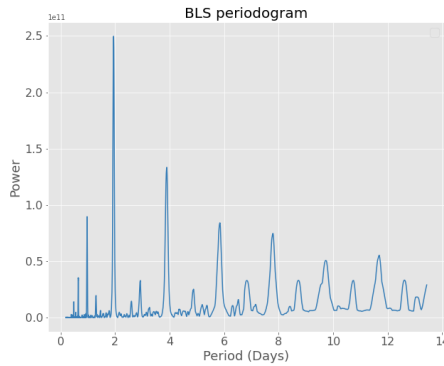


Figure 5.2: BLS Periodogram, used to estimate the spectral density of transiting stars

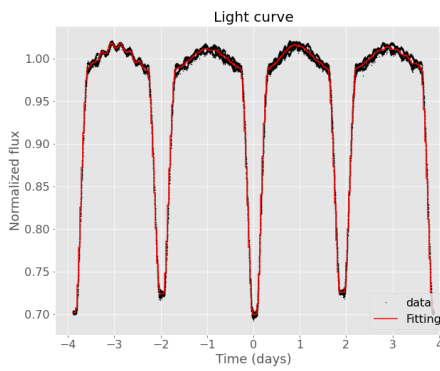


Figure 5.3: The fitted Light Curve with primary and secondary eclipse

Section 5.1.3 gives the way for analysing the RV curves. RVs generally yields P , K_1 , K_2 , & $e \sin \omega$ whereas LCs generally yield P , r_1 , r_2 , i , & $e \cos \omega$.

1. $e \sin \omega$ & $e \cos \omega$ gives e & ω of the system.
2. K_1 , K_2 , i , & e gives M_1 , M_2 , & a using the expressions,

$$M_{1,2} = \frac{P}{2\pi G} \left(\frac{\sqrt{(1-e^2)}}{\sin i} \right)^3 (K_1 + K_2)^2 K_{2,1} \quad (5.22)$$

$$a = \frac{P}{2\pi} \frac{\sqrt{(1-e^2)}}{\sin i} (K_1 + K_2) \quad (5.23)$$

3. r_1 , r_2 , & a gives R_1 & R_2 using expression,

$$R_{1,2} = r_{1,2} a \quad (5.24)$$

4. The obtained $M_{1,2}$ & $R_{1,2}$ are then used to obtain $g_{1,2}$ & $\rho_{1,2}$ by,

$$g_{1,2} = \frac{GM_{1,2}}{R_{1,2}^2} \quad (5.25)$$

$$\rho_{1,2} = \frac{3M_{1,2}}{4\pi R_{1,2}^3} \quad (5.26)$$

which, in astrophysical units, becomes,

$$\frac{\rho_{1,2}}{\rho_{\odot}} = \frac{M_{1,2}}{M_{\odot}} \left(\frac{R_{1,2}}{R_{\odot}} \right)^{-3} \quad (5.27)$$

5. Eq. 5.17 yields T_{eff} of the stars. Using that along with R_1 & R_2 , we compute Stellar Luminosity (\mathcal{L}) by,

$$\mathcal{L}_{1,2} = 4\pi R_{1,2}^2 \sigma T_{1,2}^4 \quad (5.28)$$

where, σ stands for Stefan-Boltzmann constant with value of $5.670 \times 10^{-8} \text{ W m}^{-3} \text{ K}^{-4}$.

6. Eq. 5.20 can be used to estimate the distance of the eclipsing binary system using the Stellar Radii, Apparent magnitude of star and Surface brightness in dedicated filter.

5.3.5 Circular Orbits

In circular orbits, due to the absence of eccentricity, the eclipses occur at an equal intervals of time. The transit time, the duration and the depths of eclipses yields r_1 , r_2 & i . The parameters can be estimated by using the Eqs. 5.7 - 5.11 provided we have an estimate of period from before hand.

Sec. 5.3.5 will further lights the way to completely solve the system for it's orbital parameters and physical properties.

5.3.6 Elliptical Orbits

In elliptical orbits, the light curve is affected by the involvement of e & ω . Eqs. 5.12 - 5.16 can be used to estimate e & ω . The Poincare elements are determined either separately from RVs and LCs or only from the LCs to give the estimate of e & ω .



6. Alcor-Mizar: A Case Study

6.1 Mizar and Alcor : the Famous Double Star

Mizar is a second-magnitude star in the handle of the Big Dipper asterism in the constellation of Ursa Major. It has the Bayer designation ζ Ursae Majoris (Latinised as Zeta Ursae Majoris). It forms a well-known naked eye double star with the fainter star Alcor, and is itself a [quadruple star system](#). The whole system lies about 83 light-years away from the Sun, as measured by the Hipparcos astrometry satellite ([van Leeuwen \(2007\)](#), [Perryman et al. \(1997\)](#), [Perryman \(2010\)](#)), and is part of the [Ursa Major Moving Group](#).

Alcor appears at about 12' from Mizar with a normal eyesight. Alcor is of magnitude 3.99 and spectral class A5V. It has a faint red dwarf companion separated by 1" ([Mamajek et al. \(2010\)](#)). Mizar and Alcor's proper motions show they move together, along with most of the other stars of the Big Dipper except Alpha Ursae Majoris and Eta Ursae Majoris, as members of the Ursa Major Moving Group, a mostly dispersed group of stars sharing a common birth. However, it has yet to be demonstrated conclusively that they are gravitationally bound. Gaia parallax measurements ([Gaia Collaboration \(2018\)](#)) indicate that the Alcor binary and Mizar quadruple are somewhat closer together than previously thought: 0.36 ± 0.19 ly. The uncertainty is due to our uncertainty about the exact distances from us. If they are exactly the same distance from us then the distance between them is only 17800 AU (0.281 ly) ([Mamajek et al. \(2010\)](#)).

The Discovery:

Benedetto Castelli, one of the Galileo's colleagues in the 16th century, observed Mizar through a telescope and realized that it was a binary system: Mizar A and Mizar B. Then, throughout the 19th century and the beginning of the 20th century, with the help of spectroscopy, scientists showed that Mizar A and B were both binary systems. In 1908, the Alcor-Mizar system was the first 5-star system ever discovered.

In 2009, Eric Mamajek and his colleagues from the University of Rochester, while searching for exoplanets, discovered that Alcor was also a binary system, making the Alcor and Mizar a 6-star system.

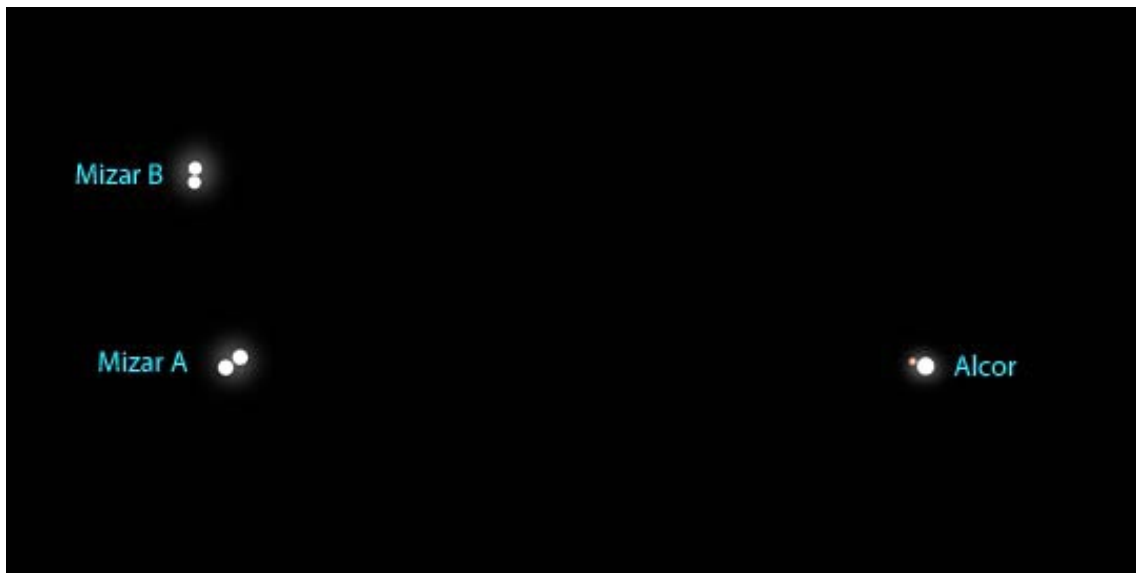


Figure 6.1: Alcor Mizar as a sextuplet system (image not to scale), credits: [Bob King, 2017](#)

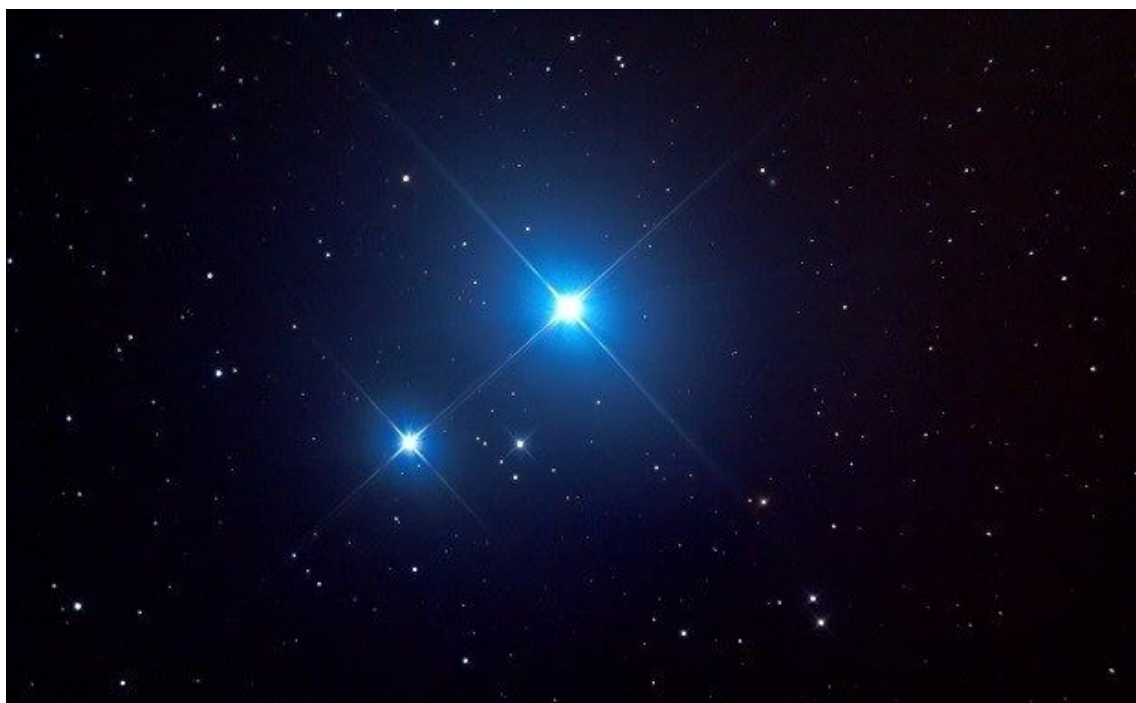


Figure 6.2: Alcor Mizar visible as a visual binary through a telescope, Credits: [Gary Fildes](#).

Constellation:	Ursa Major
Coordinates:	RA 13h 23m 55.5s
	Dec. +54° 55' 31"
Distance:	86 light years
Star Type(s):	Mizar (A2V + A2V + A1V)
	Alcor (A5V)
Mass:	Mizar Aa + Bb ($2.43 M_{\odot}$)
	Alcor ($1.8 M_{\odot}$)
Diameter:	Mizar Aa + Bb ($4.8 M_{\odot}$)
	Alcor ($1.76 M_{\odot}$)
Apparent Magnitude:	Mizar (+2.27)
	Alcor (+3.99)
Luminosity:	Mizar Aa + Bb ($33.3 M_{\odot}$)
	Alcor ($13.4 M_{\odot}$)
Surface Temperature:	Mizar Aa + Bb (9,000 K)
	Alcor (8,000 K)

Table 6.1: Physical properties of the Alcor Mizar System

6.1.1 Observation and Analysis of System in Radio at 1420 MHz

Figure 6.3: SALSA radio telescope at Onsala Space Observatory, Sweden reference: [SALSA website](#)

Aim of the experiment:

Observe the binary system (Mizar and Alcor) in radio at 1420 MHz using the 2.3 metre SALSA radio telescope and try to find the surface temperature of the stars.

Important parameters to be considered:

1. SALSA radio telescope has an angular resolution of 6° , therefore it is impossible to resolve the 2 stars using this radio telescope. The main objective of this experiment is to show that by using a larger radio telescope such as the GMRT (Giant Metrewave Radio Telescope) by [NCRA-TIFR](#) or by using the Indian SWAN (Sky Watch Array Network) by [Raman Research Institute](#), it is possible to find the stellar parameters such as temperature, relative velocity, etc by using a similar approach.
2. The telescope's antenna is not calibrated as informed by the observatory due to technical problem, it will be calibrated by the end of 2020, therefore a margin of error is expected due to lack of system calibration.

Method:

The telescope was pointed in the direction of the binary system, and a measurement at a frequency of 1420.4 MHz was taken for an integration time of 3600 seconds with the bandwidth at 10 MHz and LSR correction (Local-Standard of Rest) as well as RFI (radio frequency interference) removal switches to be on.

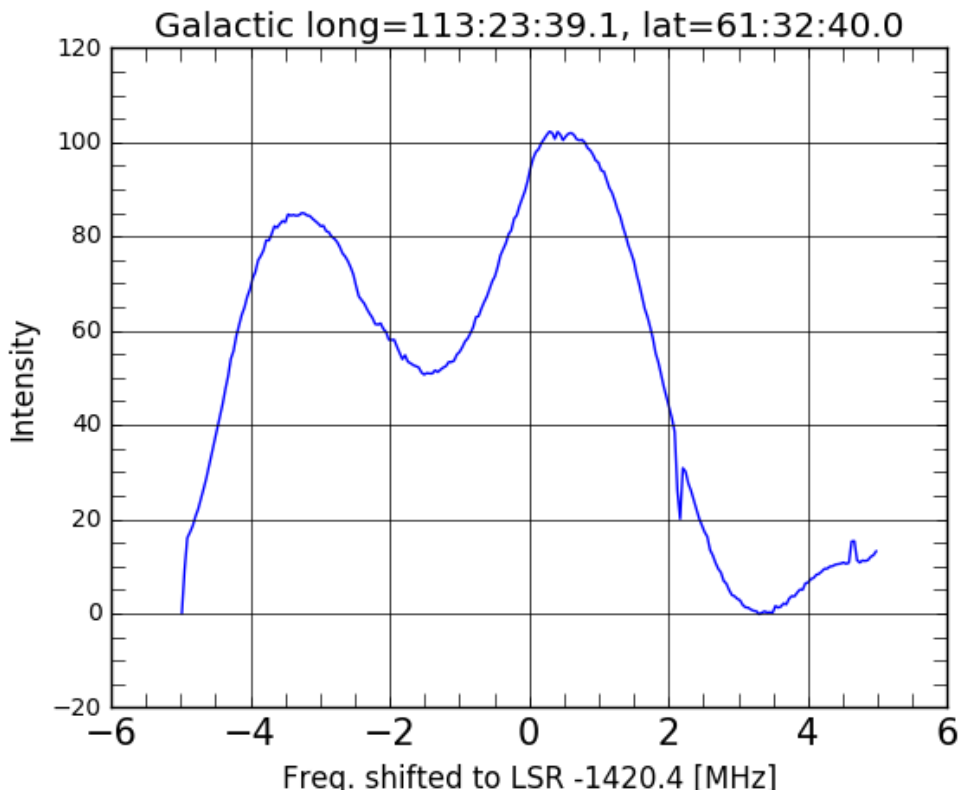


Figure 6.4: Spectrum obtained with Intensity on Y axis (Antenna Temperature in Kelvin) and Frequency shifted to LSR on X axis

A Gaussian curve was fitted and the baseline was subtracted using MATLAB (the code is available on the GitHub repository) to find the Antenna temperature of the left peak in

Figure 6.5, as the peak is blue shifted, it is assumed that the left peak is the signal from the observed stars.

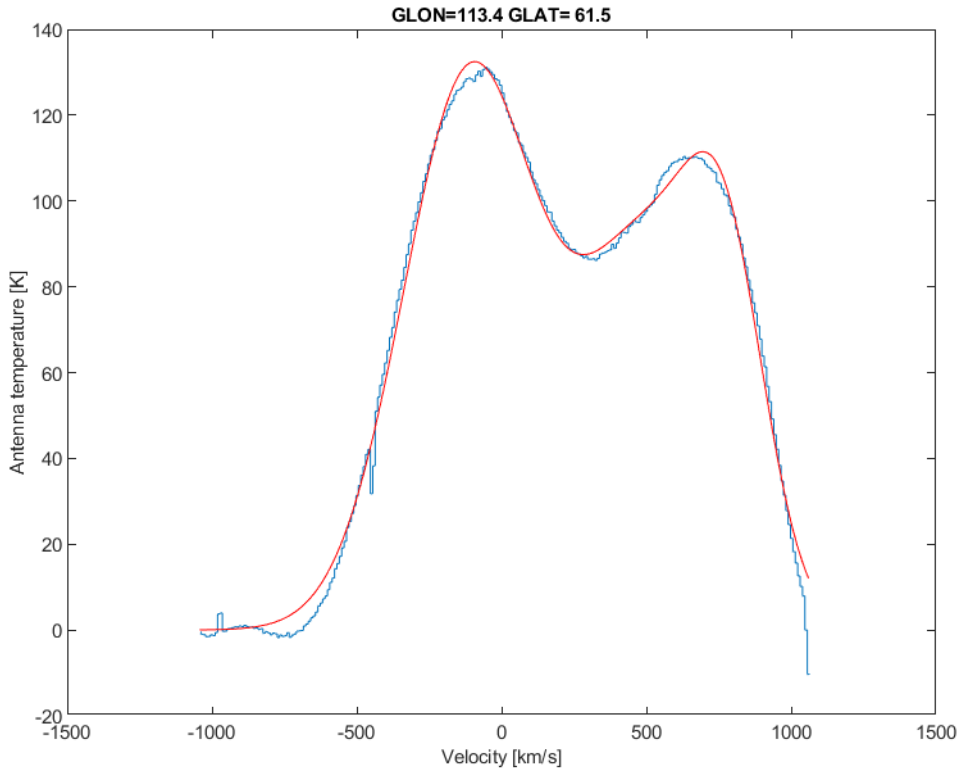


Figure 6.5: Spectrum with a Gaussian fit having Intensity on Y axis (Antenna Temperature in Kelvin) and Velocity (Km/s) on X axis.

To measure the temperature of the stars, temperature needs to be thought of in terms of brightness temperature and antenna temperature where equation equation 6.1 is defined as brightness temperature,(Draine (2011))

$$T_B = \frac{h\nu}{k * \ln(1 + \frac{2h\nu^3}{I_\nu c^2})} \quad (6.1)$$

Where T_B is brightness temperature, h is Planck's constant, ν is the frequency being observed, k is the Boltzmann constant, c is the speed of light, and I_ν the intensity of the wave at the given frequency. This intensity can be thought of as the brightness of the object at the wavelength being observed.

Brightness temperature is dependent on astronomical objects being black body radiators. Different wavelengths of light coming from a region will have different intensities, which is essentially the brightness. Brightness temperature is a way of defining temperature dependent on that brightness, causing the brightness temperature to vary depending on which section of the electromagnetic spectrum measurements are being taken in. However, since the motion of the particles moving in the magnetic field is not black body radiation, this is an effective temperature rather than a real temperature.

Antenna temperature is defined as equation 6.2 and is what the telescope is directly measuring, (Draine (2011)). In this equation all the symbols have the same meaning as

those in 6.1 with T_A being antenna temperature

$$T_A \equiv \frac{c^2}{2k\nu} * I_\nu \quad (6.2)$$

For radio waves these temperatures are approximately equal meaning the telescope is directly measuring the temperature of the object it is pointed at (in our case, the Alcor-Mizar system)

Derivation:

$$T_B = \frac{\hbar\nu}{k * \ln(1 + \frac{2\hbar\nu^3}{I_\nu c^2})} \quad (6.3)$$

$$T_A \equiv \frac{c^2}{2k\nu} * I_\nu \quad (6.4)$$

These temperatures are approximately equal because of the limit where the energy of the photon is much less than that of the thermal energy, which is true for radio waves and can be stated mathematically as $\hbar\nu \ll kT_A$. When this is true $\frac{2\hbar\nu^3}{c^2 I_\nu} \ll 1$ which allows the Taylor series approximation $|x| \ll 1$ to be used for brightness temperature. This can then be used to derive that $T_B \approx T_A$ for radio waves.

$$T_B = \frac{\hbar\nu}{k * \ln(1 + \frac{2\hbar\nu^3}{I_\nu c^2})} \quad (6.5)$$

if $|x| \ll 1$, $\ln(1 + x) \approx x$. When $\hbar\nu \ll kT_A$, $\frac{2\hbar\nu^3}{c^2 I_\nu} \ll 1$

$$T_B = \frac{\hbar\nu}{\frac{2k\nu^3}{c^2 I_\nu}} \quad (6.6)$$

$$T_B = \frac{c^2 I_\nu}{2k\nu^2} \quad (6.7)$$

$$T_B \approx T_A \quad (6.8)$$

6.1.2 Optical Analysis of the Binary System using Aperture Photometry Tool

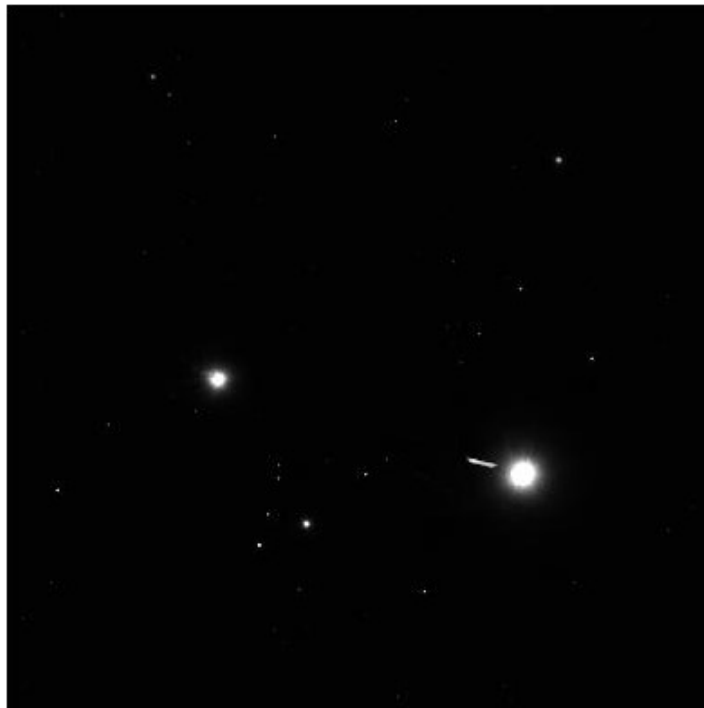


Figure 6.6: Alcor-Mizar as photographed by the Pan-STARRS1 telescope, [Pan-STARRS1, 2019](#)

Aim of the experiment :

Analyse image of the binary system (Alcor-Mizar) using Aperture Photometry Tool to find the magnitude of star and in turn, try to find the mass of the stars using Mass- Luminosity relation.

Aperture Photometry Tool:

Aperture Photometry Tool ([APT](#)) is software with a graphical user interface for computing aperture photometry on astronomical imagery. Image overlays, graphical representations, statistics, models, options and controls for aperture-photometry calculations are brought together into a single package. The software also can be utilized as a FITS-image viewer. APT is executed on desktop and laptop computers, and is free of charge under a license that limits its use to astronomical research and education. The software may be downloaded from its official website, and requires the Java Virtual Machine to be installed on the user's computer.

Method:

First, images were obtained using the website [Telescope Live](#) which offers 20 credits for free, these 20 credits can be used to take images of object to be observed. [Slooh](#) is another platform which offers access to various telescopes in the northern as well as southern hemispheres at an annual subscription fee.

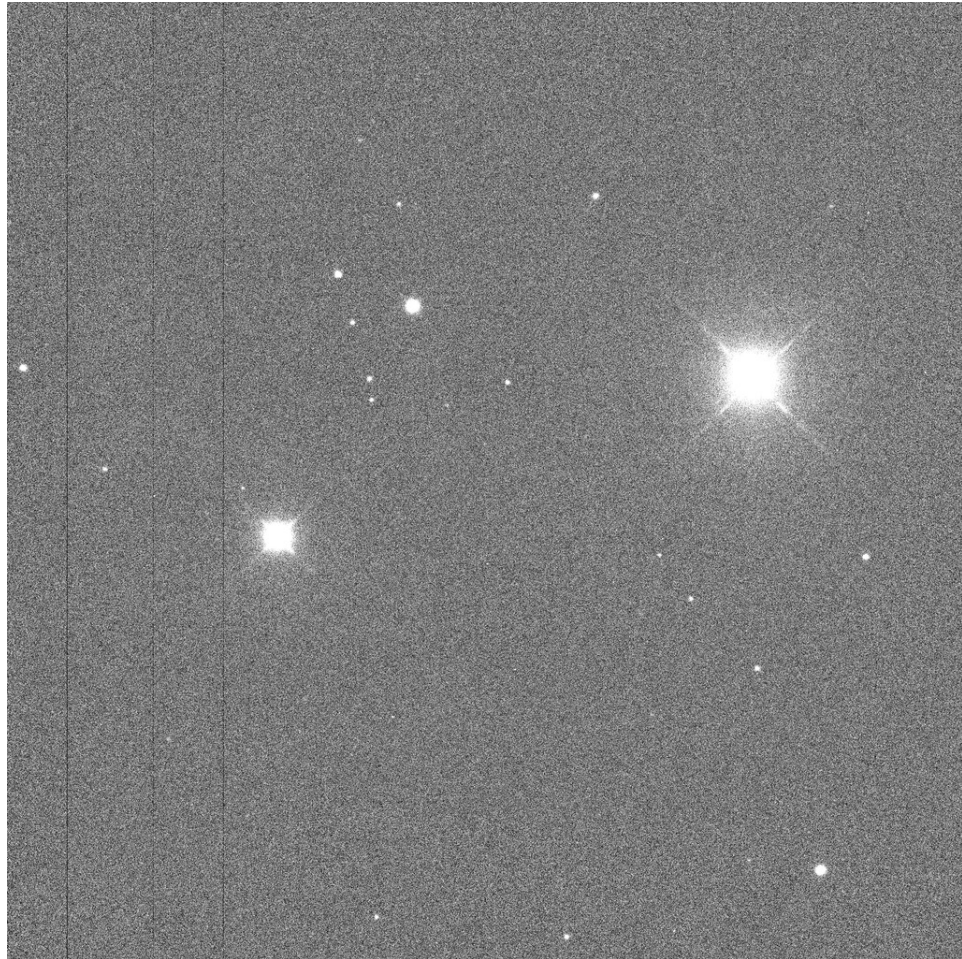


Figure 6.7: Alcor Mizar photographed using Telescope Live at 5s exposure time and a green filter

The image was then opened in Aperture Photometry Tool, and in 'more settings' option, Model 0 i.e no aperture radial profile interpolation was selected as source algorithm and Model B i.e sky annulus median subtraction was selected as sky algorithm, all other settings were default. It is also important to set a 'magnitude zero point' to get an accurate magnitude of the star. There are two kinds of photometry that are commonly done in astronomy:

- differential photometry – in which the magnitude you derive for the star is compared to the magnitude you derive for stars of known brightness in the near field at the same time, so that a “standardized magnitude” for the variable can be determined.
- all-sky photometry – a more complicated procedure in which the star magnitudes are derived directly using the results of nightly calibration of your system and current atmospheric conditions using a set of standard stars outside the field-of-view

We have used differential photometry here, therefore it is necessary to use the magnitude of a star visible in figure 6.7 which will be used to calculate the magnitude zero point. The magnitude zero point can be calculated using the following formula :

$$\text{zero point} = \text{Magnitude of known star} + (2.5 * \log_{10}(\text{source intensity of known star}))$$

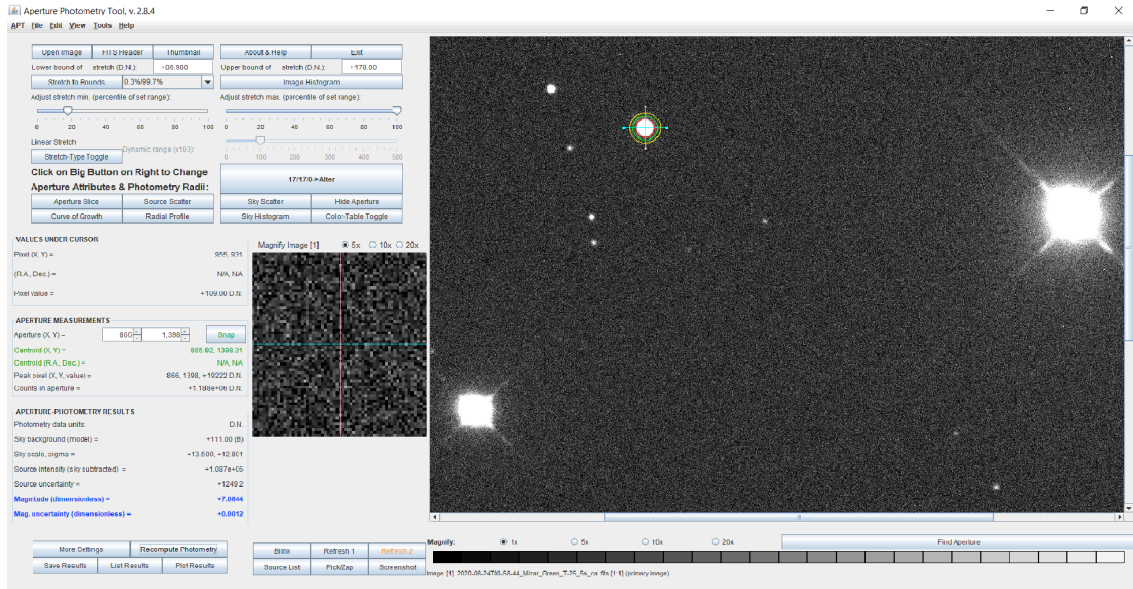


Figure 6.8: Photometry of known star in APT to find the magnitude zero point

Using the known star's source intensity of 1002000 and its magnitude of 7.55, the magnitude zero point comes out to be 22.5521693, putting this value in the magnitude zero point in 'more settings' options will give us the apparent magnitude of star we want to observe.

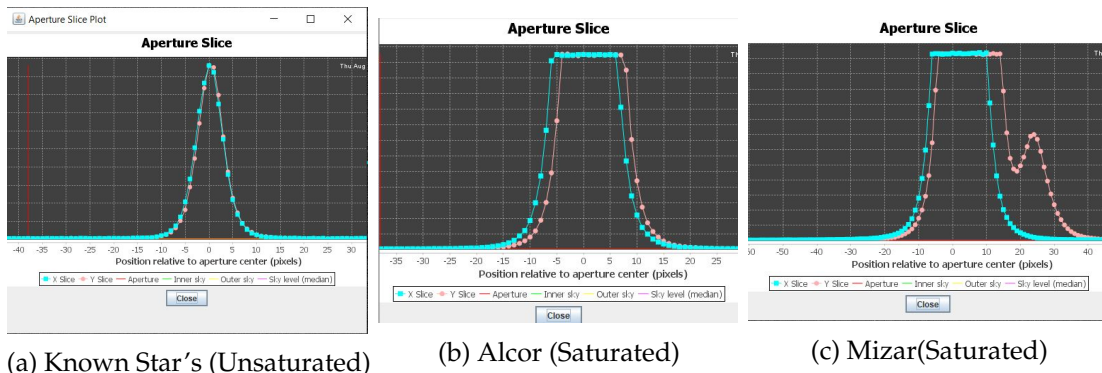


Figure 6.9: Aperture Slices of stars under observation

If the aperture slice of the star comes out to be a flat 'plateau', it indicates that the star is saturated, and therefore the magnitude that we will obtain using ATP therefore will not be accurate. The aperture slice of both Alcor as well as Mizar were a flat plateau (see Figure 6.9), the reason being that both the stars are extremely bright and the website telescope live does not allow an observation time of less than 5 seconds, whereas it should be less than 1 second for the stars to be unsaturated in a photo. Using APT, the calculated magnitude of Alcor came out to be 4.31 (actual magnitude is 3.99) and for Mizar it came out to be 2.5 (actual magnitude is 2.04), the reason for this error is the over exposure to Alcor-Mizar



7. More Complex Systems

7.1 Types of Binaries

Almost all of the discussion in the previous chapters was limited to what are known as **detached binaries**. In this section, we will delve into what are known as **contact binaries** and **semi detached binaries**.

To understand the distinction between detached, semi detached and contact binary star systems, we first need to understand the concept of **Roche Lobe**. In every binary star system, there are regions in space where, if a particle is released from rest, remains bound to that particular star, under the influence of both the gravitational forces. This region is an approximate tear-drop shaped structure that terminates at the first Lagrangian point of both the stars. The envelope of this region is at a gravitational equipotential. Both the stars have this region enveloping them, and this is called the Roche Lobe.
potential due to centrifugal force also contributes afaiik (Soumyadeep)

In the case of detached binary star systems, the distance between the stars always remains large enough so that neither of the stars have material crossing over outside their respective Roche Lobes. In the case of a semi-detached binary system, only one of the stars has its material extending into the Roche Lobe of the other star, which causes a mass transfer to take place from the donor to the accretor. Finally, contact binary star systems are defined to be stars which have both components surrounded by a common envelope lying between the inner and outer Lagrangian zero-velocity equipotential surfaces.

7.2 Stability of Complex Systems

When a star goes beyond its Roche Lobe, its surface extends out beyond its Roche Lobe, and the material that lies outside the Roche Lobe can "fall off" into the other object's Roche Lobe via the first Lagrangian Point. In binary evolution, this is called **mass transfer** via

Roche Lobe Overflow.

Theoretically, since a mass transfer would lead to shrinking of the Roche Lobe, the component should shrink until it gets completely consumed. However, this is generally not the case for a number of reasons- firstly, the donor itself shrinks, and if this shrinkage is faster, it may stop Roche Lobe Overflow when the component gets limited to its Roche Lobe. Secondly, mass transfer also leads to a change in momentum, and since angular momentum is conserved, in the case of a relatively larger donor, the orbit will reduce, but when the donor is the smaller of the two, the orbit will increase, thus leading to a stage when it gets limited to its own Roche Lobe.

To determine the outcome of mass transfer in binary star systems, one has to determine how the radius of the donor star and orbit reacts to the mass transfer taking place. Based on this, mass transfer is broken down into three classes:

1. Case A

Case A Roche Lobe Overflow happens in cases when the donor star is hydrogen burning (in its main sequence). Nelson and Eggleton further subdivided this class into subclasses:

- *AD dynamic*: This kind of evolution happens when the donor star has a deeper convective zone. The mass transfer is rapid, and the outcome may be a complete merger.
- *AR Rapid Contact*: Similar to the AD system, however the star gaining mass grows fast enough to exceed its own Roche Lobe, thus forming a contact binary star system.
- *AS Slow Contact*: Similar to AR, but there is a short period of rapid mass transfer, followed by a much longer period of slow mass transfer. Eventually, the system forms a contact binary, but the component stars have undergone a massive change.
- *AE Early Overtaking*: The star gaining mass overtakes the one donating, and evolves past its main sequence. The donor may shrink enough to stop mass transfer, but due to stellar evolution, it will begin again.
- *AL Late Overtaking*: When the star that initially was the donor goes supernova after the other star begins to donate, it falls under this class.
- *AB binary*: The case when the stars switch back and forth between becoming donor and accretor at least three times.
- *AN No Overtaking*: The star which was the donor undergoes supernova before the other star can begin its donation phase.
- *AG Giant*: Mass transfer does not begin until the donor has reached its Red Giant phase, but hasn't completely exhausted its hydrogen core.

2. Case B

Case B happens when the Roche Lobe Overflow begins in a post hydrogen burning/hydrogen shell burning star. There are two alternative methods of classification within this class:

- *Br*: The overflow happens in a star whose radiative zone is the dominating

zone.

- *Bc*: The overflow happens in a star whose convective zone is the one that dominates.

Or alternatively,

- *Ba*: Star systems with the donor undergoing Helium fusion
- *Bb*: Star systems with the donor undergoing after Helium and before Carbon fusion.
- *Bc*: Star systems with donor burning elements beyond Carbon.

3. Case C

Case C happens when RLOF starts when the donor is at or beyond the helium shell burning phase. These systems are the rarest observed, but this may be due to selection bias.

7.3 Contact Binary Systems from an Observer's Perspective

Now, since we have considered contact binaries on an absolute scale, it is not of much use if we cannot use that information to study such systems from the Earth. This section is devoted to the developments in observational astronomy regarding contact binary systems, and various subsections will deal with various physical features of stars in contact binary systems.

The first contact binary to be observed was the W Ursae Majoris, hence similar contact binary stars are called W Ursae Majoris Stars. A classification system within W Ursae Majoris stars ([Binnendijk \(1965\)](#)) is the follows: W type stars are the ones with light curves having deeper minimum corresponding to an occultation of the secondary, less massive component; A-type systems have the deeper minimum corresponding to a transit of the secondary in front of the primary, more massive, component. What this essentially means, according to ([Rucinski \(1974\)](#)), is that W type systems have the secondary star as the hotter star amongst the two whereas A type stars are the opposite. A type stars are generally older and more evolved than the W type ones.

The first instance of observation was done by [Lucy \(1967\)](#), when he proved that W Ursae Majoris is a contact binary system. He did this using a direct numerical method based on Roche Geometry to synthesize theoretical light curves, which he fit to the above star system. Improvements came when [Mauder \(1972\)](#) and [Ruciński \(1973\)](#) used Fourier techniques to more simply classify a larger number of systems in terms of the common envelope model. This method of fitting light curves agrees well between different authors, and a large collection of data for several systems is now available with excellent reviews on the subject. Some problems that still remain are: determination of gravity darkening (change in shape of the star to an oblate spheroid due to rapid rotation) and limb darkening (a phenomenon in which the center of the star appears brighter than the edge of the star) which currently use least square fitting of a large collection of stars, but this could be inaccurate and affects determination of temperature difference between the components as well as fill-out (fraction to which the Roche Lobes get filled).

The common photosphere of the binary system is defined by the following potential equation:

$$\Psi = \frac{-G(M_1 + M_2)C}{2A} \quad (7.1)$$

Here, Ψ is the gravitational potential, M_1 and M_2 are the masses of the primary and secondary components, G is the gravitational constant, C (normalised surface potential) is a constant that defines the geometry of the system, and A is the separation between the component center of masses. The geometry has been fully described mathematically by [Mochnacki & Doughty \(1972\)](#). The geometry of the system is fully defined by C and $q = \frac{M_2}{M_1}$.

However, the constant C is not convenient, and there are other parameters defined for fill-out or over-contact systems exist. As mentioned before, fill out is the degree to which the stars have achieved contact. It is defined as:

$$F = \frac{C_1 - C}{C_1 - C_2} + 1 \quad (7.2)$$

Here, C is the same as before, C_1 and C_2 are the normalized potentials for inner and outer contact, respectively. It has been observed that the W-type systems have F near 1.0 and the A-type systems have somewhat larger fill-out factors. A rough correlation can be seen with systems of larger q having lower F except for the hot contact systems, which appear to have higher F for larger q .

Papers have also been published which have accurately calculated the densities of the component stars. The densities (in terms of CGS units) are given as:

$$\rho_1 = \frac{0.079}{V_1(F, q)(1+q)p^2} \quad \rho_2 = \frac{0.079}{V_2(F, q)(1+q)p^2} \quad (7.3)$$

Here, V_i stands for the volume of the i^{th} component using A as the unit of length, and V is a function of F and q . p is the period of the system in days.

By plotting the density ρ_1 of the primary against a temperature index, a comparison with the main sequence and evolutionary models for single stars is possible.

Lucy's convective common envelope model has the secondary deriving most of its luminosity by "sideways convection" from the primary. Up to a third of the energy generated by the primary is transferred to the secondary ([Mochnacki 1971 \(unpublished\)](#); [Moses & Smith \(1976\)](#)). Following Mochnacki (1971), one can define a quantity U which is the transferred component of the secondary's luminosity expressed as a fraction of the energy radiated from the surface of the primary,

$$U = \frac{L_2 - L_2(\text{internal})}{L_1} \quad (7.4)$$

Here, L_1 and L_2 are the apparent (radiative) luminosities of the primary and secondary, respectively. The method to calculate U is the follows:

$$U = \frac{\frac{S_2}{S_1} - q^{4.4}}{1 + q^{4.4}} \quad (7.5)$$

S_1 and S_2 are the respective calculated surface areas that are found using numerical integration. Calculation of U leads us to the calculation of the primary's temperature. The increase in the primary's effective temperature at constant radius where the energy transfer shut off is given by:

$$\Delta \log(T_e) = \frac{\log(1+U)}{4} \quad (7.6)$$

and the corrected temperature is:

$$\log(T_1) = \log(T_e) + \Delta \log(T_e) \quad (7.7)$$

T_e is the calculated surface temperature from spectral data, correction is needed due to the transfer of energy from primary to secondary.

We now move on to the angular momentum of contact binary systems rotating uniformly, as calculated by Webbink(1976a). It is calculated as follows:

$$J = \left[\frac{M_1 M_2 A^2}{M_1 + M_2} + M_1 k_1^2 R_1^2 + M_2 k_2^2 R_2^2 \right] \Omega \quad (7.8)$$

Here, R_1 and R_2 are their effective radii, $k_1 R_1$ and $k_2 R_2$ are their radii of gyration, and Ω is the orbital frequency. This equation can be re-arranged accordingly, and after substituting Kepler's Law, written as:

$$J = \sqrt{GAM^3} f(q) \quad (7.9)$$

Here, M is total mass of the system, and $f(q)$ is a function, which after derivation, is as follows:

$$f(q) = \frac{q}{(1+q)^2} + \frac{k_1^2 r_1^2}{1+q} + \frac{k_2^2 r_2^2}{1+q} \quad (7.10)$$

The usage of r_i for respective i is:

$$r_i = \frac{3V_i(F, q)^{\frac{1}{3}}}{4\pi} \quad (7.11)$$

The quantities r_i and V_i are the component radii and volumes in normalized units ($A = 1$).

The rearrangement we have done here may not be apparent yet, but now equation 7.9 can be written in terms of period of the system as:

$$J = \left(\frac{G^2 M^{5/3}}{2\pi} \right) P^{\frac{1}{3}} f(F, q) \quad (7.12)$$

Now, you will appreciate the importance of this rearrangement. Since contact binaries evolve with time, taking a ratio of angular momenta at different times, we get:

$$\frac{J}{J_0} = \left(\frac{P}{P_0} \right)^{\frac{1}{3}} \frac{f(F, q)}{f(q_0)} \quad (7.13)$$

This is important because the initial period of binary systems can be calculated, further by estimating, a minimum initial period P_0 for systems, we can confirm whether A type

systems have evolved from W type systems as angular momentum can only decrease or remain constant with time. Further, as the minimum period is dependent on q , later on, we'll see how this is an important parameter in evolutionary model of contact binary systems.

The next important feature for any observer is calculation of masses and luminosities of contact binary systems. The method of determining the mass of a contact binary system relies on the fact that the mass-luminosity curve of single stars is steep whereas the formula derived from Kepler's law for the luminosity of the binary common envelope is a shallow function of mass. Because of this, the intersection point is well determined. The details of this method are described in Mochnacki(1971). A different method is used by [Wilson \(1978\)](#) in which he uses mass-radius relations of stars in a similar fashion to determine the mass and luminosity of contact systems, however both the curves of both single as well as contact systems are shallow, making the intersection point less distinct.

Moving on to luminosities, the absolute bolometric magnitude of a star is given by:

$$M_b = M_s + 2.5\log_{10}(L_s) - 2.5\log_{10}(\sigma) - 2.5\log_{10}(S) - 10\log_{10}(T_e) \quad (7.14)$$

Here M_s and L_s are the bolometric magnitude and the luminosity of the sun respectively, σ is the radiation constant, S is the surface area of the star and T_e is the effective temperature.

The surface area S is given by:

$$S = S(F, q)A^2 \quad (7.15)$$

$S(F, q)$ is the surface area of the envelope in normalized units and A is the same as previous usage. A is determined using Kepler's Law, which finally leads us to:

$$S = \left(\frac{GP^2M}{4\pi^2}\right)^{\frac{2}{3}}S(F, q) \quad (7.16)$$

Which finally leads us to the luminosity of the primary component:

$$L_1(\text{int}) = \sigma T_e^4(1 + U)S_1 \quad (7.17)$$

$L(\text{int})$ is the internally generated luminosity by the primary, U is the constant calculated in 7.4 and 7.5, T_e here is the effective temperature of the primary. Substituting this back in the equation for the bolometric magnitude, we can calculate the primary's bolometric magnitude as well.

This brings us to the final section on the topic of contact binaries: Theories of formation.

[Roxburgh \(1966\)](#), was the first paper to propose a theory. According to it, a non-uniformly radiative core forms at the center of a convective Hayashi protostar, the envelope of which is assumed to be rotating uniformly at its equatorial breakup velocity. Hayashi track is a curve on the Hertzsprung Russel diagram proposed by Hayashi, which is followed by stars whose masses are less than $3M_s$, before they enter the main sequence (protostars). It is an evolutionary curve which Hayashi stars follow before entering the main sequence. According to this theory, this radiative core can become fissionally unstable beyond $0.8M_s$, which means that it can split at a certain specific angular momentum, forming two cores,

and essentially, a contact binary system. He plotted observational data of specific angular momentum against the total mass of the Hayashi star, and estimated h_u as the upper limit for fission and h_l as the lower limit. This theory was rather rudimentary and there was an under-estimation of the specific angular momentum by a factor of two, because of which, it was dismissed.

However, this was not the only problem with the theory. The idea that a convective Hayashi star undergoes fission was itself problematic. Observational data suggests most of the W-type stars would have formed before a radiative core was formed, which is impossible, unless turbulent viscosity during contraction does not impose uniform rotation ([Ostriker \(1970\)](#)).

Larson ([Larson \(1969\)](#),[Larson \(1972a\)](#),[Larson \(1972b\)](#)) proposed a more plausible theory involving the star never entering its Hayashi phase, instead a rotating cloud of gas could collapse to form an unstable ring-like structure. Ring fragmentation has been suggested as the formation mechanism for binaries with mass ratios near 1.0 ([Lucy & Ricco \(1979\)](#)). It would appear that the W-type systems may have been formed by ring fragmentation during or near the end of the accretion phase.

None of these younger models involved the consideration of magnetic braking for the formation of contact binary stars in the computer simulations of hydrodynamic calculations. [Mestel \(1968\)](#) provide a framework for studying the effects of magnetic braking during the formation of a close binary star. A pair of tidally coupled protostars moves closer together as each component is magnetically braked by its own stellar wind. If the contraction time is sufficiently large compared with the braking time, a contact binary or a single star will be formed.

We have come a long way in determining various features of contact binaries, and research is still going on regarding theories of formation and evolution. Hopefully, in the near future, we will fully be able to understand contact binary stars completely.

Note that this chapter has skipped derivations and is to provide a basic understanding of complex systems. The reader is encouraged to read up the cited reference papers in order to get an in-depth understanding of this subject.



8. Visualizations

8.1 Introduction

Understanding all the topics discussed till now is often mathematically challenging and also involve in-depth knowledge of physics. This learning takes time, years of toil to properly understand the complicated events that are going on somewhere within the enormous universe. Residing on a tiny spot in this gigantic universe, it is very difficult to perform the experiments of events taking place light years away in our labs few meters to at most few kilometers long. Though experiments are being performed but those are in some different form, which are often as difficult as the equations to understand. These are meant for the specialized people working particularly in these fields, but they hardly mean anything for the public interested to know about these events or even the beginners starting to work in the field. But things like visualization through animation is often more interesting, appealing and accessible. These are highly simplified version of the events recreated on the computer - recreating the dynamic universe on a screen. These serve as abstraction - hiding the complicated and page-long equations describing the events, behind the movements and colours of the animation. These animations may involve simulations of certain differential equations that teach us some physics behind the event(s) being depicted, but mostly these give a qualitative picture of the events. Here, we will talk about a similar animation, made by our team.

8.2 About the Software and the Tools Used

8.2.1 Blender - a Brief Introduction

Blender is a free and open-source 3D computer graphics software toolset used for creating animated films, visual effects, art, 3D printed models, motion graphics etc. There are several tools to work with in Blender, some of which will be mentioned. Blender community has also launched several open projects to help drive innovation in Blender. Blender interface is user friendly - it has both graphical menu options but mostly work is done with the help of hotkeys which are shortcut keys for the menus. Blender also has

several modes to work in - the two most important being Object Mode and Edit Mode. Object mode is used to manipulate individual objects as a unit, while Edit mode is used to manipulate the actual object data - manipulating vertices and faces etc. The Blender version used for this project is 2.82. This version comes with two rendering engines - Cycles and EEVEE, both having their own advantages and disadvantages. The engine used for this animation is EEVEE.

8.2.2 Blender Python

Blender has an embedded Python interpreter which is loaded when Blender is started and stays active while Blender is running. This interpreter runs scripts to draw the user interface and is used for some of Blender's internal tools as well. Blender's embedded interpreter provides a typical Python environment, so code from tutorials on how to write Python scripts can also be run with Blender's interpreter. Blender provides its Python modules, such as *bpy* and *mathutils*, to the embedded interpreter so they can be imported into a script and give access to Blender's data, classes, and functions. Scripts that deal with Blender data will need to import the modules to work. This whole animation under discussion has all the modelling have been done with python scripting - the scripts can be run through Blender.

8.2.3 Tools Used

The following blender tools were used -

- Particle System - model events like mass transfer and novas
- Material Nodes - provide colour and textures to the objects
- Modifiers - enhance texturing and deform objects
- Constraints - to control influence of one body on another
- Physics; Force Fields - to create fields oh whose influence particles move

8.2.4 Python Modules Used

The following are the python modules which are mainly used in the scripts of this animation -

- *bpy* - the access blender facilities, to create objects and accessing the object data
- *scipy* - *odeint* from *scipy.integrate* is used to simulate differential equations
- *numpy* - Mainly to create and maintain arrays and carry of operations.
- *os* - to access the directory of blender and python files
- *random* - to crate random locations of objects

8.3 Topic of the Animation

In short, this animation describes the evolution of a binary system. Throughout this project, we have discussed several aspects of binary systems, several types of binary systems, several equations governing their motion, several interesting systems like interacting binaries. This evolution pathway depicted in the animation involves almost all of the events discussed so far, and also involve few extra. This depicts the formation bath a Binary Neutron Star(BNS) System, from a two high mass Main Sequence stars. This formation pathway was actually reported in a paper by K. Belczynski and V. Kalogera in 2001. This pathway involves two mass transfer events (one stable, one unstable), two envelope formations events (one single and one double), a supernova type 1c. In adition to the formation pathway, the merging of the two neutron stars formed and the gravitational

waves have also been shown. Apart from these, a satellite detecting the supernova and LIGO-India detecting Gravitational waves have also been shown. The following sections will have some detailed discussion on these.

8.3.1 Revisiting few Terms

These have been already discussed in detail, but here I give brief mention to some of the terms required to follow my animation.

- Main sequence (MS) phase - This is the part of the life of a star in which it spends the maximum time. This is the phase when the star burns Hydrogen to Helium in its core. The process by which this happens depends mainly on the mass of the star - high mass stars use CNO cycle, low mass stars use proton-proton (p-p) chain.
- Giant phase - This is the phase when the hydrogen fuel of the star gets exhausted and Helium starts to burn in the core. The star expands greatly (giant) in this phase owing to the release of energy when the core shrinks after H fuel exhausts. In later phases, outer parts of the star starts to burn Hydrogen to Helium.
- Stellar evolution in nutshell - A star starts from the MS phase, where it burns Hydrogen to Helium. Here it spends the maximum fraction of its life. As the Hydrogen fuel comes to end, the star starts to burn helium (Giant Phase). Before that, the star expands greatly (Sub giant phase). The burning of higher elements require higher temperature in the core, which in turn is brought by the high pressure. Thus, the end phase of the star is dependent on initial mass. The high mass stars, after burning helium forms CO (Carbon, Oxygen) cores, which are burnt to higher elements like Si till Iron. Iron nucleus is the most stable, thus no further burn takes place. Gravitational effect continues, which leads to core collapse. This leads to either a supernova or a black hole.
- Supernova - This is the massive explosion that happens at the end of the lifetime of a star, when it exhausts the fuel in its core that lead to gravitational collapse of the star. The collapse faces a rebound and simultaneously ejection of lot of neutrinos. This triggers the explosion. A lot of matter is ejected to space with a high kinetic energy. A supernova can leave behind either a Neutron star or a Black Hole. Supernova can be type 1 (contains Hydrogen lines in the spectra) or type 2 (which doesn't contain hydrogen lines). These types are in turn divided into several types. Among them type 1c is the core collapse supernova of the Fe cores of the massive stars. This type has a mention in the animation.
- Neutron star - Highly compact object with a Fe outer envelope and degenerate neutron core. The core is supported against gravity by the neutron degeneracy pressure. These have mass in order of several solar masses, compressed to a radius of around 10 km. They have very high magnetic fields, whose origin is unclear, but can be attributed primarily to conservation of magnetic fluxes.
- Tidal effect and Circularization - Tidal effect occurs when the two stars interact with each other. This mainly happens when one of the stars grows in size and the outer parts of the star is affected by the presence of the other star - this includes distortion by the other star (leading to distorted shape of the larger star) and also dissipation of energy in the drag, which is either gravitational in nature or due to the material ejected by the other star. This leads to loss of energy thus an elliptical orbit goes to circular (this can be thought simply as orbit with minimum energy for a given angular momentum)
- Roche lobes - These are surfaces around each star which determines mainly the 'region of influence' of a star. This is the surface on which the net potential on a third

test body co rotating with the system (consisting of the gravitational potential of both the stars and the pseudopotential associated with the centrifugal force) has a constant value. The value is the one whose corresponding equipotential surface contains the first Lagrange point (L1) which is a potential extremum between the two stars.

- Mass Transfer - This is a process in which mass is transferred from one star to another. There are several ways in which transfer can happen. One type is when one star expands to fill its Roche lobe and mass is transferred to other star through L1 point. Transfer can be broadly conservative and Non-conservative, Stable and Unstable. Conservative signifies no mass is lost from the system - mass lost by one star is taken up by the other. Non-conservative involves mass loss by several means (eg winds). Stable mass transfer signifies that the mass transfer is slow and not ever-happening. Unstable mass transfer occurs when either the other star is not capable to take up all the mass given by the primary (donating) star, or the secondary completely takes up all the matter given by the first.
- Common envelope - This happens when mass transfer is too fast, and the second star is not capable to take up the mass. Thus, the matter from the expanding primary overflows both the Roche lobes and then engulfs the whole system (forming an envelope). Envelope can be Single (when envelope matter is contributed by one star) or double (when both stars contribute in forming the envelope). What leaves behind are the small cores of the star(s).
- Gravitational Waves - Space time disturbances that arises due to accelerating bodies and travel at the speed of light. They are predictions from Einstein's General Theory of Relativity. Merging Neutron stars or black holes merger leads to production of intense gravitational waves as the components spiral inwards which can be detected on earth.
- Kilonova - Explosion that occurs in a merger event. This is a source of strong Gravitational Waves and Gamma Ray Bursts.

8.4 The Animation and its Making

The animation has several parts and each part had to be properly placed in a sequence for the animation to look continuous, self-explaining but not boring. The overall animation had few major parts - 1) Animating the main formation pathway 2) Modelling the Satellites 3) Modelling the LIGO-India 4) Modelling of earth 5) NS NS Merge. All the images are taken from the final animation. Here, will be discussed briefly each of the parts, and the physics behind them. Focus will mainly be on the formation pathway and the merger. For detailed reports including those of the satellite modelling and their corresponding codes refer

8.5 The Main Formation Pathway

This includes the formation of the NS-NS Binary starting from the two Main Sequence Stars. In this section a brief discussion will be done on how the modelling and texturing were done - the star texture, how the envelope formations were depicted or how the supernova was shown followed by few images from the animation and brief discussion of what the image depicts.

8.5.1 Texture and Modelling

This can be broadly broken up in few parts -

- Star Texture - *Musgrave* texture coupled with a *ColorRamp* was used for the color, and *Fresnel* node, coupled with a *ColorRamp* was used for the glow. These were used in conjunction with *Emission node*. The dynamic corona effect was done with separate sphere with *Cloud* texture.
- Roche Lobes - The Lobe Shape was made using *Displace* modifier with the instance object as a *Plain Axis* which was placed at a desired position.
- Mass Transfer - Emitter particle system was used along with *Curve Guide* force field with a *NurbsPath*.
- Common Envelope - Depicted mainly through scaling of spheres appropriately and making them transparent to depict ejection. Small modifications to textures were done.
- Supernova - Emitter particle system was used. The instance object for the particle was prepared separately; a sphere which is coloured with *Emission Node*.

8.5.2 Images of the Major Events

The following figures are taken from the animation. These pictures depict the major events which finally lead to the BNS system formation.

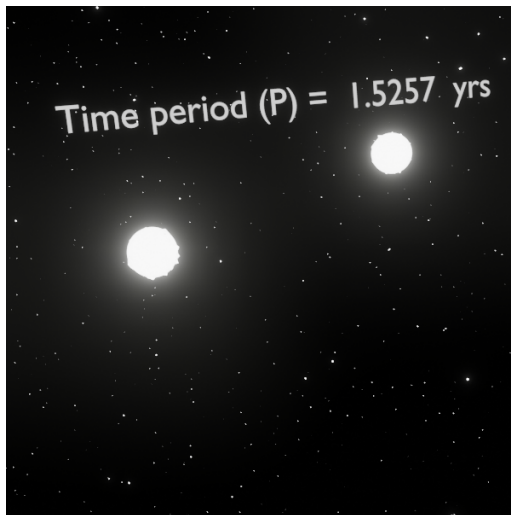


Figure 8.1: MS Binary Star

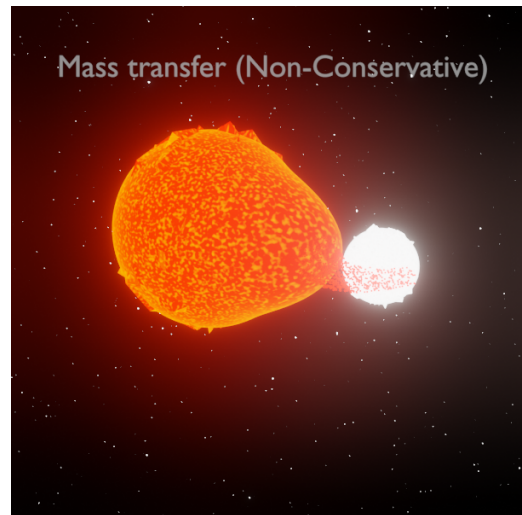


Figure 8.2: Mass Transfer

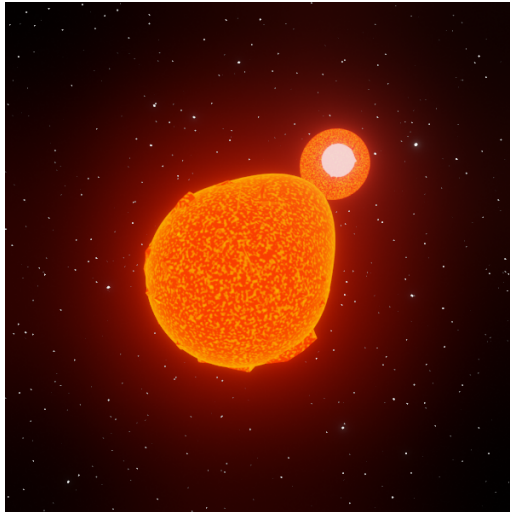


Figure 8.3: Filling of Roche Lobes

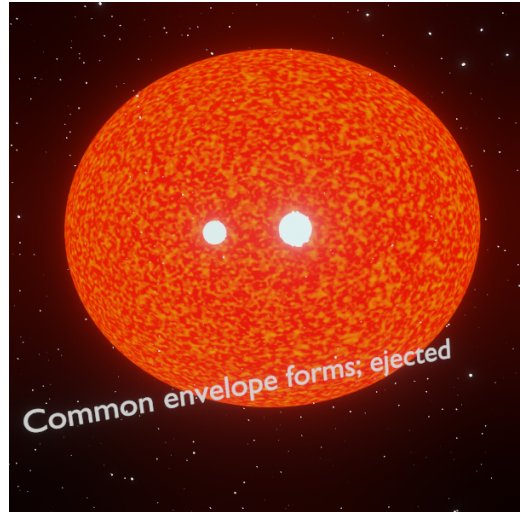


Figure 8.4: Single Common Envelope

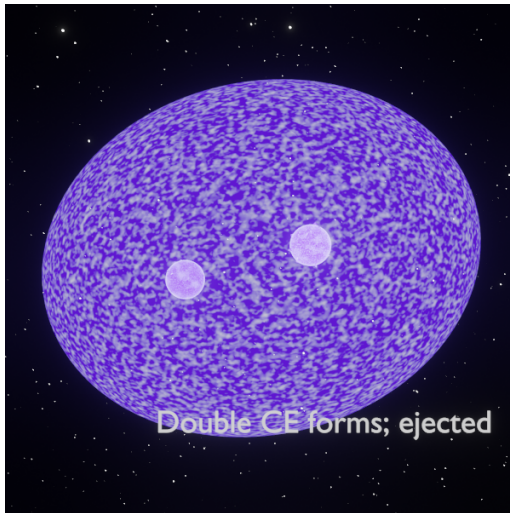


Figure 8.5: Double Common Envelope

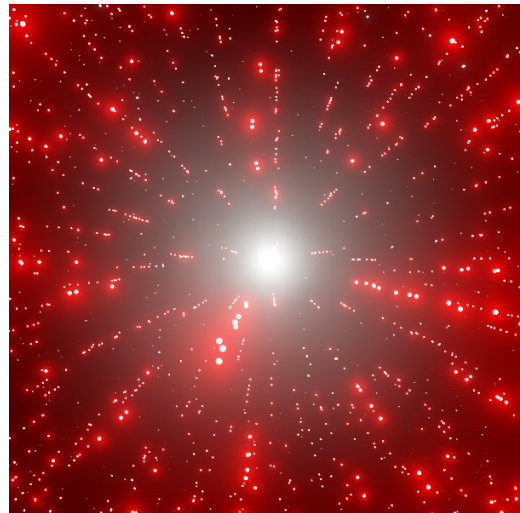


Figure 8.6: Supernova

- Fig 8.1 Depicts the Main Sequence Binary Stars. These are high mass, B type stars thus they appear bluish white. The blue is faint here thus cant be seen, thus they appear white in the animation. They follow an elliptical orbit which will later get circularized.
- Fig 8.2 depicts the mass transfer. The Lobe shape of the star is to be noted. Referring to types of transfer mentioned earlier, this is non-conservative as mentioned. The direction of the swirl of the transferred matter depends on the angular momentum of the system. The direction is governed by the Coriolis force, which prevents straight in falling o the matter. As the acceptor star is a later MS star and thus big enough, a wide accretion disc is not observed.
- Fig 8.3 This shows the overflow of both the Roche Lobe due to dynamically unstable mass transfer. The donor is a red giant, the acceptor is a He core left from the previous mass transfer.
- Fig 8.4 shows the common envelope. The two stars inside are the He cores. They lose energy due to frictional drag, spiral inward.

- Fig 8.5 depicts the second double CE phase. The two stars inside are the CO cores. The spiral-in and ejection occurs in a similar way as the previous case.
- Fig 8.6 shows the final stage - the Supernova Explosion. It is a type 1 explosion as there is no H line, and subtype c as it is a core collapse supernova, with Fe lines in spectrum.

The supernova leaves behind the two Neutron Stars. Thus completing the pathway. The merger of the two NS will be discussed next.

8.6 The BNS Merger

The Binary Neutron Star (BNS) Merger is nothing but the event when the two Neutron stars merge. The tight system formed after the supernova eventually lose energy through Gravitational Waves and come closer, and finally merge. This event produces intense gravitational waves. The modelling and then the events with images will be briefly discussed below-

8.6.1 Modelling and Texture

- The star texture was done with *Musgrave* texture node and *ColourRamp* similar to the previous stars.
- The gravitational waves were modelled using an equation to create a plane and rotating the plane to represent propagation of the waves. The following equation was used -

$$f(x, y) = 2 \times \left(\frac{\cos \left(2 \times \tan^{-1} \left(\frac{y}{x} \right) + 3.7 \times \sqrt{x^2 + y^2} \right)}{4.87 + \sqrt{x^2 + y^2}} \right) \quad (8.1)$$

- The Kilonova was modelled using emitter particles in a similar way as the Supernova.

8.6.2 Images

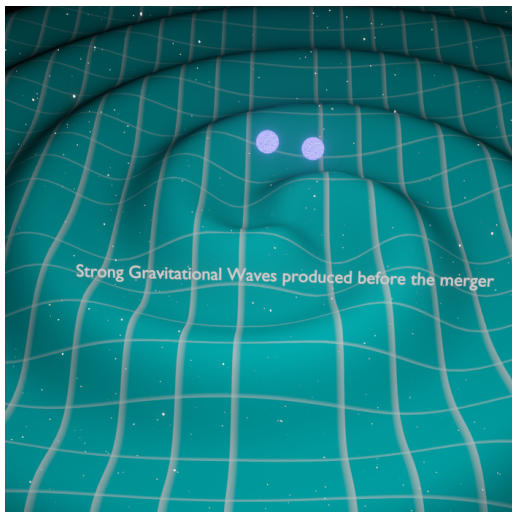


Figure 8.7: Gravitational Waves

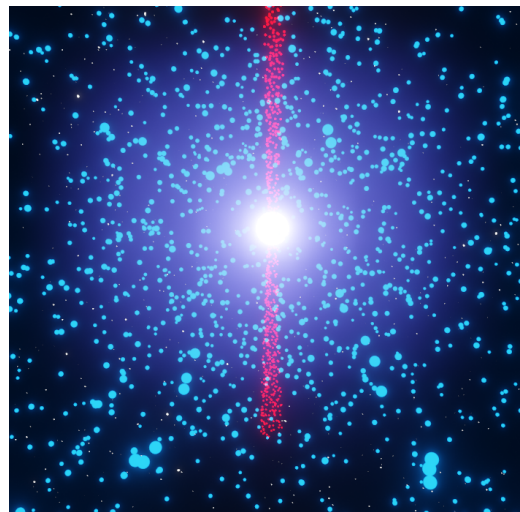


Figure 8.8: Kilonova

- Fig 8.7 shows the Gravitational waves produced during the inspiral phase. The greenish blue coloured plane depicts the space-time fabric. At earth, these waves are detected in observatories like LIGO.
- Fig 8.8 shows the Kilonova.

8.7 Detection from Earth

These events are spectacular events which can be detected from the Earth. Though there are several scopes of detection which also depends on various other factors, two very prominent detection windows are the supernova and the Gravitational Waves. The animation shows detection of these events. A satellite in the animation (modelled based on the proposed design of Daksha - a yet-to-be-launched Indian Satellite). This satellite is shown equipped with ray sensors which can be used to study high energetic events like supernovae. The second window of detection is also shown, with a model LIGO. This model was inspired by The proposed design of LIGO India. For details regarding the modelling of the satellite and LIGO refer

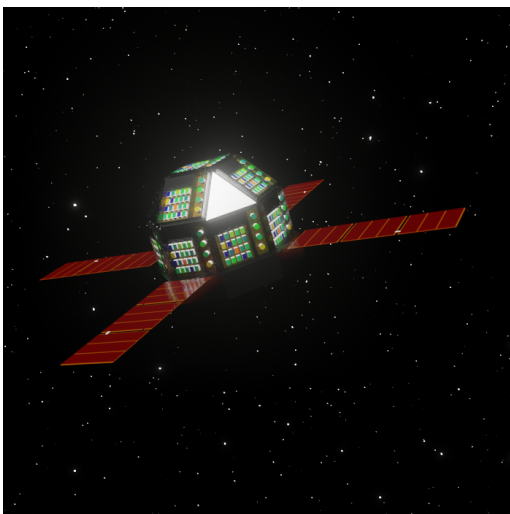


Figure 8.9: "Daksha"

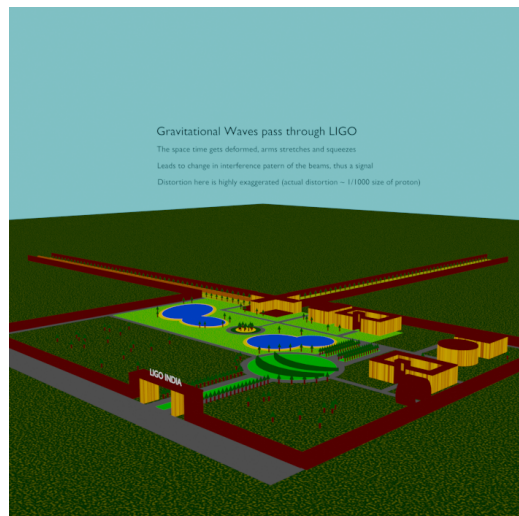


Figure 8.10: LIGO India

8.8 Putting the parts together

The total animation is actually divided in to 10 separate videos which were compiled. The first part gives the introduction to my animation (a second satellite model has been used here). The second part shows the main pathway, from the MS binaries to Supernova 1c. The third video shows the "Daksha" observing the supernova. The supernova has been shown as a white luminous path in the sky. The fourth one shows a simplistic model of X ray view, and also shows a real Xray image of SN2008D which was a type 1c supernova. The fifth video shows how the light curve SN1c looks like. The sixth video shows the merger of the Neutron Stars, the formation of the G waves and the kilonova. The seventh and the eighth video shows the LIGO India model and the deformation as the G waves passed. The ninth video shows the plot for the strain and frequency for the merger. The data of a Binary Black hole merger is used, just to show how the data may look like. The tenth video displays the names and the credit. Effort has been made to make the animation as self-explanatory, as theoretically accurate as possible.



A. Appendix

A.1 Two Body Problem

The equations of motion of 2 bodies of mass m_1 and m_2 , $M = (m_1 + m_2)$, position vectors \mathbf{r}_1 and \mathbf{r}_2 with separation vector $\mathbf{r} = \mathbf{r}_2 - \mathbf{r}_1$ and the position vector of the centre of mass is $\mathbf{R} = \frac{m_1\mathbf{r}_1 + m_2\mathbf{r}_2}{m_1 + m_2}$ under Gravitational interactions are given by :

$$m_1 \ddot{\mathbf{r}}_1 = -\frac{Gm_1m_2}{r^3} \mathbf{r} \quad (\text{A.1})$$

$$m_2 \ddot{\mathbf{r}}_2 = -\frac{Gm_1m_2}{r^3} \mathbf{r} \quad (\text{A.2})$$

Adding (A.1) and (A.2), we get:

$$(m_1 + m_2) \ddot{\mathbf{R}} = 0 \quad (\text{A.3})$$

Therefore, the centre of mass is either at rest or moves with a constant velocity.

Subtracting (A.1) and (A.2), we get:

$$m \ddot{\mathbf{r}} = -\frac{Gm_1m_2}{r^3} \mathbf{r} \quad (\text{A.4})$$

So the 2-body problem is effectively reduced to a 1-body problem with a reduced mass $m = \frac{m_1m_2}{M}$ under the attractive force given by (A.4)

A.1.1 Angular Momentum

We denote Angular Momentum of the system with \mathbf{L} . It is given by:

$$\mathbf{L} = m \dot{\mathbf{r}} \times \mathbf{r} \quad (\text{A.5})$$

It's time derivative is given by:

$$\dot{\mathbf{L}} = m(\ddot{\mathbf{r}} \times \mathbf{r} + \dot{\mathbf{r}} \times \dot{\mathbf{r}}) \quad (\text{A.6})$$

Using (A.4) and (A.6), we can clearly see that \mathbf{L} is constant as its time derivative vanishes. Therefore we can conclude that the orbit is confined to a plane whose normal is parallel to \mathbf{L} . Therefore we can write its coordinates in polar coordinates (\mathbf{r}, θ)

A.1.2 Deriving the Orbit

The position vector can be written as:

$$\mathbf{r} = r\hat{\mathbf{r}} + \theta\hat{\theta} \quad (\text{A.7})$$

Also note that $\dot{\hat{\mathbf{r}}} = \hat{\theta}$ and $\dot{\hat{\theta}} = -\hat{\mathbf{r}}$. Differentiating A.7 twice with respect to time, we get:

$$\ddot{\mathbf{r}} = (\ddot{r} - r\dot{\theta}^2)\hat{\mathbf{r}} + (r\ddot{\theta} + 2\dot{r}\dot{\theta})\hat{\theta} \quad (\text{A.8})$$

Comparing (A.4) and (A.8), we get (Taking GM=k):

$$\ddot{r} = -\frac{k}{r^3} + r\dot{\theta}^2 \quad (\text{A.9})$$

$$r\ddot{\theta} + 2\dot{r}\dot{\theta} = 0 \quad (\text{A.10})$$

(A.10) is equivalent to the derivative of (\mathbf{L}/m) which is obviously 0. We can now replace $\dot{\theta}$ by (\mathbf{L}/mr^2) into (A.9). We also take $|\mathbf{L}/m| = h$ for convenience. Then we get,

$$\ddot{r} = -\frac{k}{r^2} + \frac{h^2}{r^3} \quad (\text{A.11})$$

It is easier to solve this seemingly scary differential equation by changing the independent variable from t to θ using the relations

$$\begin{aligned} \frac{d}{dt} &= \frac{h}{r^2} \frac{d}{d\theta} \\ r &= 1/u \end{aligned}$$

As a result of this, the following terms change in A.11

$$\frac{dr}{d\theta} = \frac{-1}{u^2} \frac{du}{d\theta} \quad (\text{A.12})$$

$$\ddot{r} = \frac{d}{dt} \left(\frac{dr}{dt} \right) = \frac{h}{r^2} \frac{d}{d\theta} \left(\frac{h}{r^2} \frac{dr}{d\theta} \right) = hu^2 \frac{d}{d\theta} \left(hu^2 \frac{-1}{u^2} \frac{du}{d\theta} \right) = -h^2 u^2 \frac{d^2 u}{d\theta^2} \quad (\text{A.13})$$

Thus, A.11 changes to:

$$\frac{d^2 u}{d\theta^2} = \frac{k}{h^2} - u \quad (\text{A.14})$$

This is a much simpler Second Order Differential equation which can be easily solved. Its solution is given by:

$$u = \frac{k}{h^2} (1 + e \cos(\theta - \theta_0)) \quad (\text{A.15})$$

Here e and θ_0 are the arbitrary constants(initial conditions) which are characteristic for a 2nd order ODE. Resubstituting r , we get:

$$r = \frac{\frac{h^2}{k}}{(1 + e \cos(\theta - \theta_0))} \quad (\text{A.16})$$

This is the standard equation of a conic section with $r_0 = \frac{h^2}{k}$ as the semi latus rectum which is $a(1 - e^2)$ where a : semi major axis

The Energy of the Orbit is given by the sum of its Kinetic and Potential Energy.

$$KE = \frac{m}{2} (\dot{r}^2 + (r\dot{\theta})^2)$$

$$PE = -\frac{Gm_1 m_2}{r}$$

Adding these we get the Energy of the orbit, E as

$$E = -\frac{Gm_1 m_2}{2a}$$

Note: The individual coordinates of both the bodies in the original frame of reference can be obtained by substituting A.16 in the relations between \mathbf{r}, \mathbf{R} and $\mathbf{r}_1, \mathbf{r}_2$.

A.1.3 Laplace-Runge-Lenz Vector (Alternate Way)

(A.4) can also be written as :

$$\dot{\mathbf{p}} = -\frac{k}{r^3} \mathbf{r} \quad (\text{A.17})$$

Its cross product with \mathbf{L} can be expanded as:

$$\dot{\mathbf{p}} \times \mathbf{L} = -\frac{mk}{r^3} (\mathbf{r} \times (\mathbf{r} \times \dot{\mathbf{r}})) = -\frac{mk}{r^3} (\mathbf{r}(\mathbf{r} \cdot \dot{\mathbf{r}}) - r^2 \dot{\mathbf{r}}) \quad (\text{A.18})$$

Using

$$\mathbf{r} \cdot \dot{\mathbf{r}} = \frac{1}{2} \frac{d}{dt} (\mathbf{r} \cdot \mathbf{r})$$

, we get:

$$\dot{\mathbf{p}} \times \mathbf{L} = -\frac{mk}{r^3} (r \dot{\mathbf{r}} \mathbf{r} - r^2 \dot{\mathbf{r}}) \quad (\text{A.19})$$

(A.19), with a bit of manipulation can be rewritten as

$$\frac{d}{dt} (\mathbf{p} \times \mathbf{L}) = mk \left(\frac{\dot{\mathbf{r}}}{r} - \frac{r \dot{\mathbf{r}}}{r^2} \right) = \frac{d}{dt} \left(\frac{mk \mathbf{r}}{r} \right) \quad (\text{A.20})$$

Thus, we get the conserved vector, \mathbf{A} (LRL vector) defined as :

$$\mathbf{A} = \mathbf{p} \times \mathbf{L} - mk \frac{\mathbf{r}}{r} \quad (\text{A.21})$$

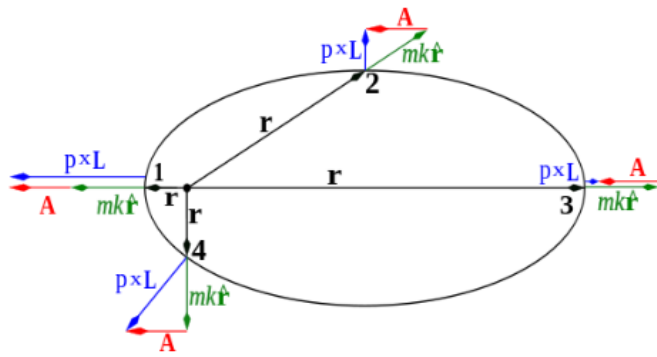


Figure A.1: Laplace-Runge-Lenz Vector, Source: Wikipedia

It can be easily seen that

$$\mathbf{A} \cdot \mathbf{L} = 0$$

It can also be seen that:

$$\mathbf{A} \cdot \mathbf{r} = Ar \cos(\theta) = \mathbf{r} \cdot (\mathbf{p} \times \mathbf{L}) - mkr \quad (\text{A.22})$$

By permutation of the triple dot product,

$$\mathbf{r} \cdot (\mathbf{p} \times \mathbf{L}) = \mathbf{L} \cdot (\mathbf{r} \times \mathbf{p}) = l^2$$

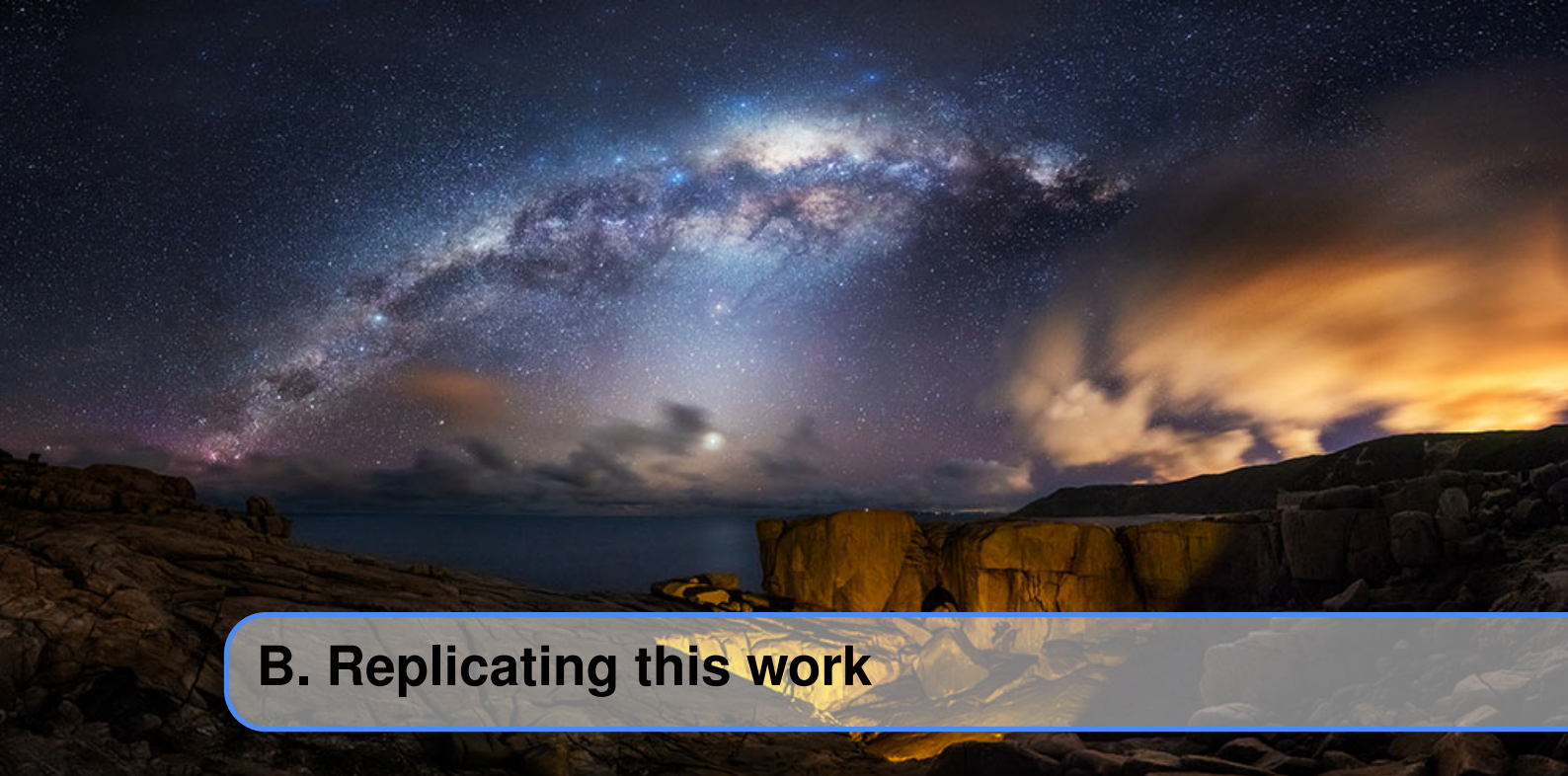
where l is the magnitude of Angular Momentum.(A.22) becomes:

$$Ar \cos(\theta) = l^2 - mkr \quad (\text{A.23})$$

or

$$\frac{1}{r} = \frac{mk}{l^2} \left(1 + \frac{A}{mk} \cos(\theta) \right) \quad (\text{A.24})$$

This is the same as the equation for a conic section we derived in (A.16) with the magnitude of $A=mke$ where e is the eccentricity of the orbit.



B. Replicating this work

B.1 RV Curves

One could go through [Double Star Astronomy](#) to get a basic understanding of Binary systems. For a more detailed understanding, one could go through [Celestial Mechanics](#) for the basics of celestial mechanics.

In order to find the radial velocities of the stars in circular orbital paths, one can use simple mathematics and some basic knowledge of vector algebra to obtain the expressions.

To find the expression of the magnitude of velocities of the stars in COM frame in the case of elliptical orbits, [Elliptic Orbits](#) is useful.

Further, in order to incorporate the orbital elements, a study of [Orbital Elements](#) is useful. The results can be verified from [Sharma \(2017\)](#).

B.2 Analysis

For the analysis, as expected, basic knowledge of Binary Systems is required.

Curve Fitting and Analysis often uses various mathematical tools such as [Non-linear Least Squares Fitting](#) and [Periodograms](#) hence a good knowledge of these tools is essential.

For the analysis of Radial Velocity curves, one can start with the [Spectroscopic Binaries](#) from [Celestial Mechanics, J. B. Tatum](#) to have a mathematical treatment of the problem.

[Russell \(1912\) & Kopal \(1979\)](#) are great starting points for the understanding of the Light Curve geometry for the analysis of Light curves.



References

- Ballesteros, F. J. 2012, EPL (Europhysics Letters), 97, 34008, doi: [10.1209/0295-5075/97/34008](https://doi.org/10.1209/0295-5075/97/34008)
- Binnendijk, L. 1965, Veroeffentlichungen der Remeis-Sternwarte zu Bamberg, 27, 36
- Bob King. 2017, Alcor Mizar as a sextuplet system (image not to scale). <http://www.astronomytrek.com/star-facts-mizar-and-alcor/>
- Boffin, H. M. J. 2016, in Society of Photo-Optical Instrumentation Engineers (SPIE) Conference Series, Vol. 9907, Optical and Infrared Interferometry and Imaging V, 99073P, doi: [10.1117/12.2232081](https://doi.org/10.1117/12.2232081)
- Brocksopp, C., Tarasov, A. E., Lyuty, V. M., & Roche, P. 1999, A&A, 343, 861. <https://arxiv.org/abs/astro-ph/9812077>
- Calçada, E. 6 March 2013, An artist's impression of eclipsing binaries. <https://www.eso.org/public/images/eso1311b/>
- da Vinci, L. 1490, Vitruvian man, Reproduced as Figure 5 in ?
- Doe, J. 2013, ApJ, 14, 1
- Draine, B. T. 2011, Physics of the Interstellar and Intergalactic Medium
- Fitzpatrick,Richard. 2016, A general planetary orbit. <https://farside.ph.utexas.edu/teaching/celestial/Celestial/node34.html>
- Gaia Collaboration. 2018, VizieR Online Data Catalog, I/345
- Günther, M. N., & Daylan, T. 2019, Allesfitter: Flexible Star and Exoplanet Inference From Photometry and Radial Velocity, Astrophysics Source Code Library. [http://ascl.net/1903.003](https://ascl.net/1903.003)

- . 2020, arXiv e-prints, arXiv:2003.14371. <https://arxiv.org/abs/2003.14371>
- Halbwachs, J.-L., Kiefer, F., Lebreton, Y., et al. 2020, Monthly Notices of the Royal Astronomical Society, 496, 1355–1368, doi: [10.1093/mnras/staa1571](https://doi.org/10.1093/mnras/staa1571)
- Hartman, J. D., & Bakos, G. Á. 2016, Astronomy and Computing, 17, 1, doi: [10.1016/j.ascom.2016.05.006](https://doi.org/10.1016/j.ascom.2016.05.006)
- Johnson, H. L., & Morgan, W. W. 1953, ApJ, 117, 313, doi: [10.1086/145697](https://doi.org/10.1086/145697)
- Kang, Y. W., Hong, K. S., & Lee, J. 2007, in Astronomical Society of the Pacific Conference Series, Vol. 362, The Seventh Pacific Rim Conference on Stellar Astrophysics, ed. Y. W. Kang, H. W. Lee, K. C. Leung, & K. S. Cheng, 19
- Kopal, Z. 1979, Language of the stars. A discourse on the theory of the light changes of eclipsing variables, doi: [10.1007/978-94-009-9466-9](https://doi.org/10.1007/978-94-009-9466-9)
- Kovács, G., Zucker, S., & Mazeh, T. 2002, A&A, 391, 369, doi: [10.1051/0004-6361:20020802](https://doi.org/10.1051/0004-6361:20020802)
- Larson, R. B. 1969, MNRAS, 145, 271, doi: [10.1093/mnras/145.3.271](https://doi.org/10.1093/mnras/145.3.271)
- . 1972a, MNRAS, 156, 437, doi: [10.1093/mnras/156.4.437](https://doi.org/10.1093/mnras/156.4.437)
- . 1972b, MNRAS, 157, 121, doi: [10.1093/mnras/157.2.121](https://doi.org/10.1093/mnras/157.2.121)
- Lucy, L. B. 1967, AJ, 72, 309
- Lucy, L. B., & Ricco, E. 1979, AJ, 84, 401, doi: [10.1086/112434](https://doi.org/10.1086/112434)
- Mamajek, E. E., Kenworthy, M. A., Hinz, P. M., & Meyer, M. R. 2010, The Astronomical Journal, 139, 919, doi: [10.1088/0004-6256/139/3/919](https://doi.org/10.1088/0004-6256/139/3/919)
- Mamajek, E. E., Kenworthy, M. A., Hinz, P. M., & Meyer, M. R. 2010, AJ, 139, 919, doi: [10.1088/0004-6256/139/3/919](https://doi.org/10.1088/0004-6256/139/3/919)
- Mauder, H. 1972, A&A, 17, 1
- McLaughlin, D. B. 1924, ApJ, 60, 22, doi: [10.1086/142826](https://doi.org/10.1086/142826)
- Mestel, L. 1968, MNRAS, 138, 359, doi: [10.1093/mnras/138.3.359](https://doi.org/10.1093/mnras/138.3.359)
- Mochnacki, S. W., & Doughty, N. A. 1972, MNRAS, 156, 51, doi: [10.1093/mnras/156.1.51](https://doi.org/10.1093/mnras/156.1.51)
- Moses, A. P., & Smith, R. C. 1976, in IAU Symposium, Vol. 73, Structure and Evolution of Close Binary Systems, ed. P. Eggleton, S. Mitton, & J. Whelan, 333
- NASA/CXC/SAO. 2000, Chandra X-ray Image with Scale Bar. <https://chandra.harvard.edu/photo/2000/0065/index.html>
- Nelson, B., & Davis, W. D. 1972, ApJ, 174, 617, doi: [10.1086/151524](https://doi.org/10.1086/151524)
- Nicholas Shanks. 2005, Rossiter-McLaughlin Effect. https://commons.wikimedia.org/wiki/File:Rossiter-McLaughlin_effect.png
- Ostriker, J. P. 1970, in IAU Colloq. 4: Stellar Rotation, ed. A. Slettebak, 147

- Pan-STARRS1. 2019, Alcor-Mizar as photographed by the Pan-STARRS1 telescope).
<http://pslimages.stsci.edu/cgi-bin/display?image=rings.v3.skycell/2380/077/rings.v3.skycell.2380.077.stack.g.unconv.fits&autoscale=99.900000&title=skycell.2380.077.stack.g>
- Perryman, M. 2010, The Making of History's Greatest Star Map, doi: [10.1007/978-3-642-11602-5](https://doi.org/10.1007/978-3-642-11602-5)
- Perryman, M. A. C., Lindegren, L., Kovalevsky, J., et al. 1997, *A&A*, 300, 501
- Popper, D. M., & Etzel, P. B. 1981, *AJ*, 86, 102, doi: [10.1086/112862](https://doi.org/10.1086/112862)
- Prša, A., Conroy, K. E., Horvat, M., et al. 2016, *ApJS*, 227, 29, doi: [10.3847/1538-4365/227/2/29](https://doi.org/10.3847/1538-4365/227/2/29)
- Rossiter, R. A. 1924, *ApJ*, 60, 15, doi: [10.1086/142825](https://doi.org/10.1086/142825)
- Roxburgh, I. W. 1966, *ApJ*, 143, 111, doi: [10.1086/148481](https://doi.org/10.1086/148481)
- Ruciński, S. M. 1973, *Acta Astron.*, 23, 79
- Ruciński, S. M. 1974, *Acta Astron.*, 24, 119
- Ruciński, S. M. 1997, *The Astronomical Journal*, 113, 407, doi: [10.1086/118263](https://doi.org/10.1086/118263)
- Russell, H. N. 1912, *ApJ*, 35, 315, doi: [10.1086/141942](https://doi.org/10.1086/141942)
- Schwarzschild, K. 1906, Nachrichten von der Königlichen Gesellschaft der Wissenschaften zu Göttingen. Math.-phys. Klasse, 195, 41
- Sharma, S. 2017, *ARA&A*, 55, 213, doi: [10.1146/annurev-astro-082214-122339](https://doi.org/10.1146/annurev-astro-082214-122339)
- Smith, J. 2012, 2, Vol. 3, Book title, 1st edn. (City: Publisher), 123–200
- Southworth, J. 2013, *A&A*, 557, A119, doi: [10.1051/0004-6361/201322195](https://doi.org/10.1051/0004-6361/201322195)
- Southworth, J., Maxted, P. F. L., & Smalley, B. 2004, *Astronomy Astrophysics*, 429, 645–655, doi: [10.1051/0004-6361:20041867](https://doi.org/10.1051/0004-6361:20041867)
- Takeda, Y., Ohshima, O., Kambe, E., et al. 2015, *Publications of the Astronomical Society of Japan*, 67, 10–10, doi: [10.1093/pasj/psu139](https://doi.org/10.1093/pasj/psu139)
- van Leeuwen, F. 2007, *Astronomy Astrophysics*, 474, 653–664, doi: [10.1051/0004-6361:20078357](https://doi.org/10.1051/0004-6361:20078357)
- VanderPlas, J. T. 2018, *The Astrophysical Journal Supplement Series*, 236, 16, doi: [10.3847/1538-4365/aab766](https://doi.org/10.3847/1538-4365/aab766)
- Wilson, R. E. 1978, *ApJ*, 224, 885, doi: [10.1086/156438](https://doi.org/10.1086/156438)
- Wilson, R. E., & Devinney, E. J. 1971, *ApJ*, 166, 605, doi: [10.1086/150986](https://doi.org/10.1086/150986)